Development of $N \times N$ SMRT for N a power of 2 and its Applications in Image Enhancement

Thesis submitted in partial fulfillment of the requirements
for the award of the Degree of
Doctor of Philosophy in Engineering
under Faculty of Engineering

by

Jaya V L
(Reg. No. 3982)

under the guidance of
Prof. (Dr.) R Gopikakumari

Division of Electronics Engineering,
School of Engineering,
Cochin University of Science and Technology,
Kochi - 682 022.

May 2015

Development of $N \times N$ SMRT for N a power of 2 and its Applications in Image Enhancement

Ph.D Thesis under Faculty of Engineering

Author

Jaya V L
Research Scholar
Division of Electronics Engineering
School of Engineering
Cochin University of Science and Technology.

E-mail: mohan.jayavl@yahoo.com

Supervising Guide

Dr. R Gopikakumari
Professor
Division of Electronics Engineering
School of Engineering
Cochin University of Science and Technology.

E-mail: gopika@cusat.ac.in, gopikakumari@gmail.com

Division of Electronics Engineering,
School of Engineering,
Cochin University of Science and Technology,
Kochi - 682 022.

May 2015

Division of Electronics Engineering,

School of Engineering,

Cochin University of Science and Technology,
Kochi - 682 022.

Certificate

Certified that the thesis entitled **Development of $N \times N$ SMRT for N a power of 2 and its Applications in Image Enhancement** is a bonafide record of the research work carried out by Jaya V L under my supervision in Faculty of Engineering, Cochin University of Science and Technology. The work presented in this thesis or part thereof has not been presented for any other degree.

Prof. (Dr.) R Gopikakumari
(Supervising Guide)

Kochi,
20 May 2015.

Declaration

I hereby declare that the thesis entitled **Development of $N \times N$ SMRT for N a power of 2 and its Applications in Image Enhancement** is a bonafide record of the research work done by me under the guidance of Prof. (Dr.) R Gopikakumari at Division of Electronics Engineering, School of Engineering, Cochin University of Science and Technology. This work or any part thereof has not been presented to any other institution for any other degree.

Jaya V L
Reg. No. 3982
Research Scholar
School of Engineering
Cochin University of Science and Technology.

Kochi,
20 May 2015.

Acknowledgements

First and foremost, I would like to express my sincere gratitude to my supervising guide, Prof. (Dr.) R Gopikakumari, Professor, Division of Electronics Engineering, School of Engineering, Cochin University of Science and Technology (CUSAT), for her valuable guidance, understanding, patience, enthusiasm and most importantly, her friendly relationship during the period of research.

I would like to express my gratitude to the Director, Institute of Human Resources Development (IHRD) for giving me an opportunity to do research on a full time basis. I also would like to thank the Vice Chancellor, Controller of Examinations, Registrar and other administrative officials of Cochin University of Science and Technology for providing me with help and assistance for the smooth completion of the research work.

I would like to acknowledge the help rendered by the Principal and office staff of School of Engineering, CUSAT for providing proper resources for research. I also would like to thank the research committee members and Dr. Binu Paul, Doctoral Committee member for their timely advice and guidance. Special thanks to Dr. S Mridula, Mrs. Anju Pradeep and Dr. Deepa Sankar for the encouragement given at various stages of my work. Thanks are also due to the faculty, office staff and technical staff of Division of Electronics Engineering for the support during the entire duration.

My sincere thanks to Manju B for the encouragement, technical assistance and timely help in carrying out my work and in preparing the thesis. I also would like to thank my fellow research scholars Preetha Basu and Anjit T A for their timely help and suggestions. Thanks are due to my friends Archana R and Mini P P for their support and encouragement. I also would like to appreciate the help

rendered by some of the Under Graduate students of the Division, Nikhil M, Vishnu J Menon, Pranoy C Vijoy and Rahul D Raj for the tool-box development based on the findings of the research work.

Let me express my gratitude to the faculty and office staff of College of Engineering, Kottarakkara for their help.

Finally, I must express my profound gratitude to my husband, Rajesh Mohan R and daughter, Parvathi for providing me with unfailing support and continuous encouragement throughout the period of research work. Without their support this accomplishment would not have been possible. I also would like to thank my parents, in-laws and all relatives for their support and prayers.

Jaya V L

Abstract

Digital Image Processing is a rapidly evolving field with growing applications in Science and Engineering. It involves changing the nature of an image in order to either improve its pictorial information for human interpretation or render it more suitable for autonomous machine perception. One of the major areas of image processing for human vision applications is image enhancement. The principal goal of image enhancement is to improve visual quality of an image, typically by taking advantage of the response of human visual system.

Image enhancement methods are carried out usually in the pixel domain. Transform domain methods can often provide another way to interpret and understand image contents. A suitable transform, thus selected, should have less computational complexity. Sequency ordered arrangement of unique MRT (Mapped Real Transform) coefficients can give rise to an integer-to-integer transform, named Sequency based unique MRT (SMRT), suitable for image processing applications. The development of the SMRT from UMRT (Unique MRT), forward & inverse SMRT algorithms and the basis functions are introduced. A few properties of the SMRT are explored and its scope in lossless text compression is presented.

The capability of SMRT in image enhancement is considered next. Linear and nonlinear algorithms based on global and block level processing are investigated. The theory of fuzzy logic offers an extensive mathematical framework to capture the uncertainties associated with human cognitive processes. So the advantages of fuzzy techniques are also examined in developing image enhancement algorithms.

Traditionally, quality of an image has been evaluated by humans.

This method, though reliable, is time consuming and impractical for real-world applications that involve the use of computers for image quality assessment. So, it is important that identification of objective quality assessment metrics, that can automatically measure image quality, are to be obtained. Analysis of existing and proposed metrics for measurement of image quality with respect to brightness, sharpness, contrast and their combination has been carried out in this work.

The important contributions of this work are listed below.

- Two dimensional Sequency ordered transform called SMRT and its inverse for a data size that is a power of 2.
- Development of Image Quality Assessment (IQA) metrics in the pixel domain and SMRT domain for measuring enhancement of images.
- Analysis of existing and proposed metrics to measure brightness, contrast, sharpness and their combination for general and medical images.
- Linear and nonlinear global image enhancement techniques in the SMRT domain for general, mammogram, fingerprint images and scanned text documents.
- Fuzzy intensification operator based and fuzzy rule based block level enhancement methods in the SMRT domain.
- Scope of SMRT for text compression is explored.

Contents

List of Figures

List of Tables

List of Abbreviations

AHE	Adaptive HE
AMBE	Absolute Mean Brightness Error
BR	Blind-Reference
CLUM	Classic Linear Unsharp Masking
CNR	Contrast-to-Noise Ratio
CSF	Contrast Sensitivity Function
CSIQ	Categorical Subjective Image Quality
CT	Computed Tomography
DCT	Discrete Cosine Transform
DFT	Discrete Fourier Transform
DIP	Digital Image Processing
DM	Distortion Measure
DST	Discrete Sine Transform
EIT	Electrical Impedance Tomography
EME	MEasure of Enhancement
EMEE	MEasure of Enhancement by Entropy
FIOP	Fuzzy INT Operator based enhancement in spatial domain
FIOS	Fuzzy INT Operator based enhancement in SMRT domain
FR	Full-Reference
FRBS	Fuzzy Rule Based enhancement in SMRT domain
FSIM	Feature SIMilarity

GFLS	Global Fuzzy rule based Linear enhancement in SMRT domain
HE	Histogram Equalization
HT	Haar Transform
HVS	Human Visual System
IEM	Image Enhancement Metric
IEMS$_{BR}$	Image Enhancement Metric in SMRT domain, Blind-Reference
IEMS$_{FR}$	Image Enhancement Metric in SMRT domain, Full-Reference
IFC	Information Fidelity Criterion
INT	INTensification
IQA	Image Quality Assessment
JPEG	Joint Photographic Experts Group
KLT	Karhunen-Loeve Transform
LET	Linear Enhancement Technique
MAE	Mean Absolute Error
MOS	Mean Opinion Score
MPEG	Moving Picture Experts Group
MRI	Magnetic Resonance Imaging
MRT	Mapped Real Transform
MSE	Mean-Squared Error
MSR	Multi Scale Retinex
MSSIM	Mean Structural SIMilarity
NLET	Nonlinear Enhancement Technique
NLUM	Nonlinear Unsharp Masking
NQM	Noise Quality Measure
PET	Positron Emission Tomography
PSNR	Peak Signal-to-Noise Ratio
RFSIM	Riesz-transform based Feature SIMilarity
RR	Reduced-Reference
SD	Standard Deviation
SDME	Second Derivative like MEasurement
SMRT	Sequency based MRT
SNR	Signal-to-Noise Ratio
SPECT	Single Photon Emission Computed Tomography
SSIM	Structural SIMilarity

SSR	Single Scale Retinex
UM	Unsharp Masking
UMRT	Unique MRT
UQI	Universal Quality Index
VIF	Visual Information Fidelity
VIFP	Visual Information Fidelity in Pixel domain
VR	Visual Representation
VSNR	Visual Signal-to-Noise Ratio
WHT	Walsh-Hadamard Transform
WSNR	Weighted Signal-to-Noise Ratio
WT	Wavelet Transform

Chapter 1

Introduction

1.1 Introduction

"A picture is worth a thousand words" is a familiar proverb referring to the notion that a complex idea can be conveyed with just an image. Trillions of images, rich in information, are stored and used for different purposes in real life every day. Humans can process large amount of visual information very quickly and can identify & classify objects easily.

Images can be acquired from many sources viz. cameras, scanners, scientific instruments, satellites etc. and can be either gray-scale or colour images. Gray-scale digital image, x, is a discrete 2-D rectangular array of N_1 rows and N_2 columns. Each element of this array is called a picture element or pixel and there are $N_1 N_2$ pixels in an image. Each pixel contains information and in many traditional image processing systems, the pixel values are represented by 8-bits that can range from 0 (black) to 255 (white). Spatial resolution is the smallest discernible detail in an image and higher the resolution, the closer the digital image to the physical world.

By convention, $x(0,0)$ is considered to be on the top left corner of the image and $x(N_1-1, N_2-1)$ to be on the bottom right corner.

The gray-scale brightness of each pixel represents the information associated with that point in an image. Colour of a pixel at each position is specified quantitatively for colour images. Each pixel is represented as a combination of brightness levels of primary colours red, green and blue in RGB colour space. Using the 8-bit monochrome standard, corresponding colour image would have 24-bits per pixel. Other colour image representations are HSI (hue, saturation, intensity), YCbCr (Y is the luminance and Cb, Cr are the blue-difference, red-difference chrominance components), CMYK (cyan, magenta, yellow and black) etc.

Histogram of an image, commonly used in image characterization, is defined as a vector that contains the count of the number of pixels in the image at each gray level. It gives many useful information such as brightness, contrast etc. of the image and is the basis for numerous spatial domain image processing techniques.

1.2 Digital Image Processing

Digital image processing (DIP) and analysis is a field that continues to experience rapid growth, with applications ranging from areas such as space exploration to the entertainment industry. It involves changing the nature of an image in order to either improve its pictorial information for human interpretation or render it more suitable for autonomous machine perception.

Digital image processing can be divided into two primary application areas based on the ultimate receiver of the visual information: machine vision applications and human vision applications, with image analysis being a key component in the development and deployment of both [1]. In machine vision applications, the processed

images are for use by a computer while in human vision applications, the output images are for human handling.

1.2.1 Machine Vision Applications

Image processing for machine vision applications involves the examination of the image data for a specific application. It requires the use of tools such as image segmentation, feature extraction, pattern classification etc.

Image segmentation is one of the first steps in finding higher level objects from raw image data. Feature extraction is the process of acquiring higher level information, such as shape or colour information and may require the use of image transforms to find spatial frequency information. Pattern classification is the act of taking this higher level information and identifying objects within the image.

1.2.2 Human Vision Applications

Human vision applications of DIP involve human beings to examine the images under study. Major topics within the field of image processing for human vision applications include image restoration, enhancement and compression. In order to restore, enhance or compress images in a meaningful way, the images are to be examined first and the relationship of raw image data to the human visual perception is to be understood.

Learning how the Human Visual System (HVS) perceives images is important to understand how an image looks better. Most important aspects of HVS are spatial frequency resolution and adaptation to a wide range of brightness levels. Visual perception depends not

only on the individual objects, but also on the background and how the objects are arranged.

Restoration methods attempt to model the image distortion and reverse this degradation, whereas enhancement methods use knowledge of the human visual system's response to improve the image visually. Image compression involves reducing the massive amount of data needed to represent an image. This is done by eliminating data that are visually unnecessary and by taking advantage of the redundancy that is inherent to most images.

1.2.3 Image Processing Applications

The field of DIP has experienced continuous and significant expansion in recent years and useful in many different disciplines covering medicine through remote sensing. The advances and wide availability of image processing hardware have further enhanced the usefulness of image processing. A few applications [2] are listed below.

1. Medicine
    - Inspection and interpretation of images obtained from various imaging modalities.
    - Locating objects of interest.
    - Taking the measurements of the extracted objects like tumours, kidney stones etc.
    - Transmission of medical images in compressed format for telemedicine applications.
2. Communication
    - Secure image and video transmission.
    - Steganography and digital watermarking.

- Image and video compression standards for faster communication.

3. Industry
   - Automatic inspection of items on a production line.
   - Inspection of fruit and vegetables distinguishing good and fresh products from old.
4. Law enforcement
   - Fingerprint analysis.
   - Sharpening of high speed camera images.
   - Forensic and investigative science.
5. Biometrics
   - Face, fingerprint, iris, vein pattern, signature etc. for personal identification and recognition.
   - Biometric access control systems, providing strong security at entrances.
6. Digital Inpainting
   - Art conservation.
   - Restoration of photographs, films and painting.
7. Remote sensing
   - Extracting information regarding natural resources, such as agricultural, hydrological, mineral, forest, geological resources etc.
   - Satellite Imaging: land-cover classification, oil slick detection, extraction of vegetation indicators.
   - Multi and hyper-spectral imaging: data reduction, galaxy detection, agricultural and environmental mapping.

- Change detection: glacier development, devastated zone mapping after a disaster.

Thus DIP has an enormous range of applications in every area of science and technology. These techniques can be carried out either in spatial domain or transform domain. The term spatial domain refers to the image plane itself and is based on direct manipulation of pixels in an image. To perform transform based image processing, a suitable transform may be employed depending on the application.

1.3 Image Transforms

A transform is simply another term for a mathematical mapping process that maps data into a different mathematical space. It can be utilized to extract properties, features etc. from images.

Image Transforms are uniquely characterized by their basis functions or basis images. Transforming an image data into another domain is equivalent to projecting the image onto the basis functions. The basis functions are typically sinusoidal or rectangular. Some of the commonly used transforms for frequency domain analysis are provided.

1.3.1 Discrete Fourier Transform

Discrete Fourier Transform (DFT) is the most widely used sinusoidal transform for 1-D spectral analysis and finds applications in analysis and design of discrete time signals and systems. It converts real data values to complex form [3].

The 2-D DFT, $Y(k_1, k_2)$, of an image $\{x(n_1, n_2),\ 0 \leq n_1, n_2 \leq$

$N-1\}$, is expressed as

$$Y(k_1,k_2) = \sum_{n_1=0}^{N-1}\sum_{n_2=0}^{N-1} x(n_1,n_2).W_N^{(n_1k_1+n_2k_2)}, \quad 0 \le k_1,k_2 \le N-1 \quad (1.1)$$

where $W_N = e^{\frac{-j2\pi}{N}}$, is the twiddle factor.

Computation of 2-D DFT, for an $N \times N$ data, requires N^4 complex multiplications and $N^3(N-1)$ complex additions. Fast Fourier Transform (FFT) is a popular algorithm for the efficient computation of DFT. Row-column FFT decomposition and vector-radix FFT algorithms reduce complex multiplications from N^4 to $N^2 log_2 N$ and $\frac{3}{4}N^2 log_2 N$ respectively [4], [5], [6].

Inverse DFT is defined by

$$x(n_1,n_2) = \frac{1}{N^2}\sum_{k_1=0}^{N-1}\sum_{k_2=0}^{N-1} Y(k_1,k_2).W_N^{-(n_1k_1+n_2k_2)}, \quad 0 \le n_1,n_2 \le N-1 \quad (1.2)$$

Here both scaling constants are placed in the inverse equation. Some prefer to use scaling constants equally in the forward and inverse transform relations.

Even though DFT possesses many desirable properties, it has some drawbacks. The computations are complex and it does not provide efficient energy compaction as other transforms. DFT is not popular for image processing applications since it converts integer data values to complex coefficients.

1.3.2 Discrete Sine and Cosine Transforms

Discrete trigonometric transforms such as Discrete Cosine Transform (DCT) and Discrete Sine Transform (DST), similar to DFT, represent data as sum of trigonometric terms (cosine or sine) with different frequencies and amplitudes [7].

Forward 2-D DCT of $N \times N$ data, $\{x(n_1, n_2),\ 0 \leq n_1, n_2 \leq N-1\}$, is expressed as

$$Y(k_1, k_2) = \alpha(k_1)\alpha(k_2) \sum_{n_1=0}^{N-1} \sum_{n_2=0}^{N-1} x(n_1, n_2) cos\Big(\frac{(2n_1+1)\pi k_1}{2N}\Big) cos\Big(\frac{(2n_2+1)\pi k_2}{2N}\Big) \tag{1.3}$$

$0 \leq k_1, k_2 \leq N-1$.

$$\text{where} \quad \alpha(k) = \begin{cases} \sqrt{\frac{1}{N}} & \text{if } k = 0 \\ \sqrt{\frac{2}{N}} & \text{if } k \neq 0 \end{cases}$$

DCT basis images are shown in Appendix A.1. While DCT makes use of cosine functions, DST makes use of sine functions and DFT uses both cosine and sine functions, in the form of complex exponentials to represent each data.

DCT was earlier used as JPEG standard for still image compression and is popular for its energy compaction capability. It concentrates most of the energy into a small number of low frequency transform coefficients for highly correlated data. In practical implementations, the floating point DCT and its inverse are usually evaluated with finite precision and may lead to accuracy mismatch.

1.3.3 Rectangular Transforms

Some transforms use square or rectangular basis functions with peaks of ± 1. Examples of such transforms are Walsh-Hadamard Transform (WHT) [8], [9], Haar Transform (HT) [10] and they possess significant computational advantages over the previously considered transforms. WHT is a simple, non-sinusoidal, orthogonal transform, whose basis functions have only two values, ± 1 (Appendix A.2). It is computationally fast and possesses energy compaction property.

2-D WHT of an image $\{x(n_1, n_2),\ 0 \leq n_1, n_2 \leq N-1\}$, is defined as

$$Y(k_1, k_2) = \frac{1}{N} \sum_{n_1=0}^{N-1} \sum_{n_2=0}^{N-1} x(n_1, n_2)(-1)^{\sum_{i=0}^{log_2 N-1} b_i(n_1)b_i(k_1)+b_i(n_2)b_i(k_2)} \tag{1.4}$$

$0 \leq k_1, k_2 \leq N-1$.
$b_i(z)$ is the i^{th} bit in the binary representation of z and N is a power of 2. Here, the transformation matrix can be generated recursively by the Kronecker product operation as

$$H_{2N} = \begin{bmatrix} H_N & H_N \\ H_N & -H_N \end{bmatrix}$$

HT is useful for real-time implementation of signal and image processing applications. The values of Haar basis functions are ± 1 and 0. They are the precise and shifted copies of each other and this property makes them popular in wavelets. It has the lowest computational cost among the above discrete orthogonal transforms, but has poor energy compaction.

1.3.4 Karhunen-Loeve Transform

Karhunen-Loeve Transform (KLT) [11] is the optimal transform in terms of decorrelation and energy compaction. It depends on the second order statistics of the data and its basis vectors are the eigenvectors of the image covariance matrix. Despite its optimal performance in terms of energy compaction, it is not popular since the transformation kernel is image-dependent and hence fast computational algorithms and architectures are not available.

1.3.5 Wavelet Transform

In the past few years, researchers in applied mathematics and signal processing have developed powerful wavelet methods [12] for the multi-scale representation and analysis of signals. This tool differs from the traditional transforms by the way in which they localize the information in the time-frequency plane. In particular, they are capable of trading one type of resolution for the other, which makes them especially suitable for analysis of non-stationary signals.

A 1-D Wavelet Transform (WT) of a signal $\{x(n),\, 0 \leq n \leq N-1\}$, is defined as

$$W_{a,b} = \int_{-\infty}^{\infty} x(n) \frac{1}{\sqrt{(|a|)}} \Psi^*(\frac{t-b}{a}) dt \tag{1.5}$$

where a, b are real constants, * denotes complex conjugation and $\Psi(t)$ is the mother wavelet.

Wavelet basis functions are shifted and expanded versions of themselves [13], [14]. The number of decomposition levels increases with the information packing ability at the expense of computational complexity. It outperforms DCT in terms of compression and quality. JPEG 2000 is a wavelet-based image compression standard. Main drawback of wavelet transforms is their inability to capture geometric regularity along singularities of the surface because of their isotropic support.

1.3.6 Directional Transforms

Discontinuity curves present in the images are highly anisotropic and they are characterized by geometrical coherence. These features are not properly captured by the standard WT that uses isotropic basis functions and fail to represent edges and contours effectively. On the other hand, anisotropic wavelets such as steerable

wavelets, wedgelets, beamlets, bandlets [15], ridgelets, curvelets [16], contourlets [17], surfacelets, platelets etc. are capable to overcome this insufficiency. The main advantages of these directional transforms lie in the fact that they possess all the advantages of classical wavelets, that is space localization and scalabilty, but additionally these transforms have strong directional character. As they are capable of capturing geometric regularity of images they are used in many image processing applications. Contourlets have less clear directional features than curvelets, which lead to artifacts in denoising and compression. Medical imaging field also finds some applications using contourlets [18], [19] and curvelets [20], [21].

Recently, shearlets [22] [23] [24], a new representation scheme based on frame elements have been introduced and yield6+5 nearly optimal approximation properties. This representation is based on a simple and rigorous mathematical framework and provides a more flexible theoretical tool for the geometric representation of multidimensional data. As a result, the shearlet approach can be associated to multiresolution analysis and leads to a unified treatment of both the continuous and discrete world.

Directionlet [25], [26] transform, has integer lattice-based anisotropic basis functions and retains separable filtering [27], [28], [29].

1.3.7 Mapped Real Transform

Eventhough DFT is popular in 1-D signal processing with the advent of FFT algorithm, 2-D DFT is not popular in the image processing applications due to its computational complexity. The FFT algorithm performs DFT computation in the complex domain and is multiplication intensive. In [30], Gopikakumari modified the 2-D DFT computation in terms of real additions by grouping the 2-D data projected on to twiddle factor planes and utilizing the sym-

metry & periodicity properties of the twiddle factor as

$$Y(k_1, k_2) = \sum_{p=0}^{M-1} Y_{k_1,k_2}^{(p)} W_N^p \tag{1.6}$$

where the scaling factor, $Y_{k_1,k_2}^{(p)}$, associated with twiddle factor was expressed as

$$Y_{k_1,k_2}^{(p)} = \sum_{\forall(n_1,n_2)|z=p} x(n_1, n_2) \; - \sum_{\forall(n_1,n_2)|z=p+M} x(n_1, n_2) \tag{1.7}$$

for $0 \leq k_1, k_2 \leq N-1$ and $0 \leq p \leq M-1$.
Here, k_1, k_2 are frequency indices and p is the phase index. The parameters, z and M are defined as $z = ((n_1k_1 + n_2k_2))_N$ and $M = N/2$. This approach enables DFT computation organized using parallel distributed computing in four stages involving only real addition except at the final stage of computation.

The properties of the DFT coefficients in terms of $Y_{k_1,k_2}^{(p)}$ were studied and understood that the frequency domain analysis of 2-D signals can be carried out without doing even single complex operation. The scaling factors, $Y_{k_1,k_2}^{(p)}$, associated with W_N^p contain the frequency and phase components of DFT and later developed as an integer-to-integer transform, namely Mapped Real Transform (originally M-dimensional Real Transform) [31], [32]. Equation (1.7) maps $N \times N$ data into M matrices of size $N \times N$, in the transform domain, using real additions only.

Inverse MRT [31] is defined as

$$x(n_1, n_2) = \frac{1}{N^2} \sum_{p=0}^{M-1} X_{n_1,n_2}^{(p)}, \qquad 0 \leq n_1, n_2 \leq N-1 \tag{1.8}$$

where

$$X_{n_1,n_2}^{(p)} = \sum_{\forall(k_1,k_2)|z=p} Y_{k_1,k_2}^{(p)} \; - \sum_{\forall(k_1,k_2)|z=p+M} Y_{k_1,k_2}^{(p)} \tag{1.9}$$

and $z = ((n_1.k_1 + n_2.k_2))_N$.

Instead of putting scaling constants equally in the forward and inverse transform relations, both scaling constants are kept in the inverse relation and this makes MRT an integer-to-integer transform.

1.3.8 Unique Mapped Real Transform

MRT of an $N \times N$ data matrix in the raw form will have MN^2 coefficients and is highly redundant. The N^2 unique MRT coefficients, corresponding to $3N - 2$ basic DFT coefficients [33], are scattered in M matrices and are to be packed in an $N \times N$ matrix. A packing technique, named Unique MRT (UMRT), was presented in [33] by placing unique coefficients from the matrices corresponding to $p = 1$ to $M - 1$ in the places of the redundant coefficients that are removed from the matrix corresponding to $p = 0$. The coefficients corresponding to (k_1, k_2) are placed at $(((k_1.q))_N, ((k_2.q))_N)$ where q is a non-negative integer, co-prime to $\frac{N}{d_m}$ and less than $\frac{N}{d_m}$ where $d_m = gcd(k_1, k_2, M)$. Table 1.1 shows the index pattern (k_1, k_2, p) of the unique MRT coefficients arranged in the form of an $N \times N$ matrix corresponding to UMRT representation for $N = 8$. The disadvantage of this transform is that the different phase terms corresponding to a particular (k_1, k_2) are scattered in the matrix. But in many applications, the coefficients corresponding to different phase terms of a particular frequency are to be accessed simultaneously. The above distribution of phase terms will become a bottleneck in such type of applications.

The image transforms are used in image processing and analysis to provide information regarding the rate at which the gray levels change within an image ie. the spatial frequency or sequency. These transforms find applications in many areas of science and engineering, including digital image enhancement.

Table 1.1: Placement of UMRT coefficients for N=8

0,0,0	0,1,0	0,2,0	0,1,1	0,4,0	0,1,2	0,2,2	0,1,3
1,0,0	1,1,0	1,2,0	3,1,1	1,4,0	5,1,2	3,2,1	7,1,3
2,0,0	2,1,0	2,2,0	6,1,1	2,4,0	2,1,2	6,2,2	6,1,3
1,0,1	3,1,0	3,2,0	1,1,1	1,4,1	7,1,2	1,2,1	5,1,3
4,0,0	4,1,0	4,2,0	4,1,1	4,4,0	4,1,2	4,2,2	4,1,3
1,0,2	5,1,0	1,2,2	7,1,1	1,4,2	1,1,2	3,2,3	3,1,3
2,0,2	6,1,0	6,2,0	2,1,1	2,4,2	6,1,2	2,2,2	2,1,3
1,0,3	7,1,0	3,2,2	5,1,1	1,4,3	3,1,2	1,2,3	1,1,3

1.4 Image Enhancement

Image enhancement is usually a preprocessing step in many image processing applications. Its aim is to accentuate relevant image features that are difficult to visualize under normal viewing conditions and thereby facilitating more accurate image analysis [34]. The enhancement process does not increase the inherent information content in the image but emphasizes certain specified image characteristics.

Various reasons for poor image quality may be due to poor illumination, lack of dynamic range in image sensor or wrong setting of lens aperture at the time of image acquisition. Visual appearance of an image can be significantly improved by brightness variation, contrast stretching, edge sharpening and/or noise reduction.

Brightness is the general intensity of pixels in an image. The image is darker when the histogram is confined to a small portion towards the lower end of gray level values and is brighter when the histogram falls to the higher end. It can be varied by changing the image mean without changing histogram shape. Contrast can be determined from its dynamic range, defined as the difference between highest and lowest intensity level present in the image. Contrast enhancement stretches the histogram to perceive more details,

normally not visible. Images are to be sharp, clear and detailed to make it look better. This can be achieved by enhancing the edges of the image by making it appear sharper. Removing noise from the image also improves the visual quality of the image.

Image restoration is an area that also deals with improving the appearance of an image. However unlike enhancement, which is subjective, image restoration is objective, in the sense that restoration attempts to recover an image that has been degraded by using a priori knowledge about degradation process. It refers to removal or minimization of known degradations in an image.

Many image enhancement techniques have been proposed in the past and they fall into two broad categories : spatial domain and transform domain methods. *Spatial domain* techniques are procedures that operate directly on the pixels in an image while *transform domain* techniques modify the transform coefficients [34]. Transformation from spatial domain to frequency domain can often permit more useful visualization of the data. Some enhancement algorithms use both spatial and frequency domain techniques.

Different image enhancement techniques include *point operations*, *mask operations* and *global operations*. *Point operations* modify each pixel according to some equation that is not dependent on other pixel values and in *mask operations* each pixel is modified according to the values in a small neighbourhood. Here, image is divided into blocks and intensity transformation is applied on each block according to the mask. *Global operations* consider all the pixel values for intensity transformation and the visual quality of low contrast image can be improved globally. All the above techniques can be used for spatial domain methods. Mask operations and global operations are used for transform domain methods also.

1.4.1 Spatial and Transform based Image Enhancement

Majority of the existing techniques have focused on the enhancement of images in the spatial domain. Histogram processing is the most common and simple spatial domain image enhancement technique. It is usually done by way of histogram stretching, equalization or matching. Histogram equalization employs a monotonic, nonlinear mapping that re-assigns the intensity values of pixels in the input image and produces an image with uniform histogram. Histogram stretching spreads the histogram to a larger range by applying a piecewise linear function while histogram matching produces an image with prespecified histogram.

Filtering with spatial masks can be used to highlight fine details, sharpen edges and remove small details. Mean/average filters are used for blurring and noise reduction. Median filters are popular for removing salt-and-pepper noise. First and second order derivative based filters, Gradient and Laplacian, are used for edge extraction and sharpening.

In transform domain techniques, transform of the image is computed first. The transform coefficients are then manipulated appropriately and inverse transform is found to obtain the enhanced image [35, 36, 37, 38]. Converting an image into transform domain offers additional capabilities that are very powerful, but requires some new way to interpret data. Images are being represented in the compressed format [35] using image transforms for efficient storage and transmission. Hence, it has become imperative to investigate compressed domain enhancement techniques to eliminate the computational overheads. If all the image processing tasks are performed in the same transform domain, processing will be computationally efficient.

1.4.2 Linear and Nonlinear Image Enhancement

Linear techniques continue to play an important role in image enhancement because they are inherently simple to implement. Such techniques modify all pixels uniformly and the gray levels in the histogram get apart equally. Entire histogram range can be utilized for maximum contrast.

Recently, nonlinear image enhancement techniques have emerged as intensive research topics since HVS includes some nonlinear effects that need to be considered in order to develop effective image enhancement algorithms. Therefore nonlinear methods may be suitable to comply with the nonlinear characteristics of the HVS. Here, a nonlinear transformation relation exists between input and outputs.

Nonlinear image enhancement can be done in the transform domain using nonlinear mapping functions. Transform coefficients can be modified nonlinearly to compress/expand the bright/dark areas in images. Most popular transform based enhancement technique is alpha-rooting [39]. Other nonlinear mapping functions used for image processing applications are twicing function, programmable-S-function, function proposed by Lee etc. (Appendix B).

Another class of nonlinear image enhancement techniques that has obtained great popularity in the last two decades is fuzzy based techniques.

Fuzzy Image Enhancement

Fuzzy techniques are nonlinear and knowledge based. They can process imperfect data if this imperfection originates from vagueness and ambiguity rather than randomness. In the real world, almost everything is uncertain and therefore a fuzzy rule based system is expected to achieve better performance than a crisp rule

based system in dealing with fuzzy data.

An image 'x' of size $N_1 \times N_2$ with L gray levels, $r = 0, 1, 2, \cdots, L-1$, can be defined as an array of fuzzy singletons (fuzzy sets with only one supporting point) indicating the membership value of each pixel regarding some predefined image property viz. brightness, contrast, sharpness etc. [40].

$$x = \bigcup_{n_1=0}^{N_1-1} \bigcup_{n_2=0}^{N_2-1} (\mu/r)_{n_1,n_2}, \qquad \text{with} \quad \mu \in [0,1] \text{ for any } (n_1, n_2) \tag{1.10}$$

where $(\mu/r)_{n_1,n_2}$ is the membership function of the $(n_1, n_2)^{\text{th}}$ pixel with gray level r.

The purpose behind this approach is to model the gray level intensities of a digital image by single fuzzy set, describing the linguistic concept of *brightness levels*. If a gray level has a membership value less than 0.5 to the *brightness levels* set, it is more likely to be dark than bright and in the opposite case it is more likely to be bright than dark.

Fuzzy image enhancement consists of three steps: fuzzification $\boldsymbol{\phi}$, modification $\boldsymbol{\tau}$ on membership values and defuzzification $\boldsymbol{\psi}$. The important step of fuzzy image enhancement is the $\boldsymbol{\tau}$ where the membership values are modified using appropriate fuzzy techniques. The output y of the system for input x is given by the processing chain

$$y = \boldsymbol{\psi}(\boldsymbol{\tau}(\boldsymbol{\phi}(x))). \tag{1.11}$$

The main difference with other methodologies in image enhancement is that input data x (gray levels, transform coefficients etc.) will be processed in the *membership plane* where one can use the great diversity of fuzzy logic and fuzzy set theory to modify the membership values. The new membership values are re-transformed

to the gray level plane or transform plane to generate enhanced image.

Fuzzy tools used to adjust image contrast in the spatial domain are fuzzy minimization, equalization using fuzzy expected value, hyperbolization, λ-enhancement, rule based approach, fuzzy relations etc.[40]. Fuzzy minimization and fuzzy rule based techniques are used here for contrast enhancement in the transform domain.

Fuzziness Minimization Approach: This is probably the first approach to image enhancement and is also known in the literature as contrast intensification (INT) operator. The main idea is to minimize the amount of fuzziness. Contrast of the image can be increased by darkening the gray levels in the lower luminance range and brightening the ones in the upper luminance range using the nonlinear INT operator given by

$$\mathrm{INT}(\mu(x)) = \begin{cases} 2(\mu(x))^2, & 0 \leq \mu(x) \leq 0.5 \\ 1 - 2(1-\mu(x))^2, & 0.5 < \mu(x) \leq 1 \end{cases} \tag{1.12}$$

A plot of this function is shown in Appendix B.5.

Fuzzy Rule Based Approach: Fuzzy rules efficiently process data by mimicking human decision making. They typically include a group of antecedent clauses that define conditions and a consequent clause that defines the corresponding action. Thus a fuzzy rule based system is formed by a set of rules that represent the knowledge base of the system and an appropriate inference mechanism that numerically processes the knowledge base to yield the result.

A typical fuzzy rule based algorithm has the following steps [40]

- Initialization of the parameters of the system (number of input and output membership functions, their shapes, locations etc.)
- Fuzzification of gray levels
- Inference procedure evaluating appropriate rules
- Defuzzification of the outputs

Several variants of fuzzy systems are available; among them, the most widely used are the *Mamdani fuzzy inference systems* (characterized by the presence of fuzzy sets over the input and output data spaces) and the *Takagi-Sugeno fuzzy inference systems* (input data space is described by fuzzy sets, but the output data space is characterized by singleton sets). Of the two, Takagi-Sugeno fuzzy systems are appealing for their simple forms and simplicity in computational requirements.

1.4.3 Colour Image Enhancement

Colour is a sensation created in response to excitation of our visual system by light, which is an electromagnetic radiation. More specifically, colour is the perceptual result of light in the region of 400 nm to 700 nm visible region of electromagnetic spectrum. Colour can be specified by a tri-component vector and the set of all colours forms a vector space or colour space.

Humans interpret a colour, based on its intensity (I), hue (H) and saturation (S) [41]. Luminance (Y) is the radiant power weighted by a spectral sensitivity function that is a characteristic of human vision. Nonlinear perceptual response to luminance is called intensity. Hue is a colour attribute associated with the dominant wavelength in a mixture of light waves. Saturation refers to the relative purity or the amount of white light mixed with a hue. Hue and saturation together describe chrominance. The perception of colour

is basically determined by luminance and chrominance. Common colour spaces are RGB, HSI, YCbCr, CMYK etc.

1.4.4 Applications

Image enhancement has potential applications in many areas of science and engineering. A few areas are listed below.

Medical Image Enhancement

Medical imaging has been undergoing a revolution in the past two decades with the advent of faster, more accurate and less invasive devices. It helps doctors to see interior portions of the body for easy diagnosis. Medical images contain values that are proportional to the absorption characteristics of tissues. Accurate interpretation may become difficult when the distinction between normal and abnormal tissue is subtle. In such cases, enhancement improves the quality of the image and facilitates easy diagnosis.

Most important clinically established medical imaging modalities are X-ray radiography, Computed Tomography (CT), Ultrasound Scan, Magnetic Resonance Imaging (MRI), Single Photon Emission Computed Tomography (SPECT), Positron Emission Tomography (PET), Electrical Impedance Tomography (EIT) etc.

Fingerprint Enhancement

A fingerprint is a pattern of ridges and furrows on the surface of a fingertip. The fingerprint of an individual is unique and remains unchanged over a lifetime. The minutiae, which are the local discontinuities in the ridge flow pattern, provide the features that are used for identification. Details such as the type, orientation, and

location of minutiae are taken into account when performing minutiae extraction.

Fingerprint identification is one of the most important biometric technologies which has drawn a substantial amount of attention recently [42]. It is commonly employed in forensic science to support criminal investigations, biometric systems such as civilian and commercial identification devices etc. A critical step in automatic fingerprint matching is to automatically and reliably extract minutiae from input fingerprint images.

Fingerprint images are rarely of perfect quality. They may be degraded and corrupted with elements of noise due to many factors including variations in skin and impression conditions. This degradation can result in a significant number of spurious minutiae being created and genuine minutiae being ignored. However, the performance of a minutiae extraction algorithm relies heavily on the quality of the input fingerprint images. In order to ensure that the performance of an automatic fingerprint identification/verification system will be robust with respect to the quality of input fingerprint images, it is essential to incorporate a fingerprint enhancement algorithm in the minutiae extraction module as a preprocessing step.

The enhancement may be useful for the following cases

- Connect broken ridges (generally produced by dry fingerprint or cuts, creases, bruises)
- Eliminate noises between the ridges
- Improve the ridge contrast

Other areas where enhancement acts as a pivotal role are in image analysis of archaeological research, recovery of paintings, underwater study, remote sensing etc.

Image enhancement methods are used to make images look better. Enhancement technique suitable for one application may not

be suitable for other applications. Expertise and problem domain knowledge are required for the development of image enhancement methods. Success of image enhancement algorithm lies in the eyes of the beholder. Suitable enhancement metrics will also help in assessing the quality of enhancement.

1.5 Image Quality Metrics

Image enhancement is basically a preprocessing step that improves the quality of the image by controlling parameters such as brightness, contrast and sharpness. Even though a number of image enhancement techniques are available, development of an Image Quality Assessment (IQA) metric [43], suitable for all types of images, is still a challenging area and newer metrics are being thought of every day [44], [45]. IQA techniques can be categorized into subjective assessment, involving humans to evaluate the image quality, and objective assessment that measures the image quality automatically.

Objective quality criteria is used to ascertain the goodness of the image enhancement result quantitatively. The human observer, however, may not perceive these results as good because his judgment is subjective. This distinction between objectivity and subjectivity is the major problem in the human-machine interaction. Another difficulty is the fact that different people judge image quality differently and is primarily due to human subjectivity.

1.5.1 Subjective Assessment

Subjective IQA is a reliable method since human beings are the ultimate users in most image processing applications. Recommendations of the International Telecommunication Union (ITU) [46]

can be applied to compare the performance of different enhancement algorithms. The observer judges the image quality using a scale from 1 to 5 where 1 is *bad*, 2 *poor*, 3 *fair*, 4 *good* and 5 *excellent*. Finally, Mean Opinion Score (MOS) is calculated as the average of the opinion scores thus obtained.

But medical image enhancement applications, this method requires the service of experts and is a time-consuming process. Hence it is not suitable for real time applications. Also, for small changes in the image, this evaluation is difficult.

1.5.2 Objective Assessment

The goal of objective quality evaluation is to obtain a quantitative measure which gives the quality of the image in a manner consistent with human perception and subjective analysis should match with objective assessment values. According to the availability of a reference image, IQA metrics are classified as Full-Reference (FR), No or Blind-Reference (BR) and Reduced-Reference (RR) image quality metrics [43].

A distortionless reference image of perfect quality is used, in FR method, to evaluate the quality of the modified image. Typically, this comparison involves measuring the distance between the two signals in a perceptually meaningful manner. Such methods are excellent for assessing the transmission and compression noise, but may not work for enhancement, since good quality enhanced image is not known a priori.

In BR method, quality is assessed without using any reference image whereas in RR method, the reference image is not fully available and some features based on statistical or texture properties extracted are employed.

Many IQA metrics, both FR and BR, have been proposed over the

past few decades (Appendix C). Each one has its own advantages and disadvantages in terms of accuracy, computational speed and application considered.

The suitability of these metrics for measurement of image brightness, contrast and sharpness are not known. Hence, it is evident that an analysis of the existing metrics for IQA is very important and there is enough scope for developing better metrics suitable for enhancement in the pixel and transform domains.

1.6 Motivation

Medical image enhancement has been a key area of research nowadays. Author had a personal experience of a medical case where the patient had to wait for a day to undergo surgery in a very serious condition due to the lack of image clarity. So proper enhancement of medical images could save life in such situations. This is the first motivation for selecting medical image enhancement as the topic of research.

Often medical images suffer from different types of noises, artifacts and inhomogeneities due to diverse reasons and hinder the image understanding process. Discussions with doctors and medical technicians revealed that built-in enhancement techniques and proper initial settings of the machine can help in providing good images due to the advancement in technology. Radiologists are now facing great difficulty in proper interpretation of mammograms. Early detection of breast cancer is important and mammography is the primary imaging modality for detection and diagnosis of breast lesions; hence a decision was taken to carry out enhancement of mammogram images from the medical image category.

Images are usually represented in the transform domain in the compressed format for efficient storage and transmission. Also, most

of the image processing tasks such as segmentation, feature extraction etc. are carried out in the transform domain. If all the image processing tasks are performed in the same transform domain, processing will be computationally efficient and real time processing of images is possible.

An integer-to-integer transform entitled MRT was developed by the former researchers of the research group and it is modified to UMRT to remove redundancy. Such an arrangement of the unique coefficients causes distribution of different phase terms associated with a particular frequency. The visual representation of the unique MRT coefficients shows specific pattern of sign changes. Hence it is useful to explore this change of signs in deriving a placement of the unique MRT coefficients in an $N \times N$ matrix form with better computational benefits.

The conventional documentation system is now changing to electronic media. Digitization of old public records, such as documents, manuscripts, drawings, title deeds, office proceedings etc. that date decades back, is a real challenge to many organizations. The easiest way to digitize old documents is to scan or photograph and store. But scanning process often makes unwanted background noises, shades etc. and removal of such disturbances is very important. So there is a strong requirement that these documents are to be enhanced using simple enhancement techniques.

Evaluation of images after enhancement is very important to find the efficiency of the enhancement technique objectively. Many metrics are available for image quality assessment. But the literature shows that none of these assessment techniques are suitable for quantifying enhancement for different classes of images. So, an analysis of existing metrics to assess images after enhancement and an investigation for newer metrics are also issues of concern.

The above set of problems motivated the author to explore the possibilities of various techniques proposed in the present research

work.

1.7 Organization of Thesis

The thesis is organized in seven chapters as

Chapter 1 is an introduction to DIP techniques, image transforms, image enhancement and IQA metrics. Basic concepts of digital images, image processing for human vision and computer vision applications are discussed. A brief description about the need of image transforms and various image transforms in literature are explained. Purpose of enhancement, different techniques employed for enhancement of images are also covered. Subjective and objective IQA techniques, the metrics available in the literature etc. are discussed. The chapter ends by explaining the motivation behind the thesis and its organization.

Chapter 2 presents a literature survey on relevant topics connected with DIP, image enhancement, image transforms, IQA metrics. Various spatial and transform domain, linear and nonlinear, global and block processing image enhancement techniques are reviewed.

Chapter 3 focuses on the development of a computationally simple N x N transform called, SMRT for N a power of 2. Visual representation, sequencies of unique MRT coefficients, basis images, algorithms for forward and inverse SMRT are also explained. Mapping relations are derived to convert between MRT and SMRT. Direct mapping relation for sequency domain representation of $N \times N$ data for N a power of 2 is also developed. Properties of SMRT representation relevant to image processing applications, especially image enhancement, are explored.

Chapter 4 explains image enhancement quality metrics. Pixel based & SMRT based full-reference and blind-reference IQA are

developed. The methodology for analysis of these metrics for variations in brightness, contrast, sharpness and a combination of the three are explained. Simulation results, analysis and identification of useful metrics for the above variations are presented. Validation of the results is also carried out.

Chapter 5 concentrates on two global enhancement techniques in SMRT domain. These techniques employ linear and nonlinear scaling of the SMRT coefficients to adjust the contrast and brightness separately and are applied to general & mammogram images with relevant quantitative assessment and comparison with existing methods. Fingerprint and scanned text documents are also enhanced using linear scaling of SMRT coefficients. The enhancement of colour images is also considered.

Chapter 6 focuses on fuzzy image enhancement techniques using block level SMRT. Fuzzy intensification operator and fuzzy rule based techniques are used for enhancement. The algorithms are applied to general & mammogram images, assessed quantitatively and the results are compared. A new method that combines the linear and fuzzy rule based methods is also employed. Finally, MOSs of all proposed methods are provided for subjective evaluation and comparison.

Chapter 7 depicts the summary and conclusion of the research work. Important research contributions and scope for future work in this area are also presented.

Chapter 2

Literature Survey

2.1 Introduction

A literature survey on DIP, Image transforms, Image enhancement techniques and IQA metrics will be helpful in grasping the history and advancements in these areas.

2.2 Digital Image Processing

Digital image processing was first used in newspaper industry, when pictures were first sent by submarine cable between London and New York. Introduction of Bartlane cable picture transmission system in the early 1920s reduced the time required to transport a picture across the Atlantic from more than a week to less than three hours. Pictures were coded using specialized printing equipment for cable transmission and reconstructed them at the receiving end [34].

Some of the initial problems in improving the visual quality of early digital pictures were related to the selection of printing procedures and the distribution of intensity levels. The early Bartlane systems were capable of coding images in five distinct levels of gray. This capability was increased to 15 levels in 1929. Improvements in processing methods for transmitted digital pictures continued and it took the combined advents of large-scale digital computers and space program to bring into focus the potential of image processing concepts.

The history of DIP is intimately tied to the development of digital computers. In fact, digital images require so much storage and computational power that progress in the field of DIP has been dependent on the development of digital computers and of supporting technologies that include data storage, display etc. Work on using computer techniques for improving images from a space probe began at the Jet Propulsion Laboratory (Pasadena, California) in 1964 when pictures of the moon transmitted by Ranger 7 were processed by a computer to correct various types of image distortion inherent in the on-board television camera. From 1960s until the present, the field of image processing has grown vigorously.

2.3 Image Transforms

The pioneering work of Joseph Fourier in developing the theory of Fourier Series, in 1807, has opened a way to spectral analysis of signals. DFT and the introduction of an efficient FFT algorithm, for its computation, have given an advancement in the field of signal processing [47]. Later, many variations of FFT and its efficient parallel implementations were also developed.

In 1923, Joseph L. Walsh published a paper in which he described a complete system of orthogonal functions on the unit interval which

take on only two values +1 or -1. These functions, later known as Walsh functions [48], exhibited many properties that are comparable with complex exponentials associated with Fourier Series and Fourier Transforms. Since the introduction of FFT in 1967, much attention has been focussed on Walsh functions because of the increased processing speed associated with algorithms involving these functions. A similar orthogonal transform matrix containing ± 1, but with different order of sequency, is due to Hadamard [49], [50] and called Hadamard Transform or Walsh-Hadamard Transform. Another orthogonal transform, called Haar Transform, is derived from the Haar matrix [51], [52] whose elements are either -1, 0 or +1 multiplied by $\sqrt{2}$.

DCT, developed by Ahmed et al. [7], has found wide application in transform image coding. It is the foundation of the JPEG standard for still image coding and the MPEG standard for the coding of moving images.

DST was introduced by Jain [11] as a fast algorithmic substitute for the KL transform of a Markov process and has shown that cosine and sine transforms are interrelated in that they diagonalize a family of tridiagonal matrices.

Major advancement in the field of wavelet theory was attributed to Jean Morlet who developed and implemented the technique of scaling and shifting of the analysis window function in analysing acoustic echoes while working for an oil company in the mid 1970s [53]. Theoretical formation of the WT was first proposed only after Jean Morlet teamed up with Alex Grossmann to work out the idea that a signal could be transformed into the form of a wavelet and then transformed back into its original form without any information loss [54]. In 1987, wavelets were first shown to be the foundation of a powerful new approach to signal processing and analysis called multiresolution theory [55]. Heil & Walnut [56] described continuous and discrete wavelets, DeVore & Lucier [57] described wavelets from an approximation theory point of view, Rioul & Vetterli [58]

looked at wavelets from a signal point of view, Strichartz [59] focused on the construction of wavelets and Strang [60] compared wavelets with Fourier techniques.

Contourlet Transform is an efficient, directional, multiresolution image representation. It was developed by Do and Vetterli [61] in 2001 and later modified in [17], [62]. It is a true two-dimensional non-separable transform that can capture the intrinsic geometrical structure of an image. It has better performance in representing the salient features of the image such as edges, lines, curves and contours than wavelet transform because of its anisotropy and directionality property. It uses fewer coefficients than wavelet transform to represent smooth curves.

Gopikakumari, in [30], modified 2-D DFT computation through a new perspective that 2x2 DFT computation involves only real arithmetic and hence found a relationship between the elements of $N \times N$ DFT and the elements of the matrix made up of 2×2 submatrices of the $N \times N$ data matrix, for any even N. She also presented a visual representation of the 2-D DFT coefficients and evolved a parallel distributed architecture for the same. The architecture involves 4 layers of which all except the fourth layer involve only real additions. The model was implemented using four different kinds of parallelism depending upon the requirements of speed and complexity.

Rajesh et al. [31], [63] continued the work of Gopikakumari and developed a new transform, named MRT by eliminating the fourth layer of the parallel distributed architecture thereby converted into an integer-to-integer transform. MRT allows to do the frequency domain analysis of 2-D signals without any complex operations. The transform coefficients showed redundancies and Unique MRT was suggested to remove redundancies [32]. These coefficients are numerically compact, unique and require only the same memory space as required for the original image. He used unique MRT coefficients to effectively to compress images.

Bhadran et al., in [64], presented a new visualization technique for the computation of 2-D DFT in terms of 2 x 2 data and its analysis. Since the visual representation gave direct relationship between spatial domain data and the frequency domain representation in terms of pictures, signal analysis was made simple. Various types of redundancies present in the visual representation were explored.

Bhadran [33] presented computation of basic set of DFT coefficients and the corresponding indices. An algorithm was also developed to find out the basic set of 2-D DFT coefficients for any matrix size even. He proposed a new algorithm for the placement of Unique MRT coefficients called UMRT. The hardware implementation reported in [30] was modified to compute UMRT. Preetha et al. [65] developed a computationally fast algorithm to compute forward and inverse UMRT.

Meenakshy [66] showed how MRT can be used for obtaining a new set of features useful for texture analysis. Experiments performed on Brodatz texture images indicated that these features can be used for texture classification. She developed a computer aided design system to predict the fragmentation of renal stones based on texture analysis of CT images using MRT.

Anish et al. [67], [68] developed optimized quadtree partitioning of images and an adaptive block size transform coder for image compression using MRT.

The present work involves modification to the placement of unique coefficients in MRT computation by exploiting sequency information from the visual representation of the MRT coefficients and its application is being explored in image enhancement.

2.4 Image Enhancement

Many spatial-domain and transform-domain image enhancement techniques have been proposed in the literature.

2.4.1 Spatial-domain Techniques

Several preprocessing techniques for enhancing selected features and removing irrelevant data are described and compared by Hall et al. in [69]. These techniques included linearization of gray level distribution, digital spatial filtering, contrast enhancement and image subtraction.

Hummel [70] developed theory of histogram modification of continuous real-valued pictures. He has shown that the transformation of image histogram to a desired histogram is unique under the constraint that the transformation function be monotonically increasing.

Histogram Equalization is a very popular spatial-domain technique [34]. Improvement in contrast can be achieved by stretching the dynamic range of image histogram based on the probability distribution of the image gray levels. It is commonly employed because of its simplicity and comparatively better performance on almost all types of images.

Trahanias et al. [71], proposed a method to extend HE for gray level image enhancement to colour images. A method of direct 3-D HE resulted in a uniform histogram of the RGB values.

Despite its popularity, HE is not always very suitable for consumer electronics applications because of the undesirable artifacts. It changes the mean brightness of the input image significantly and makes some of the uniform regions of the output image saturated with very bright or dark intensities.

Adaptive Histogram Equalization (AHE) has been recognized as a good method of contrast enhancement in block level image processing. The main advantage of AHE was that it can provide better contrast in local areas due to the block processing whereas traditional HE method uses entire image at once.

Sherrier & Johnson [72] calculated histograms locally and then modified according to both the mean pixel value of that region as well as certain characteristics of the cumulative distribution function. This method suffered from over-enhancement of noise in relatively homogeneous regions and reduced speed.

Pizer & Amburn [73] proposed modifications to AHE to reduce the above limitations. They used three approaches: interpolated AHE to increase the speed of computation, weighted AHE to improve the quality and clipped AHE to overcome over-enhancement.

T.L. Ji et al. [74] presented a novel adaptive algorithm that tailored the required amount of contrast enhancement based on the local contrast of the image and the observers Just Noticeable Difference (JND). This algorithm always produced adequate contrast in the output image and resulted in almost no ringing artifacts even around sharp transition regions. Limitation of this method was that it does not take the mean brightness of an image into account.

Many variations of HE have been developed to preserve the mean brightness of the image for consumer electronics applications. The fundamental enhancement needed in most of the images is an increase in contrast. Some of the HE techniques developed to preserve the mean brightness are Brightness preserving Bi-Histogram Equalization (BBHE) [75], Multi-Peak HE with Brightness Preserving (MPHEBP) [76], Dualistic Sub-Image Histogram Equalization (DSIHE) [77], Recursive Mean-Separate HE (RMSHE) [78] [79], Minimum Mean Brightness Error Bi-Histogram Equalization (MMBEBHE) [80], Recursive Sub-Image Histogram Equalization (RSIHE) [81], Dynamic Histogram Equalization (DHE) [82], Bright-

ness Preserving Dynamic Histogram Equalization (BPDHE) [83], Recursively Separated and Weighted HE (RSWHE) [84], Image Dependent Brightness Preserving Histogram Equalization(IDBPHE) [85], Brightness Preserving Weight Clustering Histogram Equalization (BPWCHE) [86], Histogram Modified Contrast Limited Adaptive Histogram Equalization (HM-CLAHE) [87] etc.

Debashis and Sankar [88] proposed automatic exact histogram specification for contrast enhancement. The desired histogram was obtained by subjecting the image histogram to a modification process that increases the overall discriminability among samples in the histogram and then maximizing a measure that represents increase in information entropy and decrease in average image ambiguity.

A fuzzy version of BPDHE was introduced by Sarrafzadeh et al. [89] to improve the crispness of the interval and the number of pixels in that interval. This algorithm solved problems associated with BPDHE such as the contouring effect and the loss of information in regions of detail information.

Filtering is an essential part of image contrast enhancement. The process consists of moving a filter mask from point to point in an image. At each point, the response to the filter at that point is calculated using a predefined relationship. Several filtering techniques have been reported over the years for various applications. In image processing problems, non-linear filtering techniques are preferred as they can cope with the non-linearities of the image formation model and also take into account the non-linear nature of the HVS. Thus, the filters having good edge and image detail preservation properties are highly desirable for image filtering. Several filtering approaches were already analyzed by many of the researchers which include Harmonic Mean Filter, Geometric Mean Filter, Max Filter, Contra Harmonic Filter, High Boost Filter, Average Filter, Standard Deviation filter, Trace Median Filter, Variance Filter, Correlation Filter, Midpoint Filter and Unsharp Filter under the categories of Low pass Filter, High Pass Filter and Image Scaling Filters [34].

These filters are more suitable to remove artificial noises like salt & pepper noise and Gaussian noises.

Thangavel et al. in [90] had proposed a filtering scheme based on statistical methods for the removal of speckle noise which is commonly found in the ultrasound medical images.

Unsharp Masking (UM) is a very common technique for contrast enhancement of digital images. Even though the Classic Linear Unsharp Masking (CLUM) technique [34] is simple and works well in many applications, it suffers from two drawbacks. i) The presence of the linear highpass filter makes the system extremely sensitive to noise. ii) It enhances high-contrast areas much more than the areas with low and medium contrast levels. Eventually, the resulting image observed is extremely artificial.

Various approaches based on the use of nonlinear operators had been suggested for reducing the noise sensitivity of the linear UM technique. A local mean-weighted adaptive high pass filter was proposed by Mitra & Li, in [91]. This method enhanced the details of the image uniformly, but simultaneously enhanced the noise. Consequently, the perceived noise in the output image was smaller than that for linear UM schemes, but the visual appearance was not good.

Polesel et al. [92] presented a new method for UM for contrast enhancement of images. The approach employed an adaptive filter that controlled the contribution of the sharpening path in such a way that contrast enhancement occurs in high detail areas and little or no image sharpening occurs in smooth areas.

In [93] Panetta et al. introduced nonlinear UM (NLUM) for mammogram enhancement. It offered flexibility 1) to embed different types of filters into the nonlinear filtering operator; 2) to choose different linear or non-linear operations for the fusion processes that combines the enhanced filtered portion of the mammogram with the original mammogram and 3) to allow the NLUM parameter

selection to be performed manually or by using a quantitative enhancement measure to obtain the optimal enhancement parameters.

Xiurong [94] developed an adaptive unsharp mask algorithm for contrast enhancement of medical images. The objective of the adaptive filter was to emphasize the medium-contrast details in the input image more than large-contrast details such as abrupt edges so as to avoid overshoot effects in the output image. The objective was that it controls the contribution of the sharpening path in such a way that contrast enhancement occurs in high detail areas and little or no image sharpening occurs in smooth areas.

Fuzzy techniques were now used widely for image enhancement. The theory of fuzzy set was first introduced by Zadeh [95]. Fuzzy set theory is a useful tool for handling uncertainty associated with vagueness and imprecision and has been successfully applied to image processing and pattern recognition areas. Image processing bears some fuzziness in nature due to the following factors: (a)information loss while mapping 3-D objects into 2-D images; (b)ambiguity and vagueness in definitions such as edges, boundaries, regions, features etc. and (c)fuzzy nature of contrast in an image. It has been widely applied to nonlinear signal processing to handle inherent fuzziness in tasks such as image enhancement.

Pal and King [96] adopted a fuzzy contrast intensification operator to modify the membership function, achieving an efficient enhancement result. In [97], they used smoothing method with fuzzy set to enhance images. They applied contrast intensification operations on pixels to modify their membership values. Both of the above methods are indirect contrast enhancement approaches.

Li and Yang [98] suggested an image enhancement approach, based on a fuzzy relaxation algorithm in which different orders of fuzzy membership functions and different statistics were used to improve the enhancement speed and quality respectively. In the image enhancement process using a fuzzy relaxation algorithm, pixel values

will change through iterations. If the algorithm is convergent, the pixel values will approach to some predefined constant after a certain number of iterations. But through a mathematical analysis it was found that the convergence cannot be guaranteed.

To solve the convergent problem, Zhou and Can suggested a method [99] for choosing appropriate values of the parameters in the transformation function to guarantee the expected convergence property for image enhancement. As another way of resolving the problem, they [100] have developed a new fuzzy relaxation algorithm with good convergence.

Chen and Xu [101] used fuzzy entropy principle and fuzzy set theory to map an image from space domain to fuzzy domain by a membership function, and then applied adaptive, direct, fuzzy contrast enhancement algorithm to enhance contrast.

Hasikin & Isa, in [102], proposed a fuzzy grayscale enhancement technique for low contrast image. This technique was proposed by maximizing fuzzy measures contained in the image. The membership function was then modified to enhance the image by using power-law transformation and saturation operator.

Chaira, in [103], presented a novel medical image enhancement using intuitionistic fuzzy set theory. An intuitionistic fuzzy set takes into account more (two) uncertainties as compared to fuzzy set that considers only one uncertainty in the form of membership function.

2.4.2 Transform-domain Techniques

Transform domain techniques consist of transforming images into frequency domain, modifying the coefficients and transforming back to the spatial domain representation. Some of the commonly used transforms for image enhancement are Discrete Cosine Transform, Wavelet Transform, Contourlet Transform etc.

One of the earliest transform domain techniques is alpha-rooting method [104], [105], [106] where the magnitude of DFT coefficients of the original image is raised to a power alpha, while the phase part is kept unchanged.

However, this method suffered from two drawbacks. The amplification went to infinity as the value of transform coefficients approaches zero resulting in increased low-level noise energy. The second problem was the artifacts that are correlated with certain edges in the image resulted in many spurious edges.

A simple mapping function that removes the problems associated with alpha-rooting was the twicing function [39]. Higher degree polynomial mapping, obtained by recursive usage of twicing function, can be used for getting increased amplification ratio for lower magnitudes. This function was later modified by Amore et al. [107] by introducing a parameter, β. The output showed an emphasis on the high-frequency content of the image without changing the phase of the transform coefficients, resulting in an overall contrast enhancement. This enhancement, however, can sometimes result in overall graying, tonal changes and ugly artifacts.

A simple, easily manoeuvarable, flexible, programmable-S-function was proposed by De [108] taking into account the perceptual processing capabilities of HVS. Threshold points and slope can be adjusted properly for stretching and compressing transform coefficients by varying the values of p_1, p_2, m and n. The function expands both low and high amplitude coefficients while compresses mid values. A similarly varying function with one parameter, γ, was proposed by Lee [109] .

Homomorphic Filtering is sometimes used for image enhancement [34]. It simultaneously normalizes the brightness across an image and increases the contrast. Homomorphic Filtering is usually used to remove multiplicative noise. Illumination and reflectance are not separable, but their approximate locations in the frequency domain

may be found. Since illumination and reflectance are combined multiplicatively, the components are made additive by taking the logarithm of the image intensity, so that these combine linearly in the frequency domain. Illumination variations can be thought of as a multiplicative noise, and can be reduced by filtering in the logarithmic domain.

Tang [110] proposed a method where the image is filtered by manipulating DCT coefficients according to a contrast measure. Mukherjee & Mitra, in [111], proposed enhancement in the block DCT domain. Local background illumination was adjusted by modifying DC coefficient of each block using twicing function. He preserved local contrast by multiplying block DCT by a constant.

Retinex theory was first proposed by Edwin Land in 1963. He presented the Retinex theory for colour vision in [112]. According to him, image is composed of two parts namely the incident light and the reflectance of the object. Retinex theory intends to explain how the HVS extracts reliable information from the world despite of changes of illumination. The algorithm based on Retinex theory can improve colour constancy, compress dynamic range and enhance contrast and it is used widely in recent years. Lee, in [109], suggested a method for dynamic range compression and contrast enhancement using retinex theory.

Multi Scale Retinex algorithm (MSR) by Jobson et al. [113] is based on their previous work on Single Scale Retinex (SSR) [114]. The SSR algorithm is a simple implementation of the Retinex that was developed especially for more practical image processing. Their work was inspired by Land's most recent version of the Retinex where he described a centre/surround operator to replace the random walk computation. This operator is similar to the difference of Gaussian function which is commonly used in natural vision science to model perceptual processes. Thus, as Land used a $1/r^2$ function for the operator, Jobson et al. used a Gaussian surround. They noticed that the method will produce better results by using three

scales for the Gaussian function.

The Retinex processing still had problems with images having regional and global gray-world violations, i.e., spatially averaged relative spectral reflectance is not equal in three colour spectral bands of the image. This was a consequence of processing an image by each channel independently and was shown as desaturation in the image.

Nielsen [115] presented an overview of time-frequency analysis and introduced wavelet & wavelet packets. There are many image enhancement methods based on wavelet transform. Lu et al. [116] presented a simple and effective method for image contrast enhancement based on the multi-scale edge representation of images using wavelets. The contrast of an image can be enhanced simply by stretching or upscaling the multi-scale gradient maxima of the image. This method offered flexibility to selectively enhance features of different sizes and ability to control noise magnification.

Yang and Hansell, in [117], presented a novel approach to the enhancement of feature differences between normal and diseased lung parenchyma so that reliable visual assessment can be made. The method relied on a hybrid structural filtering technique which removes pulmonary vessels appearing in the CT cross-sectional images without affecting intrinsic subtle intensity details of the lung parenchyma. In order to restore possible structural distortions introduced by the hybrid filter, a feature localization process based on wavelet reconstruction of feature extrema was used. After contrast enhancement, the resultant images were used to delineate region borders of the diseased areas and quantification was made with regard to the extent of the disease.

Fang and Qi [118] introduced a wavelet based method of image enhancement using soft threshold. The Discrete Wavelet Transform (DWT) decomposed an image into a set of different scale smaller images. Then detail coefficients were modified based on the soft-

thresholding filter, prior to obtaining the inverse transform. The results indicate that the method can effectively enhance image details, preserve image edges and improve the visual quality of image.

In contourlet transform, the Laplacian pyramid [119] was first used to capture the point discontinuities; it was then followed by a directional filter bank [120] to link point discontinuities into linear structures. The overall result was an image expansion using elementary images like contour segments, called contourlet transform, which was implemented by a pyramidal directional filter bank [61]. The Laplacian Pyramid (LP) was used to decompose an image into a number of radial subbands, and the directional filter banks (DFB) decompose each LP detail sub-band into a number of directional subbands.

Sung Kon et al. [121] proposed a new algorithm for image enhancement including highpass filtering, lowpass filtering and edge enhancement in the block DCT domain. They proposed the blocking artifacts reduction technique as well as the optimal image enhancement technique using both frequency filtering and spatial filtering method.

A new method for contrast enhancement based on the curvelet transform was presented in [122]. The curvelet transform represents edges better than wavelets, and is therefore well-suited for multiscale edge enhancement. The authors compared this approach with enhancement based on the wavelet transform, and the MSR. The findings were that curvelet based enhancement out-performed other enhancement methods on noisy images, but on noiseless or near noiseless images, curvelet based enhancement was not better than wavelet based enhancement.

Nezhadarya & Shamsollahi, in [123], proposed a new simple enhancement function and applied to coefficients in contourlet space. The directionality capability of this transform, resulted in better edge representation and enhancement in 2-D images. Aiping Jiang

et.al., in their paper [124], used contourlet transform for medical image denoising and enhancement.

Fuzzy techniques were also used in the transform domain for image enhancement. They have been applied for medical image processing since main challenge of medical image enhancement is to solve conflicts between noise resistance and detail sharpening. A multiscale enhancement method based on fuzzy logic (MEMBFL) was presented by Ping, in [125]. The proposed method prevented noise increasing during the sharpening of the image details. With this method, the original image was filtered by the hybrid low pass filter which was designed according to local context of the image in order to remove the impulse noise and no-impulse noise. Then the filtered image was decomposed into several band pass images. Each pixel in band pass image was adaptively assigned a different enhancement factor by evaluating the local feature. The processed band pass images can be composed into an enhanced image by the process opposite to the decomposition process.

Popa et al. [126] developed fuzzy image enhancement in the compressed domain, without full decompression. They [127] proposed fuzzy rule based algorithm in the compressed JPEG images and used threshold comparison in the block level to determine whether the fuzzy enhancement is to be carried out in compressed domain or decompressed domain. They, in [128], proposed a similar algorithm based on fuzzy contrast intensification operator.

An infrared image enhancement algorithm based on Non-Subsampled Contourlet Transform(NSCT) and adaptive threshold is proposed by Hong et al. [129]. At first, coefficients in different scales and different directions were obtained by image decomposition using the non-subsampled contourlet transform. Then, filter thresholds and enhancement functions were adaptively estimated according to the transform coefficients. Finally, image enhancement was implemented by reconstruction of these enhanced coefficients.

Hema and Bhavani [130] proposed a method to make the super- resolution of a high-resolution image from a sequence of low-resolution frames containing non-stationary objects. Mussarat Yasmin et al. [131] provided a short overview of different methods presented in the prospect of brain image enhancement.

Hasikin & Isa [132] developed fuzzy image enhancement for low contrast and non-uniform illumination images. A new fuzzy intensity measure was proposed to distinguish between the dark and bright regions. This measure was computed by considering the average intensity and deviation of the intensity distribution of the image. The input image was enhanced using a power-law transformation.

Leijun & Ting, in [133], proposed a modified fuzzy-shrink image enhancement algorithm in the NSCT domain and fuzzy domain. The algorithm had optimal denoising effect and the processed image was close to the original image on visual effects.

Evaluation of images after enhancement is important for assessing the quality of the image enhancement technique objectively. A literature survey of the IQA metrics will help in identifying suitable metrics for enhancement applications.

2.5 Image Quality Metrics

Evaluating the image perceptual quality is a fundamental problem in image processing and various metrics had been proposed for IQA. They can be used as a feedback tool, to monitor visual quality, to optimize parameters, algorithms etc. or to benchmark image processing applications.

Natural way to measure image quality is to solicit human opinion and is known as subjective quality assessment method. Standardized procedures for subjective IQA are described in the ITU Rec-

ommendation [46] and MOS is regarded as the best method. Here, the perception of quality is influenced by many factors such as context, lighting, degree of interaction, psychological factors etc. Such evaluations are time-consuming, cumbersome, expensive to conduct and not feasible in most practical applications. Thus there is a need to develop efficient objective IQA methods. Most of the objective methods for IQA [43] can be defined as either FR, BR or RR as discussed in section 1.5.

2.5.1 Full-Reference Metrics

There are basically two classes of FR IQA metrics, conventional IQA and HVS based IQA.

A simple and widely used conventional FR fidelity measure is the Peak Signal-to-Noise Ratio (PSNR), or the corresponding distortion metric, the Mean-Squared Error (MSE) [134] that directly measures the pixel-by-pixel differences between the images. Other conventional metrics are Mean Absolute Error (MAE) [135], a simple measure of average error; Absolute Mean Brightness Error (AMBE) [136], used to preserve image brightness and gives absolute value of the difference in mean of the enhanced image and the reference image; Signal-to-Noise Ratio (SNR) [137], [138], ratio of the average signal power to average noise power and Contrast-to-Noise Ratio (CNR) [139], ratio of signal intensity differences between two regions scaled to image noise. These are attractive metrics due to their simplicity, physical significance and mathematical convenience to measure the loss of image quality, but not well matched to perceive visual quality.

Recently, a great deal of efforts has been made for development of IQA metrics that take advantage of the known characteristics of HVS. Aim of the HVS-based IQA is to evaluate how strong the distorted information is perceived by HVS, according to characteristics

and cognitive mechanism of the HVS. A number of IQA metrics, based on HVS, has been proposed to evaluate the perceptual quality. Weighted Signal-to-Noise ratio (WSNR) [140] was defined in the same way as SNR and is the ratio of average weighted signal power to average weighted noise power, where the weights are derived from the Contrast Sensitivity Function (CSF). Distortion Measure (DM) and Noise Quality Measure (NQM) [141] are used to quantify the impact of frequency distortion and noise injection on the HVS.

Wang & Bovik, in [142], proposed Universal Quality Index (UQI) approach that does not depend on the images being tested, the viewing conditions or the individual observers and can successfully measure image similarity across distortion types.

Natural image signals are highly structured exhibiting strong dependencies between spatially proximate pixels. They carry important information about the structure of the objects in the visual scene. HVS is highly adapted to extraction of structural information from the visual field. Consequently a measure of the loss of structural information can also be regarded as a good measure of the perceived distortion. Wang et.al.[143] introduced SSIM (Structural SIMilarity), an image quality assessment method based on a structural similarity (SSIM) index. It computed mean, variance and covariance of small patches inside a frame and combined the measurements into a distortion map. Mean SSIM (MSSIM) index, extracted structural information from an image and can provide a good approximation of perceived image quality.

Sheikh et al.[144] introduced information theory into image fidelity measurement and proposed a visual Information Fidelity Criterion (IFC) for IQA by using natural scene statistics models. Later, he extended IFC to Visual Information Fidelity (VIF) [145] that quantifies Shannon information shared between distorted image and the modified image. Visual Information Fidelity in Pixel domain (VIFP) was derived from a quantification of two mutual information

quantities: the mutual information between input and output of the HVS channel when no distortion is present and the mutual information between input of the distortion channel and output of the HVS channel for the test image [146].

Chandler, in [147], proposed a wavelet-based Visual Signal-to-Noise Ratio (VSNR) which operates by using both low-level and mid-level properties of HVS and quantifies the visual fidelity of enhanced images based on psychophysical findings. A Feature SIMilarity metric (FSIM) by Zhang[148] , based on Riesz-transform (RFSIM), can extract low level image features efficiently. Feature SIMilarity (FSIM) metric index proposed by Zhang [149] employed two features to compute the local similarity map, the phase congruency and the gradient magnitude. They played complementary roles in characterizing the image local quality.

2.5.2 Blind-Reference Metrics

There are other applications where a reference image is not available, but quality assessment is desirable. Conversely, the BR methods provide an estimate of quality without any knowledge of the original reference image.

A number of BR metrics are available in literature and a few that are used frequently are mentioned here. EME (measure of enhancement) and EMEE (measure of enhancement by entropy) have been developed by Agaian et al. [150],[151],[152]. These metrics were improved as AME and AMEE, based on Michelson contrast law [153]. Later, Panetta et al. developed logAME and logAMEE [154] for better assessment of images and introduced a Second Derivative like MEasurement (SDME) [2], [93]. This measure is shown to have better performance than other measures in evaluating the image visual quality. All these metrics divide an image into blocks and calculate the average value of the measured results of all blocks.

2.5.3 Statistical Feature Metrics

A feature is a characteristic that can capture visual properties of an image either globally for the entire image or locally for regions. Visual characteristics of homogeneous regions of real-world images are often identified as texture. Since an image is made up of pixels, texture can be defined as an entity consisting of mutually related pixels or group of pixels and thus leading to visual quality of images.

An image can be described by means of first order statistics of gray values of the pixels inside a neighbourhood. Examples of such features extracted from the image histogram are mean, standard deviation (SD), entropy etc.

Statistical and texture properties can be utilized for measuring image quality. Haralick, in [155], investigated the importance of statistical & structural approaches for micro & macro textures and proposed second order features based on Gray Level Co-occurrence Matrix (GLCM). He also defined a set of 14 measures of texture features that are useful in texture recognition and classification. Some of the second order statistical features are entropy, contrast, homogeneity, energy and correlation of the gray level pixels [156].

Entropy is used to measure the content of an image, with higher value indicating richness of details. Contrast returns a measure of the intensity difference between a pixel and its neighbour over the whole image. Homogeneity measures the similarity of gray-scale levels across the image. Thus, larger the changes in the gray-scale, the higher the GLCM contrast and lower the homogeneity. GLCM energy measures the overall probability of having distinctive gray-scale patterns in image. Correlation returns a measure of how correlated a pixel is to its neighbour over the whole image and it measures the joint probability of occurrence of the specified pixel pairs.

From the literature surveyed, it is observed that enhancement us-

ing transform domain techniques were not explored much and the potential of transform domain fuzzy techniques in image enhancement has not been exploited much. As a result, transform based enhancement techniques are given emphasis in this work.

Chapter 3

Sequency Based MRT

3.1 Introduction

Feasibility of transform based image processing techniques is investigated nowadays with the advent of newer and efficient transforms. Processing with the transform of an image, instead of the image itself, may give more insight into properties of the image. Transform domain representation can be used for efficient storage and transmission by making use of its sparsity and energy compaction property. It can efficiently capture the spatial variations such as smooth, moderate, sharp etc. and these variations are appropriately refined or polished in transform based image processing.

Visual representation of unique MRT coefficients for $N \times N$ data is explored to develop a new transform named Sequency based MRT (SMRT) and its inverse when N is a power of 2. The coefficients are arranged in the order of sequencies along row, column and diagonal directions. The basis functions of SMRT are developed and the algorithms to find forward and inverse SMRT through MRT computation are presented. Direct computation of SMRT, its properties

and applications are also examined.

3.2 Development of 2-D SMRT from MRT

Proper arrangement of the N^2 unique MRT coefficients in an $N \times N$ matrix is very important for the development of MRT as an efficient transform. The relationship between the unique MRT coefficients and the data can be represented visually using '+' symbol to indicate addition of data at that position, '−' symbol for subtraction and blank to indicate no involvement of data. A thorough investigation of visual representation of unique MRT coefficients will be helpful in proper placement of coefficients.

3.2.1 Visual Representation

Visual representation (VR) of the MRT coefficients were derived in terms of 2×2 DFT in [30], 2×2 data in [33] and each data in [32]. VR of UMRT coefficients in terms of each data, represented as '+', '−' or blank for $N = 4$ was presented in [65]. A similar VR of UMRT coefficients for $N = 8$ is shown in Fig. 3.1. The '+', '−' and blank symbols in the VR indicate that the data in the respective position is to be added, subtracted and masked/ignored to get the corresponding UMRT coefficient. The digits in the number below the VR of each $Y^{(p)}_{k_1,k_2}$, in Fig. 3.1, represent k_1, k_2 and p values respectively.

Analysis of visual patterns of unique MRT coefficients in Fig. 3.1 shows that the orientation in which data elements are combined and the number of data elements involved in the computation of each of these coefficients are different. Computation of $Y^{(0)}_{0,0}, Y^{(0)}_{0,4}, Y^{(0)}_{4,0}, Y^{(0)}_{4,4}$ involves all data elements and are placed in the first and fifth positions of the first and fifth rows respectively of the UMRT ma-

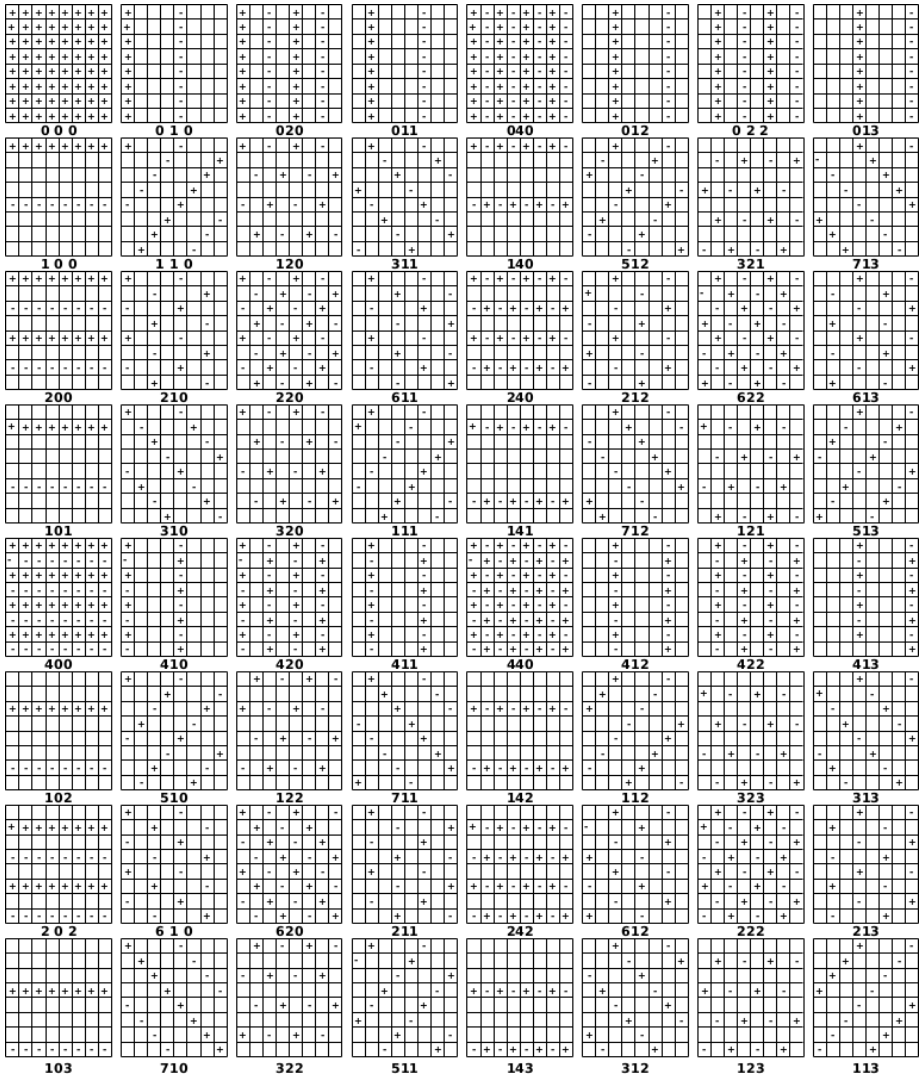

Fig. 3.1: Visual representation of UMRT for N=8 (Each box of +, − and blank symbols represent VR of a particular $Y^{(p)}_{k_1,k_2}$ with the digits below the box representing k_1, k_2, p respectively).

trix. $Y^{(0)}_{0,0}$ adds all data elements. $Y^{(0)}_{0,4}$, $Y^{(0)}_{4,0}$ and $Y^{(0)}_{4,4}$ combine

data elements along column, row and diagonal directions. $Y_{0,1}^{(p)}$ consider column-wise data separated by 4 and the columns get shifted by one, as the value of p increases. $Y_{0,2}^{(p)}$ deal column-wise data separated by 2. In UMRT, these coefficients are placed in the first row in the order $Y_{0,0}^{(0)}, Y_{0,1}^{(0)}, Y_{0,2}^{(0)}, Y_{0,1}^{(1)}, Y_{0,4}^{(0)}, Y_{0,1}^{(2)}, Y_{0,2}^{(2)}, Y_{0,1}^{(3)}$. Similarly, $Y_{1,0}^{(p)}, Y_{2,0}^{(p)}$ and $Y_{4,0}^{(p)}$ for different p's deal data elements row-wise and in UMRT, these occupy remaining positions of first column [33]. Similarly all other UMRT coefficients, $Y_{k_1,k_2}^{(p)}$ are placed as in Fig. 3.1.

Visual patterns of each coefficient show that the number of '+' and '−' symbol pairs are constant for each row and column. Hence, a parameter called sequency, c, can be defined in terms of the number of '+' and '−' symbol pairs present in one spatial direction. This is analogous to frequency in Fourier representation. Various visual patterns and the corresponding sequencies in one spatial direction can be illustrated with the help of Fig. 3.2. Here, the number of '+' and '−' symbol pairs is 1 for Fig. 3.2 (a) & (b), 2 for (c) and 4 for (d).

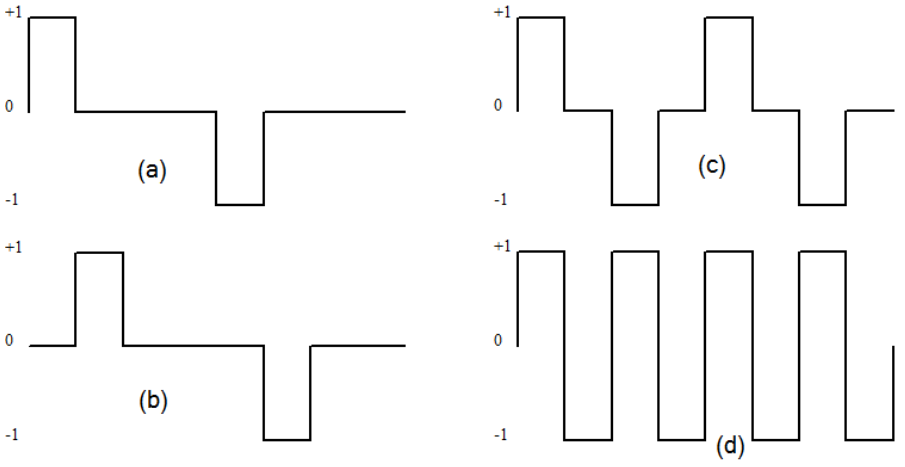

Fig. 3.2: Sequencies for N=8 (a),(b) c=1 (c) c=2 (d) c=4

Table 3.1 lists the unique MRT coefficients and the corresponding sequencies for $N = 8$. Let (c_1, c_2) denote the row-wise and column-wise sequencies of the unique MRT coefficients. Row-wise and column-wise sequencies for $Y_{0,0}^{(p)}$ are $(c_1, c_2) = (0,0)$. The sequencies of $Y_{0,1}^{(p)}, Y_{0,2}^{(p)}, Y_{0,4}^{(p)}$ are (0,1), (0,2), (0,4) respectively. The frequency indices k_1, k_2 of $Y_{0,1}^{(p)}$, $Y_{0,2}^{(p)}$ and $Y_{0,4}^{(p)}$ are related to $Y_{1,0}^{(p)}, Y_{2,0}^{(p)}$ and $Y_{4,0}^{(p)}$ as interchange of k_1 and k_2 and similar interchange is present in sequencies also. The sequencies of coefficients $[Y_{1,1}^{(p)}, Y_{3,1}^{(p)}, Y_{5,1}^{(p)}, Y_{7,1}^{(p)}]$, $[Y_{1,2}^{(p)}, Y_{3,2}^{(p)}]$ and $Y_{1,4}^{(p)}$ are (1,1), (1,2) and (1,4). Similarly, the groups $[Y_{2,1}^{(p)}, Y_{6,1}^{(p)}]$, $[Y_{2,2}^{(p)}, Y_{6,2}^{(p)}], Y_{2,4}^{(p)}$ have sequencies (2,1), (2,2), (2,4) respectively as in Table 3.1. Also, $Y_{4,1}^{(p)}, Y_{4,2}^{(p)}, Y_{4,4}^{(p)}$ have sequencies (4,1), (4,2), (4,4) respectively.

A similar analysis performed on the VR of the unique MRT coefficients for higher values of N that are power of 2 shows that the sequencies along column, row and diagonal directions vary as $0, 2^0, 2^1, 2^2, ..., M$. The UMRT placement has no sequency ordering and an arrangement of the unique MRT coefficients according to sequency is an option for placement. Thus the unique MRT coefficients corresponding to $N = 8$ can be rearranged in the increasing order of sequency along row, coloum and diagonal directions. A new sequency ordered placement, for N a power of 2, can be considered where the unique MRT coefficients are arranged in the order of sequencies.

3.2.2 Sequency-Ordered Placement

Unique MRT coefficients can be grouped, based on row-column sequencies, into groups (i, j), where 'i' and 'j' indicate row and column-wise groupings.

Placement of the 64 unique MRT coefficients corresponding to N=8 is discussed below. Coefficient having zero sequency in both direc-

Table 3.1: Sequencies of unique MRT coefficients

unique MRT coefficients	Sequency	
	row-wise (c_1)	column-wise (c_2)
$Y_{0,0}^{(p)},\ (p=0)$	0	0
$Y_{0,1}^{(p)},\ (p=0,1,2,3)$	0	1
$Y_{0,2}^{(p)},\ (p=0,2)$	0	2
$Y_{0,4}^{(p)},\ (p=0)$	0	4
$Y_{1,0}^{(p)},\ (p=0,1,2,3)$	1	0
$Y_{2,0}^{(p)},\ (p=0,2)$	2	0
$Y_{4,0}^{(p)},\ (p=0)$	4	0
$Y_{1,1}^{(p)}, Y_{3,1}^{(p)}, Y_{5,1}^{(p)}, Y_{7,1}^{(p)},\ (p=0,1,2,3)$	1	1
$Y_{1,2}^{(p)}, Y_{3,2}^{(p)},\ (p=0,1,2,3)$	1	2
$Y_{1,4}^{(p)},\ (p=0,1,2,3)$	1	4
$Y_{2,1}^{(p)}, Y_{6,1}^{(p)},\ (p=0,1,2,3)$	2	1
$Y_{2,2}^{(p)}, Y_{6,2}^{(p)},\ (p=0,2)$	2	2
$Y_{2,4}^{(p)},\ (p=0,2)$	2	4
$Y_{4,1}^{(p)},\ (p=0,1,2,3)$	4	1
$Y_{4,2}^{(p)},\ (p=0,2)$	4	2
$Y_{4,4}^{(p)},\ (p=0)$	4	4

tion, $Y_{0,0}^{(0)}$, is grouped as $(0,0)$. Its value is computed using Eq. (1.7) and is placed at the first position, $S(0,0)$, of the 8×8 SMRT matrix. Unique MRT coefficients with k_1 being zero is grouped into $(0,1),(0,2),(0,3)$ having column-sequencies $2^0, 2^1, 2^2$ respectively. Sequencies of $Y_{0,1}^{(p)}$ are (0,1) and the coefficients for various p's are sequentially arranged in the first row of SMRT matrix, starting from S(0,1). The sequencies of $Y_{0,2}^{(p)}$, $Y_{0,4}^{(p)}$ are respectively (0,2) & (0,4) and are arranged sequentially in the first row, in continuation to $Y_{0,1}^{(p)}$, in the order of sequency. Similarly $Y_{1,0}^{(p)}$, $Y_{2,0}^{(p)}$, $Y_{4,0}^{(p)}$, whose $k_2 = 0$ are placed in the first column of SMRT, in the increasing

order of p.

The row and column sequencies, (c_1, c_2), of $Y^{(p)}_{k_1,1}$, $k_1 = 1, 3, 5, 7$ are (1,1). The group index (i, j) of these coefficients is $(1, 1)$ and are placed in the second row of SMRT matrix, starting from $S(1, 1)$, in the increasing order of k_1 with the coefficients for different p's placed along respective column.

The (c_1, c_2) of $Y^{(p)}_{k_1,2}$, $k_1 = 1, 3$ are (1,2) and they are grouped as $(i, j) = (1, 2)$. These coefficients are placed sequentially in the increasing order of k_1, starting from $S(1, 5)$, with the coefficients for different p's arranged column-wise. Similarly, sequencies of $Y^{(p)}_{1,4}$ are (1,4) and are placed from $S(1, 7)$ to $S(4, 7)$ and grouped into $(i, j) = (1, 3)$.

Corresponding to groups (i, j) for $j > i$ and sequency (c_1, c_2), there exist a group (j, i) with sequencies (c_2, c_1). These group (j, i) coefficients for $j > i$ are named as related coefficients of (i, j). They are placed as the lower triangular matrix with symmetry about the diagonal formed by groups (i, i).

The related coefficients of $Y^{(p)}_{1,2}$ & $Y^{(p)}_{3,2}$, ie. $Y^{(p)}_{2,1}$ & $Y^{(p)}_{6,1}$ respectively, are grouped as (2,1) and that of $Y^{(p)}_{1,4}$, ie. $Y^{(p)}_{4,1}$, as group (3,1) and are given in Table 3.2. They are placed in S(5,1), S(6,1) and S(7,1) with the coefficients for different p's arranged in the respective rows so as to get the coefficients arranged in the form of a square matrix. Similarly, all other coefficients are grouped and placed, with the indices (k_1, k_2, p) of each SMRT coefficient arranged in the respective cell as in Table 3.3. The group of cells with boldface boundaries represent different (i, j) groups and there are 16 groups for $N = 8$. Thus SMRT matrix corresponding to $N = 8$ can be considered as a matrix of 4×4 groups. Fig. 3.3 shows the VR of the SMRT coefficients with the coefficients arranged in the respective position for $N = 8$.

Thus, SMRT can be considered as an arrangement of unique MRT

Table 3.2: Groups of unique MRT coefficients and the related coefficients

Unique MRT coefficients	group (i,j)	related coefficients	group (i,j)
$Y_{0,0}^{(p)}$	(0,0)	-	-
$Y_{0,1}^{(p)}, Y_{0,2}^{(p)}, Y_{0,4}^{(p)}$	(0,0)	-	-
$Y_{1,0}^{(p)}, Y_{2,0}^{(p)}, Y_{4,0}^{(p)}$	(0,0)	-	-
$Y_{1,1}^{(p)}, Y_{3,1}^{(p)}, Y_{5,1}^{(p)}, Y_{7,1}^{(p)}$	(1,1)	-	-
$Y_{1,2}^{(p)}, Y_{3,2}^{(p)}$	(1,2)	$Y_{2,1}^{(p)}, Y_{6,1}^{(p)}$	(2,1)
$Y_{1,4}^{(p)}$	(1,3)	$Y_{4,1}^{(p)}$	(3,1)
$Y_{2,2}^{(p)}, Y_{6,2}^{(p)}$	(2,2)	-	-
$Y_{2,4}^{(p)}$	(2,3)	$Y_{4,2}^{(p)}$	(3,2)
$Y_{4,4}^{(p)}$	(4,4)	-	-

Table 3.3: Placement of SMRT coefficients for N=8

0,0,0	0,1,0	0,1,1	0,1,2	0,1,3	0,2,0	0,2,2	0,4,0
1,0,0	1,1,0	3,1,0	5,1,0	7,1,0	1,2,0	3,2,0	1,4,0
1,0,1	1,1,1	3,1,1	5,1,1	7,1,1	1,2,1	3,2,1	1,4,1
1,0,2	1,1,2	3,1,2	5,1,2	7,1,2	1,2,2	3,2,2	1,4,2
1,0,3	1,1,3	3,1,3	5,1,3	7,1,3	1,2,3	3,2,3	1,4,3
2,0,0	2,1,0	2,1,1	2,1,2	2,1,3	2,2,0	6,2,0	2,4,0
2,0,2	6,1,0	6,1,1	6,1,2	6,1,3	2,2,2	6,2,2	2,4,2
4,0,0	4,1,0	4,1,1	4,1,2	4,1,3	4,2,0	4,2,2	4,4,0

coefficients according to row-wise and column-wise sequencies with lower sequencies placed at the upper left corner and highest sequencies at the bottom right corner. In otherwords, SMRT can be considered as an ordered arrangement of sequency packets formed of coefficients with same row and column sequencies.

Similarly placement procedure for $N = 8$ is extended to any N, a power of 2. Placement of 256 SMRT coefficients for $N = 16$ is shown in Table 3.4. Unique MRT coefficients with either k_1 and/or k_2 being zero are grouped into $(0,0)$, $(0,1)$, $(0,2)$, $(0,3)$, $(1,0)$, $(2,0)$,

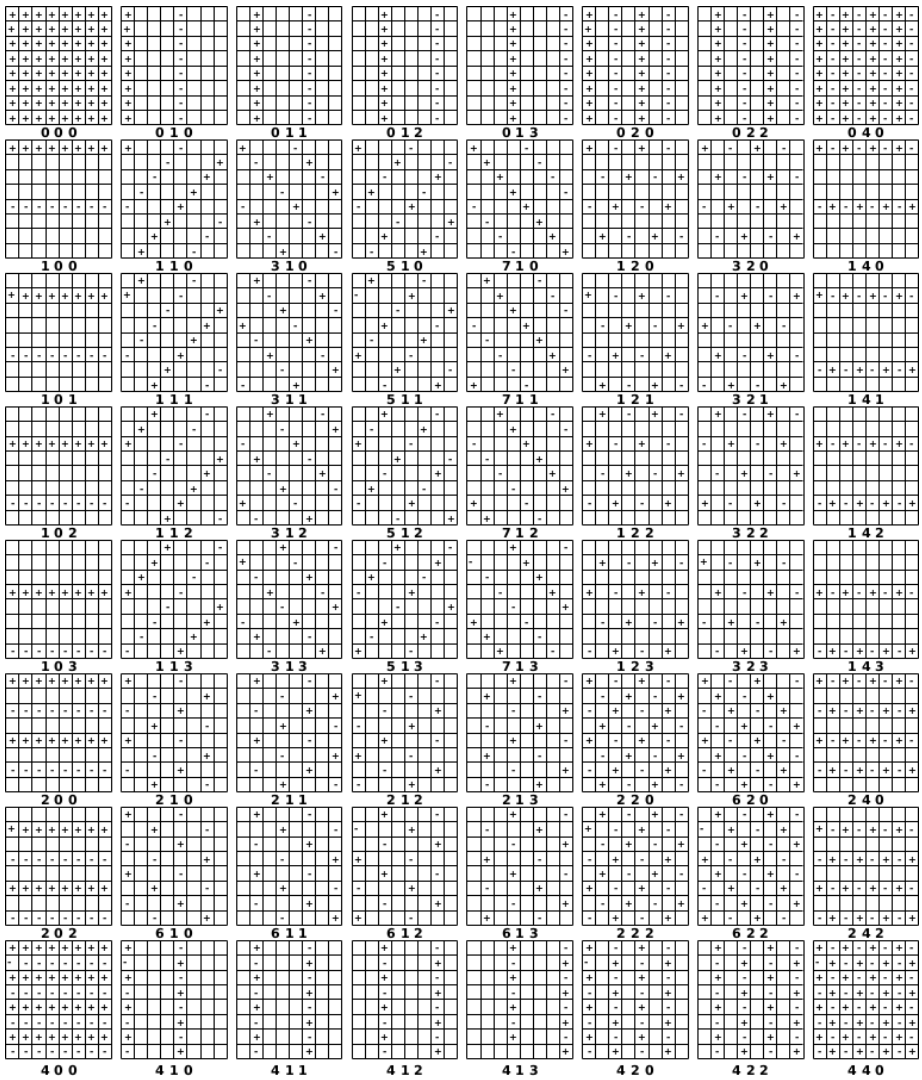

Fig. 3.3: Visual representation of SMRT for N=8

$(3, 0)$. There are 31 coefficients in these groups and their sequencies are $0, 2^0, 2^1, 2^2, 2^3$ in one direction and 0 in the other direction. The remaining 225 coefficients are grouped along rows and columns into

4 groups each. All coefficients having $c_1 = 1$ and $c_2 = 1, 2, 4, 8$ fall under groups with indices $i = 1$ and $j = 1, 2, 3, 4$ respectively. Similarly, coefficients with $c_1 = 2$ & $c_2 = 2, 4, 8$ are grouped under indices $i = 2$ & $j = 2, 3, 4$ respectively and so on. In general, total number of groups of unique MRT coefficients organized based on sequencies in the SMRT placement can be obtained as $(1 + log_2 N)^2$.

Table 3.4: Placement of SMRT coefficients for N=16

0,0,0	0,1,0	0,1,1	0,1,2	0,1,3	0,1,4	0,1,5	0,1,6	0,1,7	0,2,0	0,2,2	0,2,4	0,2,6	0,4,0	0,4,4	0,8,0
1,0,0	1,1,0	3,1,0	5,1,0	7,1,0	9,1,0	11,1,0	13,1,0	15,1,0	1,2,0	3,2,0	5,2,0	7,2,0	1,4,0	3,4,0	1,8,0
1,0,1	1,1,1	3,1,1	5,1,1	7,1,1	9,1,1	11,1,1	13,1,1	15,1,1	1,2,1	3,2,1	5,2,1	7,2,1	1,4,1	3,4,1	1,8,1
1,0,2	1,1,2	3,1,2	5,1,2	7,1,2	9,1,2	11,1,2	13,1,2	15,1,2	1,2,2	3,2,2	5,2,2	7,2,2	1,4,2	3,4,2	1,8,2
1,0,3	1,1,3	3,1,3	5,1,3	7,1,3	9,1,3	11,1,3	13,1,3	15,1,3	1,2,3	3,2,3	5,2,3	7,2,3	1,4,3	3,4,3	1,8,3
1,0,4	1,1,4	3,1,4	5,1,4	7,1,4	9,1,4	11,1,4	13,1,4	15,1,4	1,2,4	3,2,4	5,2,4	7,2,4	1,4,4	3,4,4	1,8,4
1,0,5	1,1,5	3,1,5	5,1,5	7,1,5	9,1,5	11,1,5	13,1,5	15,1,5	1,2,5	3,2,5	5,2,5	7,2,5	1,4,5	3,4,5	1,8,5
1,0,6	1,1,6	3,1,6	5,1,6	7,1,6	9,1,6	11,1,6	13,1,6	15,1,6	1,2,6	3,2,6	5,2,6	7,2,6	1,4,6	3,4,6	1,8,6
1,0,7	1,1,7	3,1,7	5,1,7	7,1,7	9,1,7	11,1,7	13,1,7	15,1,7	1,2,7	3,2,7	5,2,7	7,2,7	1,4,7	3,4,7	1,8,7
2,0,0	2,1,0	2,1,1	2,1,2	2,1,3	2,1,4	2,1,5	2,1,6	2,1,7	2,2,0	6,2,0	10,2,0	14,2,0	2,4,0	6,4,0	2,8,0
2,0,2	6,1,0	6,1,1	6,1,2	6,1,3	6,1,4	6,1,5	6,1,6	6,1,7	2,2,2	6,2,2	10,2,2	14,2,2	2,4,2	6,4,2	2,8,2
2,0,4	10,1,0	10,1,1	10,1,2	10,1,3	10,1,4	10,1,5	10,1,6	10,1,7	2,2,4	6,2,4	10,2,4	14,2,4	2,4,4	6,4,4	2,8,4
2,0,6	14,1,0	14,1,1	14,1,2	14,1,3	14,1,4	14,1,5	14,1,6	14,1,7	2,2,6	6,2,6	10,2,6	14,2,6	2,4,6	6,4,6	2,8,6
4,0,0	4,1,0	4,1,1	4,1,2	4,1,3	4,1,4	4,1,5	4,1,6	4,1,7	4,2,0	4,2,2	4,2,4	4,2,6	4,4,0	12,4,0	4,8,0
4,0,4	12,1,0	12,1,1	12,1,2	12,1,3	12,1,4	12,1,5	12,1,6	12,1,7	12,2,0	12,2,2	12,2,4	12,2,6	4,4,4	12,4,4	4,8,4
8,0,0	8,1,0	8,1,1	8,1,2	8,1,3	8,1,4	8,1,5	8,1,6	8,1,7	8,2,0	8,2,2	8,2,4	8,2,6	8,4,4	8,4,4	8,8,4

Analysis of the placement for different values of N reveals that the coefficients under the different groups can be organized in the following manner. The coefficients that come under the group $(i, j) = (1, 1)$ are the coefficients having frequency indices $k_1 = 1, 3, 5, ..., N - 1$ and $k_2 = 1$. The frequency indices for group $(i, j) = (1, 2)$ are $k_1 = 1, 3, 5, ..., \frac{N}{2} - 1$ and $k_2 = 2$ and that for group $(i, j) = (1, 3)$, are $k_1 = 1, 3, 5, ..., \frac{N}{4} - 1$ and $k_2 = 4$ etc. Computation of the related coefficients, row & column sequencies interchanged, can be implemented with the other set of coefficients. The frequency indices of the related coefficients can be obtained as $(k_1/2^{(j-1)}, k_2.2^{(j-1)})$. The related coefficients in each group are arranged in the matrix row-wise for increasing values of p.

The implementation of SMRT is illustrated with an example for $N = 8$ derived through MRT and is compared with UMRT also. Data matrix is given in (3.1) and the MRT matrices $Y^{(p)}_{k_1,k_2}, p = 0, 1, 2, 3$ are given by (3.2), (3.3), (3.4), (3.5) respectively. UMRT

and SMRT coefficients are given in (3.6) and (3.7) respectively.

$$X = \begin{bmatrix} 28 & 26 & 22 & 23 & 15 & 15 & 15 & 18 \\ 26 & 25 & 24 & 17 & 15 & 13 & 16 & 24 \\ 28 & 25 & 17 & 14 & 17 & 16 & 26 & 30 \\ 26 & 19 & 16 & 24 & 22 & 26 & 35 & 32 \\ 22 & 20 & 28 & 24 & 29 & 42 & 51 & 51 \\ 24 & 30 & 22 & 19 & 39 & 51 & 56 & 54 \\ 26 & 19 & 04 & 24 & 46 & 49 & 48 & 38 \\ 24 & 15 & 05 & 36 & 52 & 51 & 44 & 28 \end{bmatrix} \tag{3.1}$$

$$Y^{(0)}_{k_1,k_2} = \begin{bmatrix} 1766 & -31 & 10 & -31 & -30 & -31 & 10 & -31 \\ -105 & -72 & 43 & 38 & 5 & 42 & 25 & 72 \\ 2 & -17 & -58 & 47 & -6 & -17 & -30 & 47 \\ -105 & 38 & 25 & -72 & 5 & 72 & 43 & 42 \\ -54 & 25 & -10 & 25 & 6 & 25 & -10 & 25 \\ -105 & 42 & 43 & 72 & 5 & -72 & 25 & 38 \\ 2 & 47 & -30 & -17 & -6 & 47 & -58 & -17 \\ -105 & 72 & 25 & 42 & 5 & 38 & 43 & -72 \end{bmatrix} \tag{3.2}$$

$$Y^{(1)}_{k_1,k_2} = \begin{bmatrix} 0 & -84 & 0 & -94 & 0 & 84 & 0 & 94 \\ -135 & 41 & 29 & 39 & 15 & -29 & 3 & 53 \\ 0 & 52 & 0 & -26 & 0 & -52 & 0 & 26 \\ -55 & 21 & -19 & 145 & 3 & -41 & -41 & 3 \\ 0 & 20 & 0 & -10 & 0 & -20 & 0 & 10 \\ 135 & 29 & -29 & -53 & -15 & -41 & -3 & -39 \\ 0 & -32 & 0 & 42 & 0 & 32 & 0 & -42 \\ 55 & 41 & 19 & -3 & -3 & -21 & 41 & -145 \end{bmatrix} \tag{3.3}$$

$$Y^{(2)}_{k_1,k_2} = \begin{bmatrix} 0 & -153 & -14 & 153 & 0 & -153 & 14 & 153 \\ -81 & 110 & -5 & 0 & 9 & 12 & -31 & 2 \\ 0 & 57 & -54 & -17 & -4 & 57 & -22 & -17 \\ 81 & 0 & 31 & -110 & -9 & -2 & 5 & -12 \\ 0 & 15 & -6 & -15 & 0 & 15 & 6 & -15 \\ -81 & 12 & -5 & 2 & 9 & 110 & -31 & 0 \\ 0 & 17 & 22 & -57 & 4 & 17 & 54 & -57 \\ 81 & -2 & 31 & -12 & -9 & 0 & 5 & -110 \end{bmatrix} \tag{3.4}$$

$$Y^{(3)}_{k_1,k_2} = \begin{bmatrix} 0 & -94 & 0 & -84 & 0 & 94 & 0 & 84 \\ -55 & 145 & -41 & 21 & 3 & 3 & -19 & -41 \\ 0 & 42 & 0 & -32 & 0 & -42 & 0 & 32 \\ -135 & 39 & 3 & 41 & 15 & 53 & 29 & -29 \\ 0 & -10 & 0 & 20 & 0 & 10 & 0 & -20 \\ 55 & -3 & 41 & 41 & -3 & -145 & 19 & -21 \\ 0 & -26 & 0 & 52 & 0 & 26 & 0 & -52 \\ 135 & -53 & -3 & 29 & -15 & -39 & -29 & -41 \end{bmatrix} \tag{3.5}$$

$$U = \begin{bmatrix} 1766 & -31 & 10 & -84 & -30 & -153 & -14 & -94 \\ -105 & -72 & 43 & 21 & 5 & 12 & -19 & -53 \\ 2 & -17 & -58 & -32 & -6 & 57 & 22 & -26 \\ -135 & 38 & 25 & 41 & 15 & -2 & 29 & -3 \\ -54 & 25 & -10 & 20 & 6 & 15 & -6 & -10 \\ -81 & 42 & -5 & 41 & 9 & 110 & 3 & 39 \\ 0 & 47 & -30 & 52 & -4 & 17 & -54 & 42 \\ -55 & 72 & 31 & 29 & 3 & 0 & -41 & 145 \end{bmatrix} \tag{3.6}$$

$$S = \begin{bmatrix} 1766 & -31 & -84 & -153 & -94 & 10 & -14 & -30 \\ -105 & -72 & 38 & 42 & 72 & 43 & 25 & 5 \\ -135 & 41 & 21 & 29 & 41 & 29 & -19 & 15 \\ -81 & 110 & 0 & 12 & -2 & -5 & 31 & 9 \\ -55 & 145 & 39 & -3 & -53 & -41 & 3 & 3 \\ 2 & -17 & 52 & 57 & 42 & -58 & -30 & -6 \\ 0 & 47 & -32 & 17 & -26 & -54 & 22 & -4 \\ -54 & 25 & 20 & 15 & -10 & -10 & -6 & 6 \end{bmatrix} \tag{3.7}$$

Every transform should have a mapping function to map the data onto the transform coefficients. They are known as basis functions and should be linearly independent. The VR of the unique MRT coefficients organized as SMRT can be utilized to derive the basis function so as to convert the SMRT into a stand-alone transform.

3.2.3 Basis Images

Any data can be expressed as a linear combination of basis functions. DCT basis functions are cosine functions that take real values between -1 & 1 and hence DCT computation involves real multiplications and additions. The pictorial representation of the basis functions are called basis images. The basis images corresponding to DCT are shown in Appendix A.1. Basis images of SMRT can be easily obtained from the visual representation of the unique MRT coefficients organized based on sequency as explained in section 3.2.1. Basis functions of the SMRT will be in the form of rectangular functions of +1, -1 or 0 and hence will give integer-to-integer transform that involves additions only.

Set of 64 basis images corresponding to the 2-D SMRT, for $N = 8$, are shown in Fig. 3.4, where black, grayish white and mid-gray boxes correspond to +1, -1 and 0 respectively. These basis images

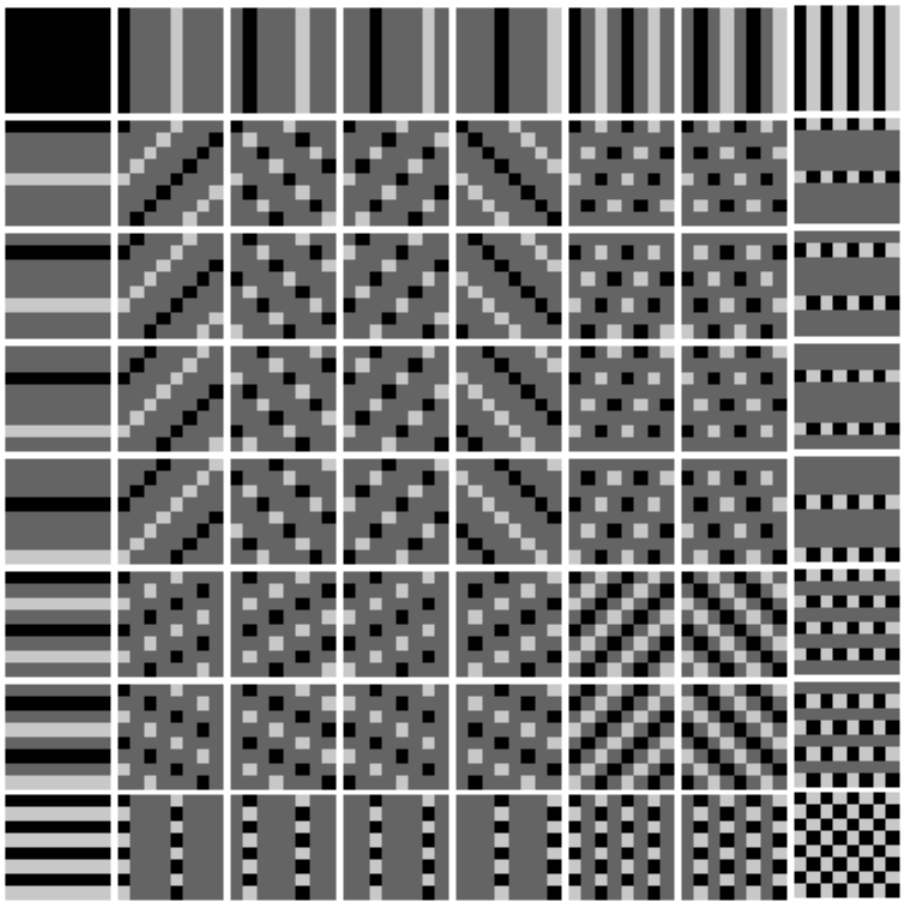

Fig. 3.4: 2-D SMRT basis images for N=8.

exhibit a progressive increase of their sequency, along horizontal, vertical and diagonal directions. SMRT coefficients can be obtained by projecting the data onto the basis images. Thus any image can be decomposed into weighted sum of basis images, where the SMRT coefficients are the weights.

$S(0,0)$ is the only coefficient with zero sequency in both directions and is called "DC SMRT coefficient". It is the sum of all data ele-

ments and holds most of the energy. The remaining (N^2-1) coefficients, named as "AC SMRT coefficients", are derived by combining the data elements based on the respective basis image.

An algorithm to compute and place the SMRT coefficients in an $N \times N$ matrix, based on the analysis performed using the VR of the SMRT coefficients, can be developed by grouping the coefficients according to sequency.

3.2.4 Forward SMRT Algorithm

Let X be the $N \times N$ data matrix and S be the corresponding SMRT matrix. The SMRT coefficients are computed based on the MRT coefficients, $Y^{(p)}_{k_1,k_2}$, in Eq. 1.7

1. *Computation of divisors of M*

   $v = log_2(M)$

   for $i = 0$ to v

   $d(i) = 2^i$

   end

2. *Computation of DC SMRT coefficient,* $S(0,0)$

   $S(0,0) = Y^{(0)}_{0,0}$

3. *Computation and placement of first row and column of coefficients*

   $a = 1$

   for $i = 0$ to v

   $j = d(i)$

   for $p = 0$ to $M-1$ in steps of j

$S(0, a) = Y_{0,j}^{(p)}$

$S(a, 0) = Y_{j,0}^{(p)}$

$a = a + 1$

end

end

4. *Computation and placement of other coefficients*

a=1

for $i = 0$ to v

$b = i$, $r = a$, $c = a$.

for $j = 0$ to $v - i$

$s_1 = 2.d(i)$, $s_2 = d(i)$.

$s_3 = \frac{N}{d(j)}$, $s_4 = d(j)$

for $k_1 = s_2$ to s_3 in steps of s_1

$k_2 = d(i + j)$

for $p = 0$ to $M - 1$ in steps of s_2

$S(r, c) = Y_{k_1,k_2}^{(p)}$

if $(i \neq b)$ (*%Computation of related coefficients*)

$S(c, r) = Y_{k_1.s_4,\frac{k_2}{s_4}}^{(p)}$

end

$r = r + 1$

end

$r = r - \frac{M}{s_2}$, $c = c + 1$

end

$b = b + 1$

end for $i = 0$ to v

$a = a + \frac{M}{s_2}$

end

3.2.5 Inverse SMRT Algorithm

The data elements can be retrieved from the N^2 SMRT coefficients. Original MRT representation involves a set of redundant coefficients with exactly same or sign-reversed values and corresponding same or complement visual representations. A redundancy factor associated with each unique MRT coefficient is defined as the number of times it repeats as mentioned above. Thus associated with every SMRT matrix there will be a redundancy matrix. Hence all SMRT coefficients are to be multiplied by the redundancy factor while calculating inverse SMRT.

1. *Computation of divisors of M*

   $v = log_2(M)$

   for $i = 0$ to v

   $d(i) = 2^{(i)}$

   $d'(i) = \frac{M}{d(i)}$

   end

2. *Contributions of* $S(0, 0)$

   for $n_1 = 0$ to $N - 1$

   for $n_2 = 0$ to $N - 1$

   $x(n_1, n_2) = S(0, 0)$

end

end

3. *Contributions due to first row and column*

for $n_1 = 0$ to $N - 1$

for $n_2 = 0$ to $N - 1$

$a = 1$

for $i = 0$ to v

$j = d(i)$

$z = ((n_2.j))_N$

for $p = 0$ to $M - 1$ in steps of j

if $z = p$

$x(n_1, n_2) = x(n_1, n_2) + d'(i).S(1, a)$

$x(n_2, n_1) = x(n_2, n_1) + d'(i).S(a, 1)$

elseif $z = p + M$

$x(n_1, n_2) = x(n_1, n_2) - d'(i).S(1, a)$

$x(n_2, n_1) = x(n_2, n_1) - d'(i).S(a, 1)$

end

$a = a + 1$

end

end

end

end

4. *Contributions of other coefficients*
   for $n_1 = 0$ to $N - 1$

   for $n_2 = 0$ to $N - 1$

   a=1

   for $i = 0$ to v

   $b = i$, $r = a$, $c = a$.

   for $j = 0$ to $v - i$

   $s_1 = 2.d(i)$, $s_2 = d(i)$

   $s_3 = \frac{N}{d_m(j)}$, $s_4 = d_m(j)$

   for $k_1 = s_2$ to s_3 in steps of s_1

   $k_2 = d_m(i + j)$

   $z = ((n_1.k_1 + n_2.k_2))_N$

   for $p = 0$ to $M - 1$ in steps of s_2

   if $z = p$

   $x(n_1, n_2) = x(n_1, n_2) + d'(i).S(r, c)$

   elseif $z = p + M$

   $x(n_1, n_2) = x(n_1, n_2) - d'(i).S(r, c)$

   end

   if $(i \neq b)$

   $z = ((n_1.k_1.s_4 + n_2.k_2/s_4))_N$

   if $z = p$

   $x(n_1, n_2) = x(n_1, n_2) + d'(i).S(c, r)$

   elseif $z = p + M$

$$x(n_1, n_2) = x(n_1, n_2) - d'(i).S(c, r)$$

end

end

$r = r + 1$

end

$r = r - \frac{M}{s_2}$, $c = c + 1$

end

$b = b + 1$

end

$a = a + \frac{M}{s_2}$

end

end

end

$x = \frac{x}{N^2}$

3.2.6 Implementation of Algorithm

The forward and inverse SMRT algorithms are coded with the help of C Programming and MEX file integration (Appendix D). The better performance of MEX files over MATLAB is accomplished by the usage of pointers, dynamically assigned during program run and cleared after program execution. Another main advantage of MEX file is the easy integration to MATLAB. All the required MEX files, integrated into a tool-box, are included to MATLAB working directory automatically when MATLAB is launched [157].

An attempt is also made to code the algorithm using Python and Cython languages in linux platform. Cython language is a superset

of the Python language that additionally supports calling C functions and declaring C types on variables and class attributes. The Cython files are integrated into a tool-box which can be included to Python working directory [158].

Computation time of SMRT and ISMRT algorithms, written in MATLAB, Python, Cython and with MEX file integration to MATLAB, are tabulated in Tables 3.5 & 3.6 respectively using an Intel i7 processor (Quad core), 8 GB RAM and 64 bit OS. The results show that the computation time increases drastically as the data size exceeds 64×64. Computation time for SMRT and ISMRT is less with Mex files. Computation time can be further reduced by hardware implementation of the algorithms.

Table 3.5: Comparison of execution time for 2-D SMRT using various methods

Data size	Computation time in seconds			
	MATLAB	Python	Cython	Mex
2×2	0.005291	0.000106	0.0000177	0.000968
4×4	0.006338	0.001050	0.000026	0.000983
8×8	0.006607	0.013900	0.000079	0.000980
16×16	0.009639	0.212000	0.000625	0.001204
32×32	0.044499	3.260000	0.007980	0.005248
64×64	0.577565	51.90000	0.114000	0.064761
128×128	8.910743	-	0.680000	1.081716
256×256	140.7894	-	27.60000	16.27126

3.3 Properties

A transformation of the signal is a change of its independent parameter. Thus the properties existing in the transform domain will be entirely different from that in the data domain. Hence it is important to analyze the properties existing in the new transform

Table 3.6: Comparison of execution time for 2-D ISMRT using various methods

Data size	Computation time in seconds			
	MATLAB	Python	Cython	Mex
2×2	0.010902	0.000185	0.000019	0.000993
4×4	0.012793	0.002240	0.000071	0.000982
8×8	0.013090	0.026300	0.000548	0.000997
16×16	0.016844	0.333000	0.004830	0.001231
32×32	0.059485	0.530000	0.045800	0.004569
64×64	0.669377	65.73000	0.494000	0.059040
128×128	9.790258	-	2.530000	0.822007
256×256	-	-	82.20000	12.97599

domain representation and a few properties of SMRT are explored here under. The properties will help in sequency domain analysis of signals and systems for various signal processing applications.

3.3.1 General Properties

Let the SMRT of an $N \times N$ data matrix, $x(n_1, n_2)$, $0 \leq n_1, n_2 \leq N-1$, be $S(s_1, s_2)$, $0 \leq s_1, s_2 \leq N-1$. A few properties that hold true for SMRT are presented below.

3.3.1.a Effect of Addition with a Constant

Basis images of AC SMRT coefficients in Fig. 3.4 show that same number of data elements are involved in addition and subtraction of each coefficient. Hence, addition of a constant, 'c' , with all data elements does not change the values of AC SMRT coefficients. DC SMRT coefficient is the sum of all data elements and addition of 'c' with all data elements increases the value of DC SMRT coefficient by cN^2.

3.3.1.b Linearity

Let $x_1(n_1, n_2)$ and $x_2(n_1, n_2)$ be two data matrices of size $N \times N$, such that

$$x_1(n_1, n_2) \overset{\text{SMRT}}{\longleftrightarrow} S_1(s_1, s_2) \tag{3.8a}$$

and

$$x_2(n_1, n_2) \overset{\text{SMRT}}{\longleftrightarrow} S_2(s_1, s_2) \tag{3.8b}$$

then for any constants a and b

$$\mathrm{a}x_1(n_1, n_2) + \mathrm{b}x_2(n_1, n_2) \overset{\text{SMRT}}{\longleftrightarrow} \mathrm{a}S_1(s_1, s_2) + \mathrm{b}S_2(s_1, s_2). \tag{3.8c}$$

This linearity property indicates that SMRT satisfies superposition principle and allows the analysis of multicomponent signals. Linearity of different sized matrices also holds true when the smaller matrix is zero padded to have the same size as the larger matrix.

3.3.1.c Orthogonality

Basis images have to be orthogonal if the inner product of any basis with another basis should produce a zero value, whereas inner product of any basis with itself should yield a constant value. SMRT basis images hold this, confirming that they are orthogonal to each other.

$$\langle A_{c_1,c_2,i_1,i_2}, A_{c_1',c_2',i_1',i_2'} \rangle = \begin{cases} k, & c_1 = c_1' \ \& \ c_2 = c_2' \ \& \ i_1 = i_1' \ \& \ i_2 = i_2' \\ 0, & \text{otherwise} \end{cases} \tag{3.9}$$

where k is some constant.

3.3.1.d Redundancy Factor

MRT representation as given in Sec. 1.3.8 introduces redundancy and some of the coefficients are either exactly same or sign reversed. But SMRT representation is carrying unique elements present in MRT leaving the redundant components. This causes loss of a portion of the information from the data. This loss can be avoided by incorporating a redundancy factor associated with each unique coefficient. Thus a matrix of redundancy factor is to be computed along with the SMRT matrix to have complete information about the data. Redundancy of each MRT coefficient $Y^{(p)}_{k_1,k_2}$ can be obtained as $\frac{M}{d_m}$, where $d_m = gcd(k_1, k_2, M)$ as given in Sec. 1.3.8.

Redundancy matrix of SMRT for N=8 is

$$R(s_1, s_2) = \begin{bmatrix} 1 & 4 & 4 & 4 & 4 & 2 & 2 & 1 \\ 4 & 4 & 4 & 4 & 4 & 4 & 4 & 4 \\ 4 & 4 & 4 & 4 & 4 & 4 & 4 & 4 \\ 4 & 4 & 4 & 4 & 4 & 4 & 4 & 4 \\ 4 & 4 & 4 & 4 & 4 & 4 & 4 & 4 \\ 2 & 4 & 4 & 4 & 4 & 2 & 2 & 2 \\ 2 & 4 & 4 & 4 & 4 & 2 & 2 & 2 \\ 1 & 4 & 4 & 4 & 4 & 2 & 2 & 1 \end{bmatrix} \tag{3.10}$$

3.3.1.e Energy Conservation (Parseval's Theorem)

Energy has to be conserved when the data is transformed into another domain. Here, the redundancy factor has to be taken into account while considering energy compaction. The Parseval's relation, applied to SMRT, is given below.

$$\sum_{n_1=0}^{N-1} \sum_{n_2=0}^{N-1} |x(n_1, n_2)|^2 = \frac{1}{N^2} \sum_{s_1=0}^{N-1} \sum_{s_2=0}^{N-1} R(s_1, s_2) \, |S(s_1, s_2)|^2 \tag{3.11}$$

3.3.1.f Energy Compaction

Energy compaction of a transform is its ability to redistribute signal energy into small number of transform coefficients. This implies that many transform coefficients will contain very little energy since total energy is preserved. Energy compaction property can be characterized by the fraction of the total number of transform coefficients that carry a certain percentage of signal energy. For a given percentage of energy, lower this fraction, better is the compaction property of the transform.

Examples of two highly correlated artificial images (*square, chess*) of size 64×64 are shown in Fig. 3.5. Position and value of DC

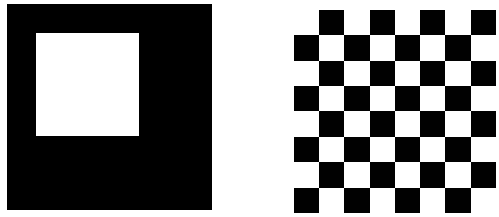

Fig. 3.5: Artificial images (a)*square* (b)*chess*

coefficient of both DCT, normalized UMRT and normalized SMRT are same. Absolute values of the normalized AC coefficient plots of DCT, UMRT and SMRT are shown in Fig. 3.6. DCT packs most of the signal energy into lower frequency coefficients and SMRT packs signal energy to very few coefficients. SMRT of *square* concentrates 100 % and DCT packs 97.36 % of its energy into the first 33×33 AC coefficients (27%). SMRT coefficients of *chess* concentrates full AC energy to 8×8 (1.6%) coefficients starting from (50,50) and DCT only packs 32.21 % energy to the first 8×8 AC coefficients starting from (1,1).

Thus, SMRT exhibits excellent energy compaction for highly cor-

related images. For uncorrelated images, large valued transform coefficients are spread out, whereas for correlated images, high valued transform coefficients are packed. In this way, many coefficients can be discarded through quantization prior to encoding.

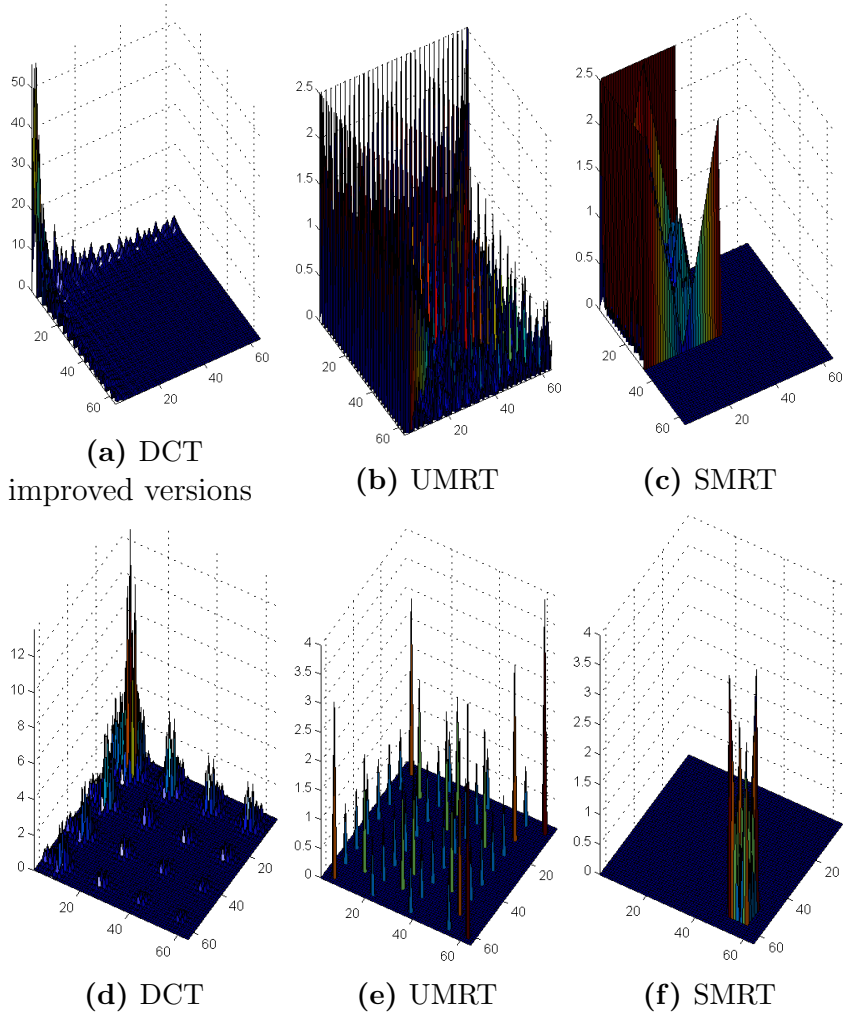

(a) DCT improved versions **(b)** UMRT **(c)** SMRT

(d) DCT **(e)** UMRT **(f)** SMRT

Fig. 3.6: Surface plots of absolute value of normalized transform coefficients (a), b), (c) *square*, (d), (e), (f) *chess*

3.3.2 Statistical Properties

In image processing, it is common to use statistical descriptors for finding the pixel distributions. In the transform domain, image parameters like mean, standard deviation, variance, minimum and maximum pixel values are not directly available. If these values can be computed directly in the transform/compressed domain, inverse transform/decompression can be eliminated in many applications.

Mean and variance play important roles in wide range of image processing applications. They provide strong indications of how bright, uniform or regular a region is.

3.3.2.a Mean

Average brightness of an image is defined as the mean of the image. DC SMRT coefficient holds most of the image energy and the mean/average of an image can be found from $S(0,0)$ as

$$\text{Mean } (\mu_s) = \frac{S(0,0)}{N^2} \tag{3.12}$$

3.3.2.b Standard Deviation and Variance

Standard deviation (SD) is a measure of dispersion from the mean and shows how the pixel values fluctuate around the mean. Variance represents the power of this fluctuation. Standard Deviation can be obtained as the mean of root of sum of squares of all AC SMRT coefficients considering redundancy.

$$\text{SD } (\sigma) = \frac{\sqrt{\sum_{s_1=0}^{N-1}\sum_{s_2=0}^{N-1}\left[S(s_1,s_2).R(s_1,s_2)\right]^2 - S^2(0,0)}}{N^2-1} \tag{3.13}$$

$$\text{Variance } (\sigma^2) = \frac{\sum_{s_1=0}^{N-1} \sum_{s_2=0}^{N-1} [S(s_1, s_2).R(s_1, s_2)]^2 - S^2(0,0)}{(N^2-1)^2} \tag{3.14}$$

3.3.2.c Coefficient-of-Variation

Coefficient-of-variation (CV) is a well-known measure of relative precision which is invariant to scale changes, but is not invariant to location changes. It is defined as

$$CV = \frac{\sigma}{\mu_s}.100\% \tag{3.15}$$

It is dimensionless and quantifies the degree of variability relative to mean.

3.3.2.d Histogram Span

Histogram span is the dynamic range of the histogram. When the histogram is symmetrical and bell shaped, 95.45 % and 99.73 % of histogram population lies within $\pm$ 2σ and $\pm$ 3σ respectively. So span or range of an image can be approximately represented as

$$\text{Span} \approx 4\sigma \tag{3.16}$$

$$\text{Minimum pixel value} \approx \text{Mean} - \frac{\text{Span}}{2} \tag{3.17}$$

$$\text{Maximum pixel value} \approx \text{Mean} + \frac{\text{Span}}{2} \tag{3.18}$$

3.3.2.e Shape and Span of Histogram from Block SMRT

When block processing is used (usually is the case for image compression) in the transform domain, the mean of each block can

be computed directly from DC SMRT coefficient. Histogram constructed from the block mean values would give an approximation of the image histogram. However, this preserves the shape and span of the original histogram. The histogram of 512×512 *lena* image and histogram built from DC SMRT coefficients of the 8×8 blocks are shown in Fig. 3.7 which justifies the above statement.

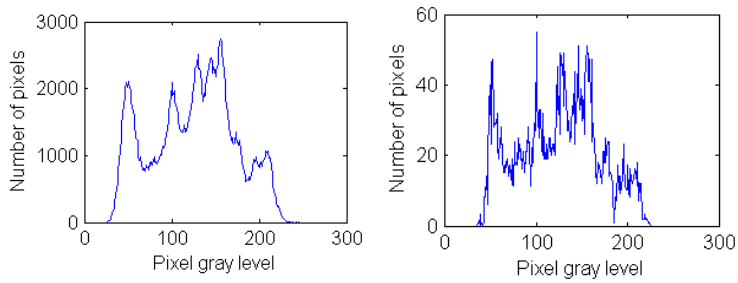

(a) **(b)**

Fig. 3.7: Histogram (a)Original image (b)Built from block DC SMRT coefficients

3.3.3 Pattern based Properties

3.3.3.a Pattern Generation

Basis images of each SMRT coefficient are the visual representation of the patterns in which the data elements are combined. New visual patterns can be derived from the basis images of coefficients from suitable combinations. Group patterns of the basic DFT coefficients [33] can be obtained by combining the basis images, $Y_{k_1,k_2}^{(p)}$, for all p. The diagonal patterns thus obtained, for $N = 8$, are shown in Fig. 3.8. These basis images are highly directional and the pixels in a specified orientation can be found using selected coefficients. Dominant orientation in a data matrix can be easily found by sensibly selecting the coefficients.

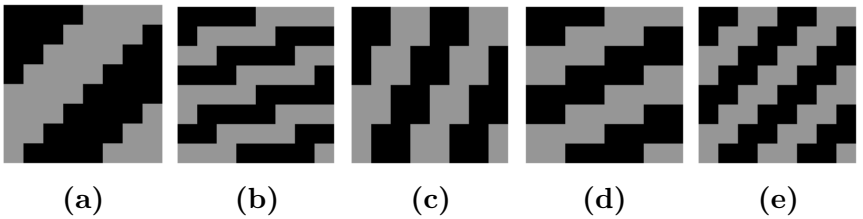

Fig. 3.8: Group diagonal patterns of SMRT coefficients for $N = 8$ (a)$Y_{1,1}^{(p)}$ (b)$Y_{3,1}^{(p)}$ (c)$Y_{1,2}^{(p)}$ (d)$Y_{2,1}^{(p)}$ (e)$Y_{2,2}^{(p)}$

Fig. 3.9 shows diagonal group patterns by combining $p's$ of the basic DFT coefficients for $N = 16$. These patterns clearly show the convenience in finding the directional patterns in images.

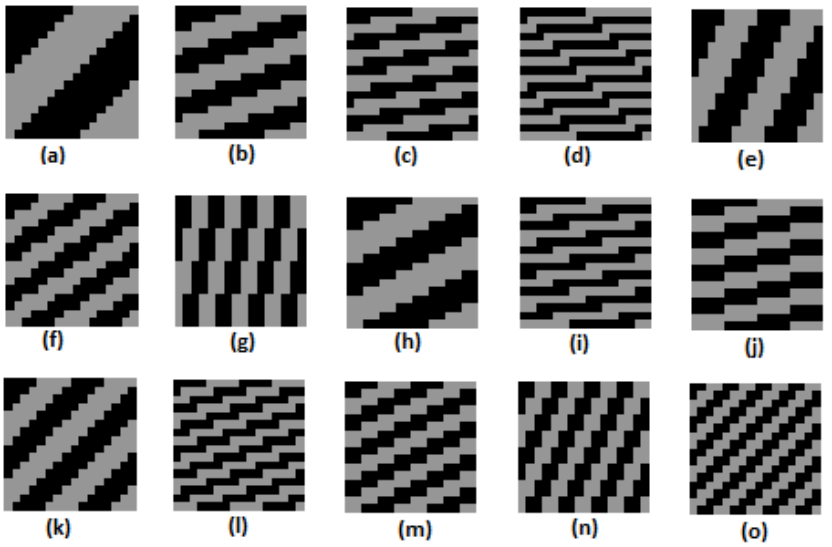

Fig. 3.9: Group diagonal patterns of SMRT for N=16 (a)$Y_{1,1}^{(p)}$ (b)$Y_{3,1}^{(p)}$ (c)$Y_{5,1}^{(p)}$ (d)$Y_{7,1}^{(p)}$ (e)$Y_{1,2}^{(p)}$ (f)$Y_{3,2}^{(p)}$ (g)$Y_{1,4}^{(p)}$ (h)$Y_{2,1}^{(p)}$ (i)$Y_{6,1}^{(p)}$ (j)$Y_{4,1}^{(p)}$ (k)$Y_{2,2}^{(p)}$ (l)$Y_{6,2}^{(p)}$ (m)$Y_{4,2}^{(p)}$ (n)$Y_{2,4}^{(p)}$ (o)$Y_{4,4}^{(p)}$

These group patterns can be combined again to derive new patterns.

Figs. 3.10 & 3.11 show the patterns thus obtained by combining two and three group patterns respectively. Thus deriving new patterns by combining coefficients helps in extracting texture patterns and features from images.

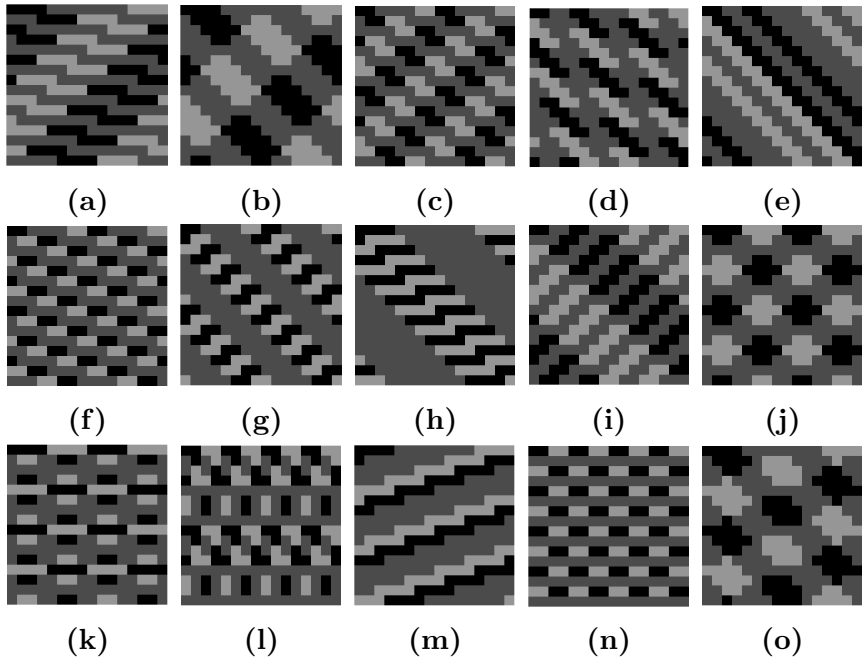

Fig. 3.10: Combined group patterns of two $Y^{(p)}_{k_1,k_2}$ for $N = 16$ (a) $Y^{(p)}_{1,1}$ &$Y^{(p)}_{10,2}$ (b) $Y^{(p)}_{1,1}$ &$Y^{(p)}_{14,2}$ (c) $Y^{(p)}_{2,2}$ &$Y^{(p)}_{12,4}$ (d) $Y^{(p)}_{12,4}$ &$Y^{(p)}_{13,1}$ (e) $Y^{(p)}_{12,4}$ &$Y^{(p)}_{15,1}$ (f) $Y^{(p)}_{4,4}$ &$Y^{(p)}_{10,2}$ (g) $Y^{(p)}_{4,4}$ &$Y^{(p)}_{6,2}$ (h) $Y^{(p)}_{7,1}$ &$Y^{(p)}_{6,2}$ (i) $Y^{(p)}_{4,4}$ &$Y^{(p)}_{15,1}$ (j) $Y^{(p)}_{2,2}$ &$Y^{(p)}_{14,2}$ (k) $Y^{(p)}_{6,2}$ &$Y^{(p)}_{10,2}$ (l) $Y^{(p)}_{2,4}$ &$Y^{(p)}_{12,4}$ (m) $Y^{(p)}_{3,1}$ &$Y^{(p)}_{6,2}$ (n) $Y^{(p)}_{4,4}$ &$Y^{(p)}_{12,4}$ (o) $Y^{(p)}_{2,1}$ &$Y^{(p)}_{14,2}$

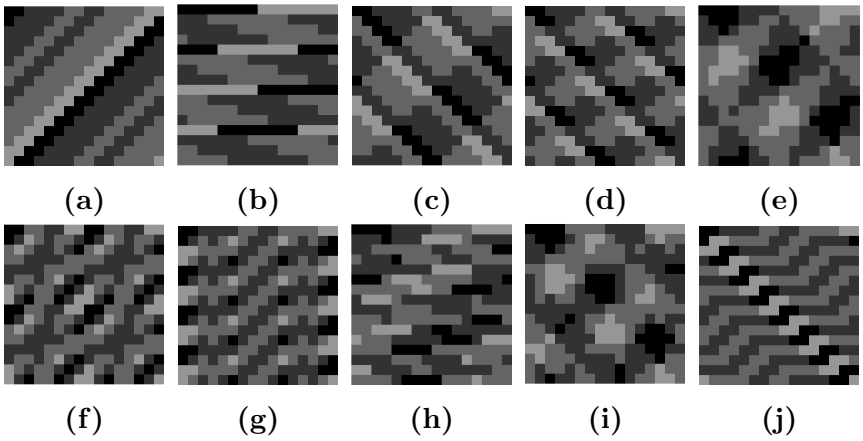

Fig. 3.11: Combined group patterns of three $Y^{(p)}_{k_1,k_2}$ for $N = 16$ (a) $Y^{(p)}_{1,1}$, $Y^{(p)}_{2,2}$ & $Y^{(p)}_{4,4}$ (b) $Y^{(p)}_{1,1}$, $Y^{(p)}_{5,1}$ & $Y^{(p)}_{9,1}$ (c) $Y^{(p)}_{1,1}$, $Y^{(p)}_{12,4}$, & $Y^{(p)}_{14,2}$ (d)$Y^{(p)}_{3,1}$, $Y^{(p)}_{12,4}$ & $Y^{(p)}_{14,2}$ (e) $Y^{(p)}_{1,2}$, $Y^{(p)}_{2,1}$ & $Y^{(p)}_{15,1}$ (f) $Y^{(p)}_{2,4}$, $Y^{(p)}_{4,2}$ & $Y^{(p)}_{4,4}$ (g) $Y^{(p)}_{4,1}$, $Y^{(p)}_{4,2}$ & $Y^{(p)}_{4,4}$ (h) $Y^{(p)}_{1,1}$, $Y^{(p)}_{4,1}$, & $Y^{(p)}_{10,2}$ (i) $Y^{(p)}_{1,2}$, $Y^{(p)}_{2,1}$ & $Y^{(p)}_{14,2}$ (j) $Y^{(p)}_{4,4}$, $Y^{(p)}_{6,2}$ & $Y^{(p)}_{7,1}$

3.3.3.b Template Matching

Template matching, in spatial domain, is done from the product of image and shifted versions of target image. This helps to locate the regions identical to the target.

In SMRT domain, the magnitude of the coefficients shows the presence of templates similar to the basis images and thus helps to identify and locate specified patterns within images directly.

3.4 Applications

SMRT is a general purpose tool that can be applied to a variety of applications. It has significance in signal analysis due to its sequency ordering and its simple implementation in terms of integer

additions for transformation. The coefficients give a direct measure of the variations in the signal. Some potential applications of SMRT are presented in this section.

Texture can be defined from an image processing view point as the spatial distribution of intensity variations in an image. The different patterns present in the VR of SMRT make it suitable for texture analysis. MRT based texture features were used for identification and classification of objects [66], [159].

UMRT has been used for optimized Quad-tree partitioning of images and an adaptive block size transform coder for image compression [68]. The purpose of the algorithm is to take advantage of large uniform regions that can be coded as a single large unit instead of smaller units and fine details of the image can be coded using smaller units. This method is capable of partitioning images according to the statistics of the pixel values, which leads to a much better image segmentation, consequently to higher image compression ratios with lower image degradation.

3.4.1 Text Compression

Compression serves to save both storage space and transmission time. Text compression provides an attractive option to store large amounts of text efficiently. Documents can be scanned, compressed and stored for later use. Compression is usually done in the transform domain followed by quantization and entropy coding.

A transform, best suited for image compression, decorrelates the image coefficients and transforms it into a sparse matrix with most of its large valued elements concentrated into a small region. More compression can be achieved by discarding irrelevant coefficients. Then the resultant coefficients are entropy coded to achieve further compression.

Here, the potential of SMRT in text compression is explored. Text, being binary data, takes two values 0 and 1 and hence better scope for sparse SMRT matrix. Simulation is done in text documents of different fonts, file extensions and sizes. Five documents, doc1 to doc5, the first three of size 256×256 and the other two of size 512×512 are taken here for documentation. Documents chosen are of different fonts and file extensions. The analysis is done for lossless compression and hence the transform coefficients are not quantized.

First, the image is partitioned into 8×8 non-overlapping blocks and SMRT is applied on these blocks and are entropy coded. In the decompression stage, the sequence is decoded and block-wise inverse transform is performed.

Number of zeros and number of symbols of DCT, WT and SMRT for lossless compression are computed and tabulated in Table 3.7. It is found that amount of sparsity is more pronounced and hence less number of symbols for SMRT based computation. This makes SMRT more suitable for text compression.

Table 3.8 gives a comparison of compression ratios and bpp of SMRT based lossless text compression using Huffman and arithmetic coding schemes. It is found that arithmetic coding gives better compression compared to Huffman coding.

Table 3.7: Comparison of sparsity and number of symbols of DCT and SMRT for lossless compression

File name	No. of zero values			No.of symbols		
	DCT	WT	SMRT	DCT	WT	SMRT
doc1	24583	8941	36508	14112	3421	63
doc2	29651	9218	39797	13499	3501	70
doc3	28702	9496	39998	12361	2673	78
doc4	144511	44044	177182	30316	5861	75
doc5	152475	44886	184113	27825	6730	78

Table 3.8: Comparison of CR and bpp of SMRT for different coding schemes for lossless compression

File name	Huffman coding		Arithmetic coding	
	CR	bpp	CR	bpp
doc1	3.43	2.33	3.46	2.31
doc2	3.62	2.21	3.69	2.17
doc3	3.68	2.21	3.71	2.16
doc4	3.99	2.01	4.19	1.91
doc5	4.12	1.94	4.41	1.81

Now through this SMRT placement the MRT computation has been modified by eliminating the redundant coefficients and organized in a structured manner based on the variation in sequency. Thus the computation of SMRT at present is a placement technique to arrange unique MRT coefficients based on MRT computation.

3.5 Direct Computation of SMRT for N a Power of 2

The computation of SMRT coefficients in Sec. 3.2.4 is through MRT. Development of SMRT as an independent transform demands a corresponding transform kernel.

3.5.1 Relation Between Independent Parameters of MRT and SMRT Representations

SMRT is developed through MRT by the identification and arrangement of unique MRT coefficients in the order of sequency and it is found that a group of coefficients are with the same sequency and can be considered as a sequency packet. Analysis of VR, corresponding to different values of N, shows that size of the sequency

packet depends on the values of N, c_1 and c_2. Number of rows or columns of sequency packet can be obtained as $\frac{M}{c_1}$ or $\frac{M}{c_2}$, except for $c_1 = c_2 = 0$. When c_1 and/or c_2 is zero, the size of the sequency packet in that direction is 1. For all other values of c_1 and c_2, the size of sequency packet will be $\frac{M}{c_1} \times \frac{M}{c_2}$.

Analogous to frequency indices k_1, k_2 in MRT, sequencies c_1, c_2 rule SMRT. Also the role of phase index p in MRT can be replaced with the row-column indices of the coefficients in a sequency packet. These packets can be classified into two according to the way the phase terms associated with a particular frequency of MRT representation are arranged. ie $c_2 = 0$ and $c_1 \leq c_2$ (class 1) or $c_1 = 0$ and $c_1 > c_2$ (class 2). Sequency packets with $c_1 = c_2$, $c_1 < c_2$ and $c_1 > c_2$ are placed in the increasing order of sequency along diagonal, upper triangular and lower triangular part of the SMRT matrix respectively. Within any sequency packet of class 1, the coefficients with same (k_1, k_2) and different p's are arranged along column while those of different k_1 and same k_2 & p are placed, in the increasing order, in different rows. For class 2 sequency packet, the coefficients with same (k_1, k_2) and different p's are arranged along rows while those of different k_1 and same k_2 & p are placed, in the increasing order, in different columns.

Thus, each sequency packet in SMRT matrix can be represented as S_{c_1,c_2} and each SMRT coefficient within the packet can be represented as $S_{c_1,c_2}(i_1, i_2)$, where (i_1, i_2) represents row and column indices of the coefficients within the packet with sequency (c_1, c_2).

A relation between the independent parameters k_1, k_2, p of the MRT coefficients and c_1, c_2, i_1, i_2 of SMRT coefficients can be obtained by properly analysing them. Table 3.9 shows the MRT parameters and the corresponding SMRT parameters for sequency packet with sequency $(1, 2)$, when $N = 8$. Similarly, the parameters for all the sequency packets are tabulated and observed that there exists a relationship. Identical relations are observed between these parameters for higher values of N. Table 3.10 shows the index relation

between MRT and SMRT.

Table 3.9: MRT and SMRT parameters for SMRT coefficients within the sequency packet $(1, 2)$, when N=8

MRT parameters			SMRT parameters			
k_1	k_2	p	c_1	c_2	i_1	i_2
1	2	0	1	2	0	0
1	2	1	1	2	1	0
1	2	2	1	2	2	0
1	2	3	1	2	3	0
3	2	0	1	2	0	1
3	2	1	1	2	1	1
3	2	2	1	2	2	1
3	2	3	1	2	3	1

Table 3.10: Relationship between MRT and SMRT parameters

	$c_1 \leq c_2$ $c_2 = 0$	$c_1 > c_2$ $c_1 = 0$
k_1	$c_1(1 + 2.i_2)$	$c_1(1 + 2.i_1)$
k_2	c_2	c_2
p	$c_1 i_1$	$c_2 i_2$

Generally, SMRT coefficients $S_{c_1,c_2}(i_1, i_2)$; $c_1, c_2 = 0, 2^0, 2^1, 2^2, ..., M$; $i_1 = 0, 1, 2, ..., \frac{M}{c_1} - 1$ and $i_2 = 0, 1, 2, ..., \frac{M}{c_2} - 1$ for any 2-D data, $x(n_1, n_2), 0 \leq n_1, n_2 \leq N - 1$, can be represented in terms of a kernel, $A_{c_1,c_2,i_1,i_2}(n_1, n_2)$, as

$$S_{c_1,c_2}(i_1, i_2) = \langle X, A_{c_1,c_2,i_1,i_2} \rangle = \sum_{n_1=0}^{N-1} \sum_{n_2=0}^{N-1} x(n_1, n_2) A_{c_1,c_2,i_1,i_2}(n_1, n_2) \tag{3.19}$$

where for class 1 sequency packet,

$$A_{c_1,c_2,i_1,i_2}(n_1,n_2) = \begin{cases} +1, & \text{if } ((n_1c_1(1+2i_2)+n_2c_2))_N - c_2i_1 = 0 \\ -1, & \text{if } ((n_1c_1(1+2i_2)+n_2c_2))_N - c_2i_1 = M \\ 0, & \text{otherwise} \end{cases} \tag{3.20}$$

and for class 2 sequency packet,

$$A_{c_1,c_2,i_1,i_2}(n_1,n_2) = \begin{cases} +1, & \text{if } ((n_1c_1(1+2i_1)+n_2c_2))_N - c_2i_2 = 0 \\ -1, & \text{if } ((n_1c_1(1+2i_1)+n_2c_2))_N - c_2i_2 = M \\ 0, & \text{otherwise} \end{cases} \tag{3.21}$$

Eqs. 3.20 and 3.21 differ only by the interchange of i_1 and i_2 according to the column wise or row wise arrangement of phase terms within a packet.

$\langle X, A_{c_1,c_2,i_1,i_2} \rangle$ denotes the inner product of the two $N \times N$ matrices X and A_{c_1,c_2,i_1,i_2}. The SMRT coefficient corresponding to c_1, c_2, i_1, i_2 is simply the inner product of the data matrix with the corresponding basis image. Eq. 3.19 expresses SMRT coefficients, $S_{c_1,c_2}(i_1,i_2)$, as a linear combination of N^2 matrices, A_{c_1,c_2,i_1,i_2} in accordance with data matrix. All basis images of SMRT can be obtained using Eqs. 3.20 & 3.21 by appropriately selecting c_1, c_2, i_1 and i_2. Thus Eq. 3.19 maps an $N \times N$ data $x(n_1,n_2)$, $0 \leq n_1, n_2 \leq N-1$ into a matrix of SMRT coefficients $S_{c_1,c_2}(i_1,i_2)$, $c_1, c_2 = 0, 2^0, 2^1, 2^2, ..., M$; $i_1 = 0, 1, 2, ..., \frac{M}{c_1} - 1$ and $i_2 = 0, 1, 2, ..., \frac{M}{c_2} - 1$. Thus SMRT has become an independent transform rather than a placement algorithm.

3.5.2 Forward SMRT Algorithm

An algorithm to compute and place the SMRT coefficients based on the kernel is presented below. Let X be the $N \times N$ data matrix and

S be the corresponding SMRT matrix. The kernel matrix A_{c_1,c_2,i_1,i_2} can be computed using Eqs. 3.20 and 3.21.

1. *Initialization*

   $v = log_2(M)$

2. *Computation of DC SMRT coefficient,* $S(0,0)$

   $S(0,0) = \langle X, A_{0,0,0,0} \rangle$

3. *Computation and placement of first row and column*

   $a = 1$
   for $i = 0$ to v
   $c_2 = 2^i$
   for $j = 0$ to $\frac{M}{c_2} - 1$
   $S(0,a) = \langle X, A_{0,c_2,0,i_2} \rangle$
   $S(a,0) = \langle X, A_{c_2,0,i_2,0} \rangle$
   $a = a + 1$
   end
   end

4. *Computation and placement of other coefficients*

   $a = 1$
   for $i = 0$ to v
   $c_1 = 2^i$, $i_{1s} = a$, $i_{2s} = a$.
   for $j = 0$ to $log(\frac{M}{c_1})$
   $c_2 = c_1.2^j$
   for $i_2 = 0$ to $\frac{M}{c_2} - 1$

for $i_1 = 0$ to $\frac{M}{c_1} - 1$

$S(i_{1s}, i_{2s}) = \langle X, A_{c_1,c_2,i_1,i_2} \rangle$

if $(c_1 < c_2)$ (*% Computation of related coefficients*)

$S(i_{2s}, i_{1s}) = \langle X, A_{c_2,c_1,i_2,i_1} \rangle$

end

$i_{1s} = i_{1s} + 1$

end

$i_{1s} = i_{1s} - \frac{M}{c_1}$, $i_{2s} = i_{2s} + 1$

end Mapping

end

$a = a + \frac{M}{c_1}$

end

3.5.3 Inverse SMRT Algorithm

Inverse SMRT algorithm based on the kernel is presented below. Let S be the SMRT matrix and X be the corresponding data matrix. Redundancy factors can be found from the sequencies. For class 1 sequency packets, $R(c_1, c_2) = \frac{M}{c_2}$ and for class 2 sequency packets, $R(c_1, c_2) = \frac{M}{c_1}$.

1. *Initialization*

   $v = log_2(M)$

2. *Contributions of DC SMRT coefficient,* $S(0, 0)$
   for $n_1 = 0$ to $N - 1$

   for $n_2 = 0$ to $N - 1$

$x(n_1, n_2) = S(0, 0)$

end

end

3. *Contributions due to first row and column*

$a = 1$
for $i = 0$ to v

$c_2 = 2^i$

for $j = 0$ to $\frac{M}{c_2} - 1$

$X = X + A_{0,c_2,0,i_2} * S(0, a) * \frac{M}{c_2}$

$X = X + A_{c_2,0,i_2,0} * S(a, 0) * \frac{M}{c_2}$

$a = a + 1$

end
end

4. *Contributions due to other coefficients*

$a = 1$
for $i = 0$ to v

$c_1 = 2^i$, $i_{1s} = a$, $i_{2s} = a$.

for $j = 0$ to $log(\frac{M}{c_1})$

$c_2 = c_1.2^j$

for $i_2 = 0$ to $\frac{M}{c_2} - 1$

for $i_1 = 0$ to $\frac{M}{c_1} - 1$

$X = X + A_{c_1,c_2,i_1,i_2} * S(i_{1s}, i_{2s}) * \frac{M}{c_1}$

if $(c_1 < c_2)$

$X = X + A_{c_2,c_1,i_2,i_1} * S(i_{2s}, i_{1s}) * \frac{M}{c_2}$

end

$i_{1s} = i_{1s} + 1$

end

$i_{1s} = i_{1s} - \frac{M}{c_1}$, $i_{2s} = i_{2s} + 1$

end

end

$a = a + \frac{M}{c_1}$

end

$x = \frac{x}{N^2}$

3.6 Conclusion

Sequency ordered placement of unique MRT coefficients in the form an $N \times N$ matrix is proposed. The important highlight is that being an integer-to-integer transform, computations require only additions. SMRT basis functions and placement are discussed. Certain properties under general, statistical and pattern based categories are explored and good results are obtained. SMRT, with its unique sequency ordered basis images, finds applications in many image processing applications. Based on the placement derived for the unique MRT coefficients, SMRT computation is developed as a stand-alone transform.

Chapter 4

Image Quality Assessment Metrics

4.1 Introduction

Evaluation of images, after processing, is an important step to determine how well the images are being processed. Literature shows that most of the commonly used Image Quality Assessment (IQA) metrics cannot adequately describe the visual quality of the enhanced image and there is no universal measure, that specifies both objective and subjective validity of the enhancement for all types of images.

Many metrics are available for the quantitative evaluation of images after processing in the spatial domain. PSNR, SNR, CNR, WSNR, VSNR, NQM, UQI, IFC, SSIM, MSSIM, FSIM, RFSIM, VIF, VIFP, MAE and AMBE are some of the commonly used FR metrics in the literature. EME, EMEE, AME, AMEE, SDME are some of the commonly used BR metrics. Statistical features like entropy, contrast, correlation, homogeneity, energy, mean, standard

deviation etc. can also be used for quality assessment along with other metrics. A study of the existing metrics will be helpful to find a suitable metric for image enhancement.

This chapter is a study about the existing FR & BR IQA metrics for changes in brightness, contrast & sharpness considered separately and a combination of all the three parameters. Analysis is done for general as well as medical images and exposes the importance of image statistical features in quantitative evaluation of image enhancement. A FR IQA metric, entitled Image Enhancement Metric (IEM), is proposed.

Enhancement techniques described in this work are mostly SMRT based and hence a metric that can directly measure the image quality in the SMRT domain will be of much use. SMRT based FR and BR metrics, $\text{IEMS}_{FR}, \text{IEMS}_{BR}$, are also proposed.

4.2 Development of Image Enhancement Metrics

Spatial domain and transform domain metrics, suitable to assess the image quality, are important depending on whether the enhancement is carried out in the spatial or transform domain. Also, a metric which is capable to measure both contrast and sharpness can effectively measure the image quality after enhancement.

4.2.1 Spatial Domain

Changes in sharpness and contrast reflect intensity difference between a pixel and its neighbours. Therefore, it is a straightforward idea to compare the absolute value of intensity difference between

every pixel and its neighbours corresponding to the reference and enhanced images.

Proposed spatial domain FR IQA metric, IEM, can approximate the contrast and sharpness of an image by dividing the image into non-overlapping blocks. The absolute difference between the center pixel and its 8-neighbours for all local windows corresponding to the reference and enhanced image can give an indication of the change in contrast and sharpness. Window size of 3×3 is enough as the metric uses only eight neighbours.

IEM is defined as the ratio of sum of absolute values of the difference of each pixel from its 8-neighbours of all non-overlapping blocks of the enhanced image to the reference image and is mathematically expressed as

$$\mathrm{IEM}_{8n} = \frac{\sum_{l=1}^{b_1} \sum_{m=1}^{b_2} \sum_{n=1}^{8} \left| I_{e,c}^{l,m} - I_{e,n}^{l,m} \right|}{\sum_{l=1}^{b_1} \sum_{m=1}^{b_2} \sum_{n=1}^{8} \left| I_{r,c}^{l,m} - I_{r,n}^{l,m} \right|} \tag{4.1}$$

where the image is divided into $b_1 b_2$ blocks of size 3×3 and $I_{e,c}^{l,m}$, $I_{r,c}^{l,m}$ are the intensities of the centre pixel in $(l,m)^{\text{th}}$ block of the enhanced and reference images respectively. $I_{e/r,n}^{l,m}$, $n = 1, 2, ..., 8$ indicate the 8 neighbours of the centre pixel.

When the reference and enhanced images are identical, IEM=1. IEM > 1 indicates improvement in contrast and sharpness of the image whereas there is deterioration otherwise. Higher the value of IEM, better the improvement in image contrast and sharpness.

The metric can also be defined from the difference of each pixel from its 4-neighbours to reduce the computational overhead.

$$\mathrm{IEM}_{4n} = \frac{\sum_{l=1}^{b_1} \sum_{m=1}^{b_2} \sum_{n=1}^{4} \left| I_{e,c}^{l,m} - I_{e,n}^{l,m} \right|}{\sum_{l=1}^{b_1} \sum_{m=1}^{b_2} \sum_{n=1}^{4} \left| I_{r,c}^{l,m} - I_{r,n}^{l,m} \right|} \tag{4.2}$$

It can be defined alternatively to understand the prominence of vertical or horizontal edges in an image from the horizontal neighbours or vertical neighbours alone as shown below.

$$\mathrm{IEM}_v = \frac{\sum_{l=1}^{b_1}\sum_{m=1}^{b_2}\left|I_{e,c}^{l,m} - I_{e,ls}^{l,m}\right| + \left|I_{e,c}^{l,m} - I_{e,rs}^{l,m}\right|}{\sum_{l=1}^{b_1}\sum_{m=1}^{b_2}\left|I_{r,c}^{l,m} - I_{r,ls}^{l,m}\right| + \left|I_{r,c}^{l,m} - I_{r,rs}^{l,m}\right|} \tag{4.3}$$

$$\mathrm{IEM}_h = \frac{\sum_{l=1}^{b_1}\sum_{m=1}^{b_2}\left|I_{e,c}^{l,m} - I_{e,t}^{l,m}\right| + \left|I_{e,c}^{l,m} - I_{e,b}^{l,m}\right|}{\sum_{l=1}^{b_1}\sum_{m=1}^{b_2}\left|I_{r,c}^{l,m} - I_{r,t}^{l,m}\right| + \left|I_{r,c}^{l,m} - I_{r,b}^{l,m}\right|} \tag{4.4}$$

where $I_{e,ls}^{l,m}$, $I_{e,rs}^{l,m}$, $I_{e,t}^{l,m}$ and $I_{e,b}^{l,m}$ are the intensity of the pixels in the left, right, top and bottom of the centre pixel in $(l,m)^{\text{th}}$ block of the enhanced image.

The metric is later modified to accommodate small variations in pixel values. The modified form of Eq. 4.2 is expressed mathematically as

$$\mathrm{IEM} = \frac{1}{b_1.b_2}\sum_{l=1}^{b_1}\sum_{m=1}^{b_2} 20.\ln\frac{\sum_{n=1}^{4}\left|I_{e,c}^{l,m} - I_{e,n}^{l,m}\right|}{\sum_{n=1}^{4}\left|I_{r,c}^{l,m} - I_{r,n}^{l,m}\right|} \tag{4.5}$$

When the reference and modified images are the same, this measure takes the value as 0 whereas +ve or -ve when there is improvement in contrast and sharpness or deterioration respectively.

4.2.2 SMRT Domain

Spatial domain metrics are disadvantageous for transform based image enhancement techniques due to the added burden of the inverse transform. Hence, it is essential to derive a metric in the same transform domain to assess the quality of the enhanced image.

Thus, a new IQA metric based on SMRT is proposed in this section to assess the quality of SMRT based enhancement techniques.

The basis functions associated with the SMRT coefficients include different combinations of +1 and -1. So the different combinations of the SMRT coefficients can vary the contrast and sharpness of images in the desired manner. The changes in contrast and sharpness of an image in the spatial domain can reflect in a similar manner in SMRT coefficients also. This enables the development of an SMRT based IQA metric.

The analysis of various combinations of SMRT coefficients from different sequency packets shows that the diagonal sequency packets are representative of the changes in contrast and sharpness. Computational complexity is directly related to number of SMRT coefficients involved in the metric computation. Considering these facts and from the analysis of various combinations of the coefficients of the diagonal sequency packets, the diagonal elements of the AC SMRT coefficients are found to be a better choice for the formation of metric in the SMRT domain.

The proposed Blind-Reference SMRT metric, IEMS_{BR}, is defined as the square root of the sum of squares of all diagonal AC SMRT coefficients with respect to size. The Full-Reference SMRT metric, IEMS_{FR} is defined as the ratio of the IEMS_{BR} of the enhanced image to the reference image.

$$\text{IEMS}_{BR} = \frac{100}{N^2}\sqrt{\sum_{i=1}^{N-1} S^2(i,i)} \tag{4.6}$$

$$\text{IEMS}_{FR} = \sqrt{\frac{\sum_{i=1}^{N-1} S_e^2(i,i)}{\sum_{i=1}^{N-1} S_r^2(i,i)}} \tag{4.7}$$

where S_e and S_r correspond to the SMRT matrix of the enhanced and reference images respectively.

For block level enhancement techniques, the evaluation method based on Eqs. 4.6 and 4.7 are not suitable for block level enhancement technique since they consider SMRT as a whole. So modified metrics based on diagonal AC SMRT coefficients of all the blocks of size $B \times B$ are proposed as given below.

$$\text{IEMS}_{BR} = \frac{1}{N^2}\sqrt{\sum_{l=1}^{b_1}\sum_{l=1}^{b_2}\left(\sum_{i=1}^{B-1} S^2(i,i)\right)} \tag{4.8}$$

$$\text{IEMS}_{FR} = \sqrt{\sum_{l=1}^{b_1}\sum_{l=1}^{b_2}\left(\frac{\sum_{i=1}^{B-1} S_e^2(i,i)}{\sum_{i=1}^{B-1} S_r^2(i,i)}\right)} \tag{4.9}$$

4.3 Methodology for Analysis of Assessment Metrics

This study focuses on the usefulness of existing metric and the metrics proposed in sections 4.2.1 & 4.2.2 for various enhancement features such as brightness, contrast and sharpness. The image data chosen to categorize the existing and proposed IQA metrics should carry adequate diversity in contrast, sharpness and spread of histograms etc. Hence eight images each from the general and medical categories are selected. These include standard images like *lena, barbara, cameraman, pelicans, peppers, boat, aeroplane, goldhill* and eight medical images of *lung, brain, prostate, breast* and *bone* as shown in Figs. 4.1 and 4.2.

Primary objectives of the analysis are :

1. Explore the importance of the proposed metrics, IEM, IEMS_{BR} and IEMS_{FR}, in brightness, contrast and sharpness measurements.

Fig. 4.1: General images considered for analysis

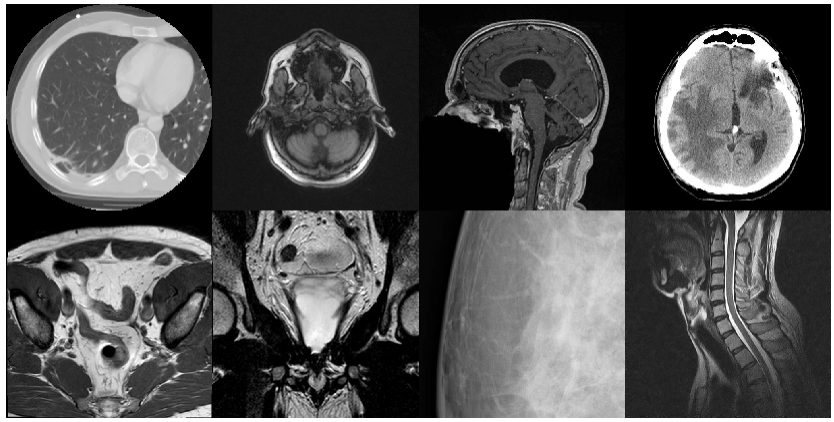

Fig. 4.2: Medical images considered for analysis

2. Performance comparison of the proposed metrics with existing IQA metrics, for image enhancement.

3. Suitability analysis of metrics for quantifying enhancement of both general and medical images.

4. Assessment of statistical parameters for image enhancement.

Variations in image brightness, contrast and sharpness are derived through modification of the images in Figs. 4.1 & 4.2 and a data set of five images each are formed for all 16 images. Brightness is obtained from the linear shift of the histograms with no effect on other two parameters. The image histogram is linearly stretched to the required level for the adjustment of contrast alone. Averaging filters are applied repeatedly to modify sharpness of the images. Five sets each of brightness, contrast and sharpness adjusted images of *lena*, as an example, with their respective histograms are shown in Figs. 4.3, 4.4 & 4.5 respectively.

In Fig. 4.3 the brightness is increased by shifting the image histogram gradually without changing contrast and sharpness The contrast is varied by compressing the image histogram to its centre without changing brightness and sharpness in Fig. 4.4. The image is smoothened successively by averaging filter as in Fig.4.5. However, contrast and brightness values seem to change when averaging filters are used and hence cannot be made constant. All the three parameters are varied simultaneously and the corresponding images with their histograms are shown in Fig. 4.6.

Image Quality 1 (IQ1) stands for the poorest quality image (ie. dark, low contrast, blurred) while IQ5 signifies the best quality image (ie. bright, high contrast, sharp) with respect to brightness, contrast and sharpness. Since optimal enhanced image is not known a priori for image enhancement, most degraded/poor image of the data set, IQ1, is considered as the reference image for the use of FR metrics. IQ2, IQ3, IQ4 and IQ5 are progressively enhanced images. The five images are considered separately for BR metrics and statistical features.

SMRT based BR and FR metrics are computed from the SMRT of the images (IQ1 to IQ5) through the application of Eqs. 4.6 and 4.7.

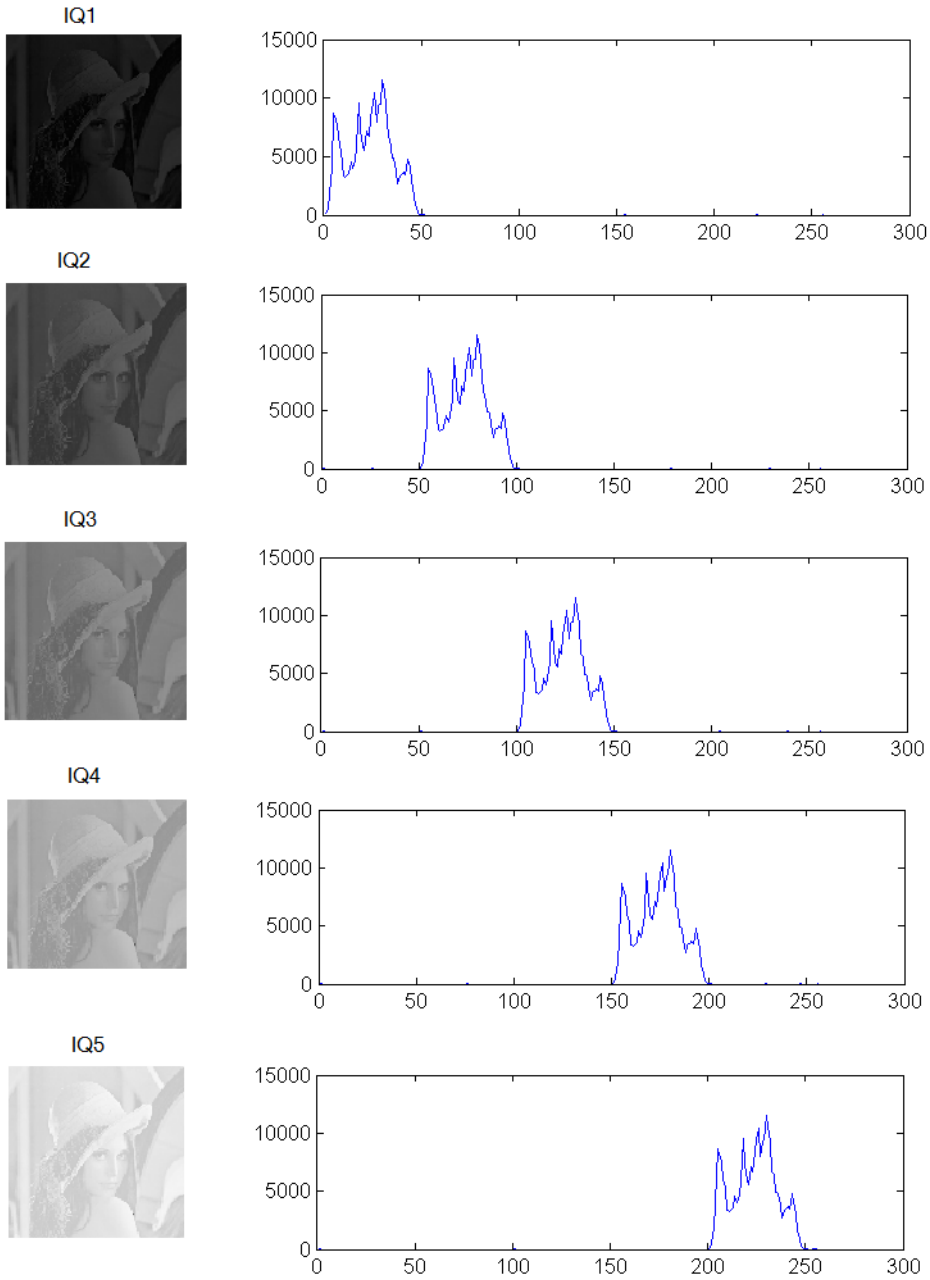

Fig. 4.3: *lena* images of varying brightness and their histograms

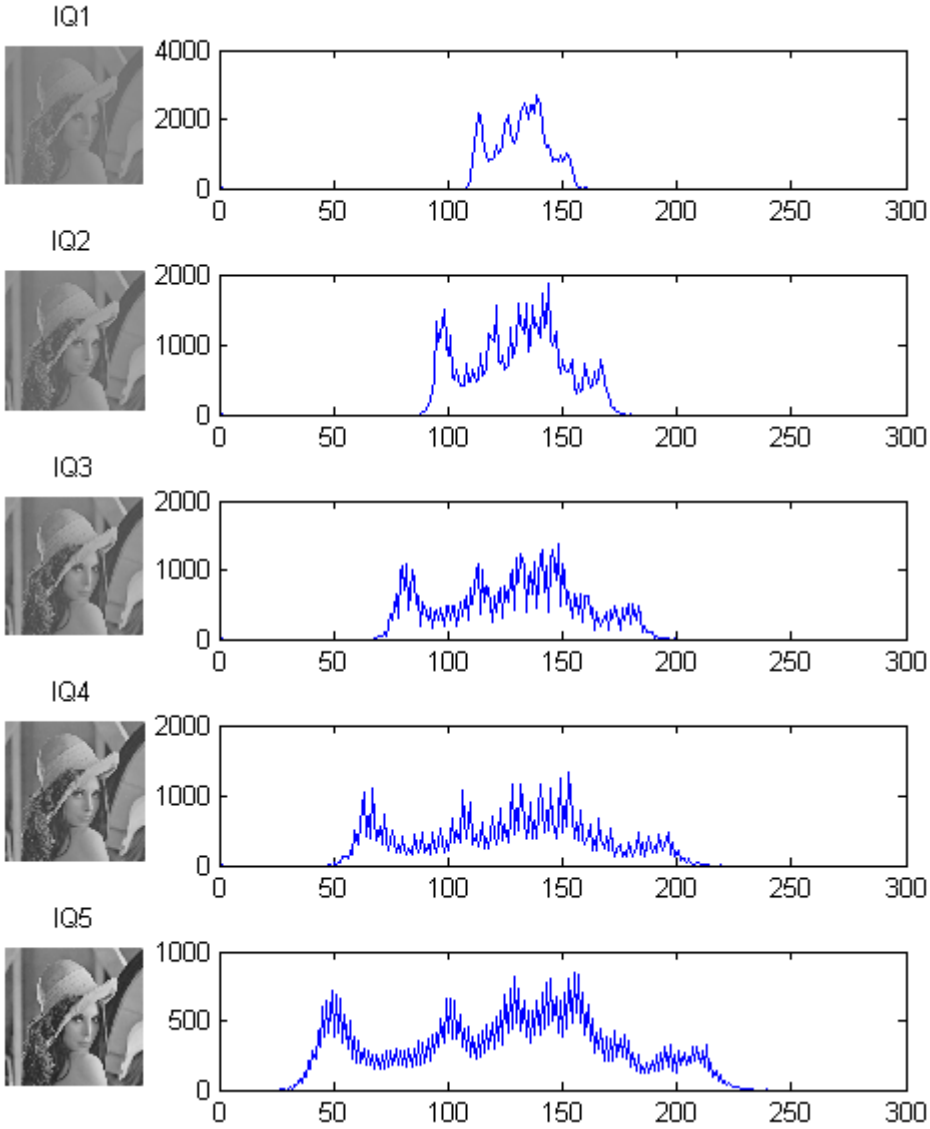

Fig. 4.4: *lena* images of varying contrast and their histograms

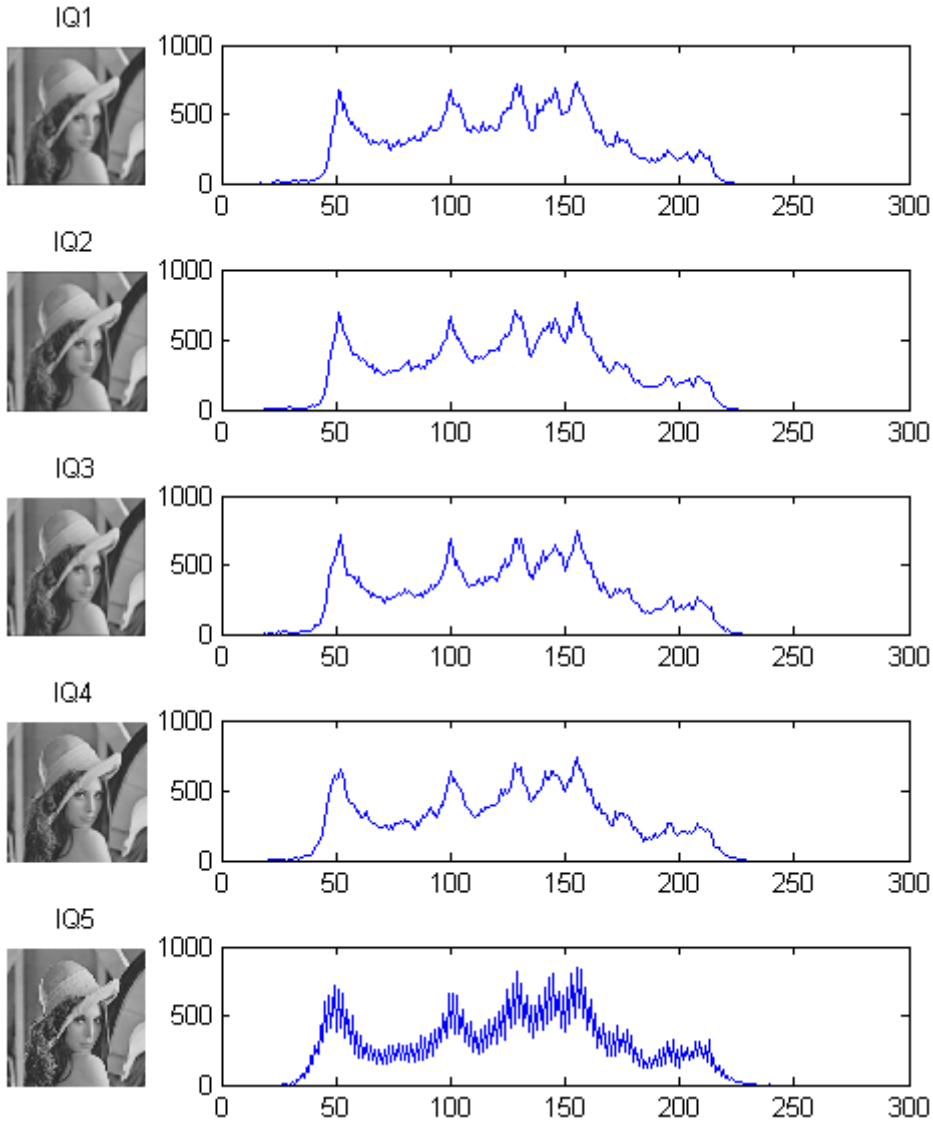

Fig. 4.5: *lena* images of varying sharpness and their histograms

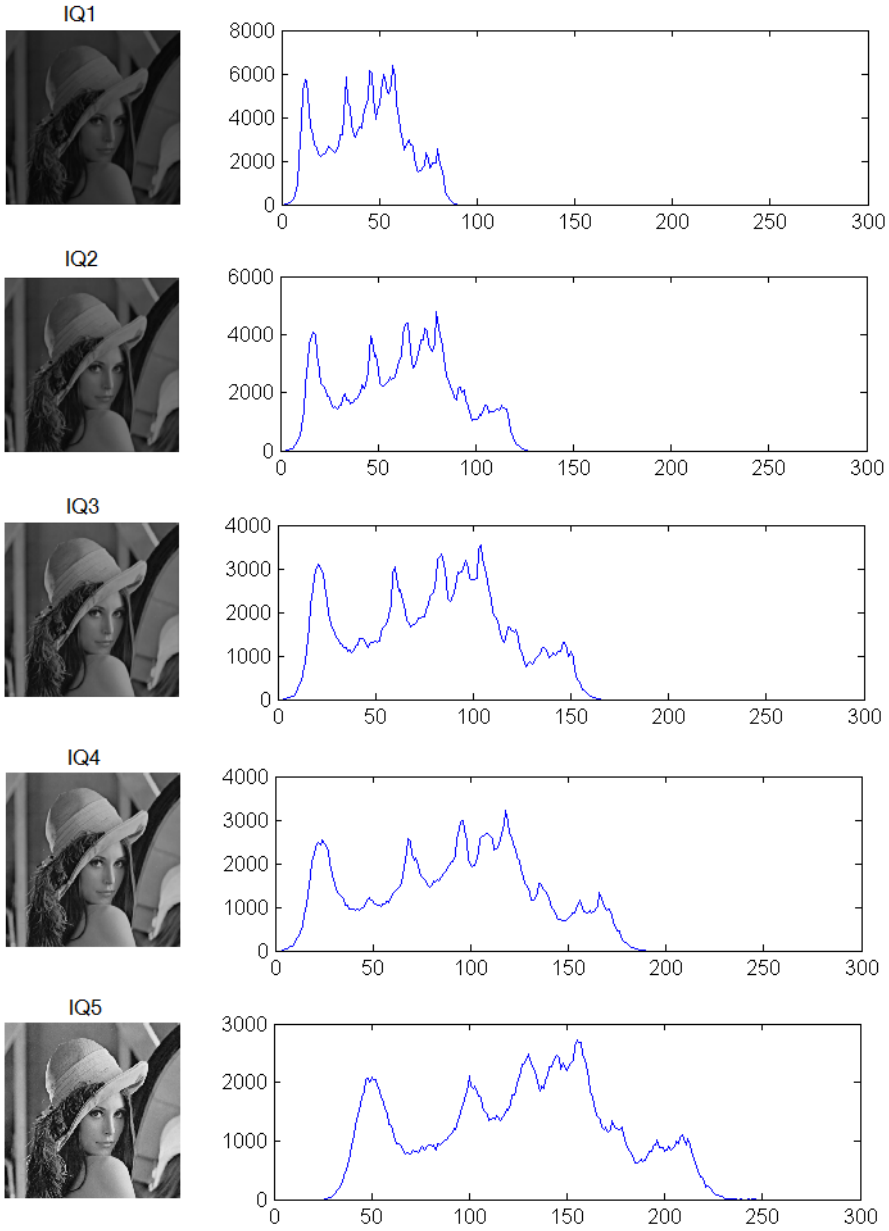

Fig. 4.6: *lena* images of varying combinations of brightness, contrast & sharpness and their histograms

4.4 Simulation Results

The usefulness of the proposed metrics can be analyzed for measurements of brightness, contrast, sharpness & their combination. Existing IQA metrics, as mentioned in section 1.5, along with the proposed metrics, in sections 4.2.1 & 4.2.2, are considered for analysis.

MeTriX MuX package of the Cornell Visual Communication Lab [160] is used to compute PSNR, SNR, WSNR, VSNR, NQM, UQI, IFC, SSIM, MSSIM, VIF, VIFP metrics. FSIM and RFSIM metrics are computed using the on-line code available [161], [162].

Changes in the values of IQA metrics for variations in brightness, contrast, sharpness and their combination are tested. A high value is expected for all FR and BR metrics except MAE & AMBE where these error values should be as small as possible for better similarity between images. Statistical feature values such as correlation and homogeneity should decrease as the contrast and sharpness increases. Homogeneity measures the pixel similarity and correlation measure how adjacent pixels are correlated. The metric values are tabulated for all 16 images and their variations with different parameters are noted. The values in respect of brightness variations for the BR metrics & statistical features, obtained for *lena* image, are listed in Table 4.1 and that for FR metric in Table 4.2. The corresponding contrast metrics values are listed in Tables 4.3 & 4.4, sharpness metrics values in Tables 4.5 & 4.6 and that for a combination of all the three parameters are shown in Tables 4.7 & 4.8 respectively.

Table 4.1: BR metric and statistical feature values of *lena* image for brightness variations

	Metrics	IQ1	IQ2	IQ3	IQ4	IQ5
BR metrics	EME	6.20	1.26	0.73	0.51	0.39
	EMEE	0.94	0.07	0.04	0.03	0.02
	AME	50.36	76.32	86.82	93.62	98.66
	AMEE	0.20	0.10	0.07	0.05	0.04
	SDME	24.29	20.03	11.15	5.46	0
	IEMS_{BR}	3.60	3.60	3.60	3.60	3.60
Statistical features	Entropy	5.30	5.30	5.30	5.30	5.30
	Contrast	0.031	0.042	0.046	0.052	0.054
	Correlation	0.904	0.882	0.899	0.865	0.893
	Homogeneity	0.985	0.979	0.977	0.974	0.973
	Energy	0.65	0.60	0.50	0.61	0.45
	Mean	22.54	72.54	122.54	172.54	222.54
	SD	10.88	10.88	10.88	10.88	10.88

Table 4.2: FR metric values of *lena* image for brightness variations

Metrics	IQ1,IQ2	IQ1,IQ3	IQ1,IQ4	IQ1,IQ5
PSNR(dB)	14.15	8.13	4.61	2.11
SNR(dB)	-6.01	-12.03	-15.55	-18.05
CNR	∞	∞	∞	∞
WSNR(dB)	-5.84	-11.87	-15.39	-17.89
VSNR(dB)	-1.34	-2.88	-3.32	-3.35
NQM	11.84	6.80	4.52	3.00
UQI	0.53	0.34	0.25	0.20
IFC	66.97	66.95	66.94	66.93
SSIM	0.53	0.34	0.25	0.20
MSSIM	0.92	0.87	0.83	0.80
FSIM	0.99	0.98	0.98	0.98
RFSIM	1	1	1	1
VIF	1	1	1	1
VIFP	1	1	1	1
MAE	50	100	150	200
AMBE	50	100	150	200
IEM	0	0	0	0
IEMS_{FR}	1	1	1	1

Table 4.3: BR metric and statistical feature values of *lena* image for contrast variations

	Metrics	IQ1	IQ2	IQ3	IQ4	IQ5
BR metrics	EME	0.74	1.36	2.06	2.90	3.98
	EMEE	0.04	0.08	0.13	0.21	0.35
	AME	87.11	76.17	68.45	62.45	57.31
	AMEE	0.07	0.10	0.13	0.16	0.18
	SDME	11.03	13.72	14.30	15.63	16.60
	IEMS_{BR}	3.94	6.95	9.96	12.99	15.98
Statistical features	Entropy	5.43	6.21	6.69	7.07	7.45
	Contrast	0.04	0.11	0.12	0.20	0.23
	Correlation	0.91	0.90	0.93	0.94	0.95
	Homogeneity	0.98	0.95	0.94	0.91	0.91
	Energy	0.49	0.32	0.23	0.16	0.13
	Mean	130.80	130.80	130.80	130.80	130.80
	SD	11.76	20.77	29.80	38.83	47.85

Table 4.4: FR metric values of *lena* image for contrast variations

Metrics	IQ1,IQ2	IQ1,IQ3	IQ1,IQ4	IQ1,IQ5
PSNR(dB)	28.86	22.85	19.33	16.83
SNR(dB)	23.10	17.08	13.56	11.06
CNR	14.29	7.06	4.64	3.44
WSNR(dB)	23.47	17.45	13.93	11.43
VSNR(dB)	05.40	-0.62	-4.06	-6.47
NQM	23.69	17.67	14.15	11.65
UQI	0.83	0.66	0.53	0.44
IFC	9.44	9.45	9.74	10.17
SSIM	0.96	0.89	0.81	0.73
MSSIM	0.93	0.81	0.70	0.62
FSIM	0.96	0.88	0.81	0.74
RFSIM	0.50	0.17	0.07	0.03
VIF	1.55	2.01	2.40	2.74
VIFP	1.42	1.72	1.95	2.15
MAE	7.50	14.99	22.48	29.97
AMBE	1.68	3.37	5.06	6.75
IEM	10.80	17.76	22.92	29.90
IEMS_{FR}	3.12	6.41	10.89	16.50

Table 4.5: BR metric and statistical feature values of *lena* image for sharpness variations

	Metrics	IQ1	IQ2	IQ3	IQ4	IQ5
BR metrics	EME	1.88	2.06	2.25	2.63	3.98
	EMEE	0.124	0.142	0.161	0.201	0.351
	AME	73.53	73.38	72.39	69.79	57.31
	AMEE	0.11	0.12	0.13	0.14	0.18
	SDME	12.74	13.10	13.60	14.39	16.60
	IEMS_{BR}	13.39	13.66	14.03	14.50	15.98
Statistical features	Entropy	7.39	7.40	7.41	7.42	7.45
	Contrast	0.09	0.10	0.11	0.13	0.23
	Correlation	0.98	0.98	0.97	0.97	0.95
	Homogeneity	0.96	0.95	0.95	0.94	0.91
	Energy	0.16	0.16	0.15	0.15	0.13
	Mean	130.80	130.80	130.80	130.80	130.80
	SD	45.78	46.14	46.58	46.97	47.85

Table 4.6: FR metric values of *lena* image for sharpness variations

Metrics	IQ1,IQ2	IQ1,IQ3	IQ1,IQ4	IQ1,IQ5
PSNR(dB)	35.48	35.59	30.55	26.63
SNR(dB)	29.74	29.84	24.81	20.88
CNR(dB)	28.81	29.22	16.37	10.45
WSNR(dB)	31.44	33.71	27.84	24.77
VSNR(dB)	25.42	26.49	20.02	16.31
NQM	23.59	26.59	20.62	17.49
UQI	0.91	0.88	0.78	0.56
IFC	4.42	4.32	2.71	1.93
SSIM	0.98	0.96	0.92	0.80
MSSIM	0.99	0.99	0.97	0.94
FSIM	0.98	0.98	0.95	0.92
RFSIM	0.73	0.78	0.59	0.47
VIF	0.72	0.78	0.58	0.48
VIFP	0.74	0.76	0.60	0.45
MAE	2.29	2.22	3.97	6.54
AMBE	0.12	0.26	0.38	0.69
IEM	1.12	2.95	5.92	19.86
IEMS_{FR}	1.04	1.10	1.17	1.42

Table 4.7: BR metric and statistical feature values of *lena* image for brightness, contrast and sharpness variations

	Metrics	IQ1	IQ2	IQ3	IQ4	IQ5
BR metrics	EME	2.10	2.24	2.47	2.97	6.24
	EMEE	0.15	0.16	0.18	0.25	1.02
	AME	56.00	62.13	65.41	67.65	51.46
	AMEE	0.118	0.123	0.129	0.140	0.199
	SDME	17.22	17.33	16.82	16.28	18.52
	IEMS_{BR}	5.8	8.4	11.1	14.2	18.5
Statistical features	Entropy	6.13	6.65	7.04	7.35	7.45
	Contrast	0.032	0.046	0.069	0.100	0.288
	Correlation	0.962	0.972	0.976	0.976	0.954
	Homogeneity	0.984	0.977	0.956	0.950	0.889
	Energy	0.396	0.269	0.195	0.157	0.105
	Mean	42.28	60.19	78.21	96.37	114.82
	SD	19.19	27.51	36.06	45.02	55.46

Table 4.8: FR metric values of *lena* for brightness, contrast and sharpness variations

Metrics	IQ1,IQ2	IQ1,IQ3	IQ1,IQ4	IQ1,IQ5
PSNR(dB)	22.21	16.14	12.55	9.88
SNR(dB)	7.41	1.35	-2.24	-4.91
CNR	7.18	4.59	3.67	3.05
WSNR(dB)	7.59	1.52	-2.06	-4.66
VSNR(dB)	7.30	-1.76	-7.86	-12.52
NQM	7.65	1.51	-2.13	-4.82
UQI	0.78	0.58	0.39	0.16
IFC	6.10	5.27	4.28	3.27
SSIM	0.93	0.79	0.64	0.42
MSSIM	0.95	0.86	0.74	0.60
FSIM	0.97	0.91	0.82	0.72
RFSIM	0.69	0.34	0.14	0.05
VIF	1.26	1.46	1.52	1.42
VIFP	1.21	1.23	1.09	0.71
MAE	17.91	35.94	54.10	72.69
AMBE	17.91	35.93	54.09	72.54
IEM	4.82	9.12	13.71	29.52
IEMS_{FR}	2.10	3.72	6.03	10.31

4.5 Analysis of Assessment Metrics

A comparison of changes in the values of the IQA metrics and statistical features for variations in brightness, contrast, sharpness and a combination of the three corresponding to the 16 images are shown in Table 4.9. The symbols used in the table have the following meaning.

- D : Decreases.
- I : Increases.
- C : Constant.
- NP : Variation not in Proper order.
- * : For majority of images, the mentioned variation is true but for a few images there is deviation from the mentioned variation.

Following observations are made based on Table 4.9.

1. Brightness :
   (a) Values of PSNR, SNR, WSNR, VSNR, NQM, UQI, IFC, SSIM, MSSIM, FSIM, EME, EMEE, AMEE and SDME decrease with increase in image brightness for medical as well as general images.
   (b) Values are constant for CNR, RFSIM, VIF, VIFP, IEM, IEMS_{FR}, IEMS_{BR}, entropy and SD.
   (c) MAE, AMBE, AME and mean give increasing values with increase in image brightness.
   (d) The values of statistical features such as contrast, correlation and homogeneity have no fixed variation pattern for all types of images.

Table 4.9: Comparison of assessment metrics and statistical features

Metrics	Brightness		Sharpness		Contrast		Combination	
	General	Medical	General	Medical	General	Medical	General	Medical
PSNR	D	D	D *	D *	D	D	D	D
SNR	D	D	D *	D *	D	D	D	D
CNR	∞	∞	D *	D *	D	D	D	D
WSNR	D	D	D *	D *	D	D	D	D
VSNR	D	D	D *	D *	D	D	D	D
NQM	D	D	D *	D *	D	D	D	D
UQI	D	D	D	D	D	D	D	D
IFC	D *	D	D	D	D *	D	D	D
SSIM	D	D	D	D	D	D	D	D
MSSIM	D	D	D	D *	D	D	D	D
FSIM	D	D	D	D *	D	D	D	D
RFSIM	C	C	D *	D *	D	D	D	D
VIF	C	C	D *	D *	I	I	NP	NP
VIFP	C	C	D *	D *	I	I	NP	NP
MAE	I	I	I *	I *	I	I	I	I
AMBE	I	I	I	I *	I	I	I	I
IEM	C	C	I	I	I	I	I	I
$IEMS_{FR}$	C	C	I	I	I	I	I	I
EME	D	D	I	I *	I	I *	I	NP
EMEE	D	D	I	I *	I	I	I	NP
AME	I	I	D *	D *	D	D *	NP	NP
AMEE	D	D	I	I *	I	I *	NP	NP
SDME	D	D	I	I *	I *	I *	NP	NP
$IEMS_{BR}$	C	C	I	I	I	I	I	I
Entropy	C	C	I *	NP	I	I	NP	NP
Contrast	NP	NP	I	I	I	NP	NP	I
Correlation	NP	NP	D	D	I *	NP	NP	NP
Homogeneity	NP	NP	D	D	D	NP	D	D
Mean	I	I	NP	NP	C	C	I	I
SD	C	C	NP	NP	I	I	I	I

(e) Objective scores obtained for AME and mean are highly consistent with increase in brightness for general as well as medical images. Hence these metrics can be used for measuring the brightness improvement for all types of images. A plot of the above metrics for brightness variations in the case of general images is shown in Fig.4.7

2. Contrast :

(a) Values of PSNR, SNR, CNR, WSNR, VSNR, NQM,

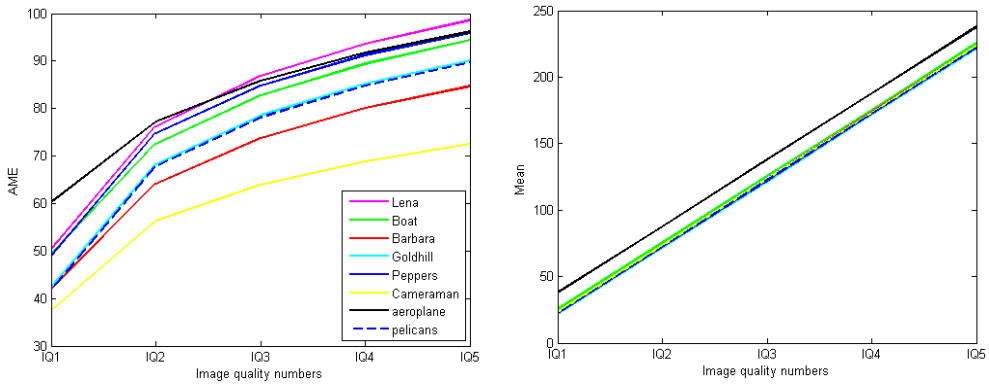

Fig. 4.7: Plot of useful parameters for increasing variations of brightness

UQI, SSIM, MSSIM, FSIM and RFSIM decrease with increase in image contrast for all medical as well as general images under study.

(b) VIF, VIFP, MAE, AMBE, IEM, IEMS$_{FR}$, IEMS$_{BR}$, EMEE, entropy and SD give increasing values with increase in image contrast for all images. EME, AMEE, SDME values increase for most of the images.

(c) Statistical parameters like contrast and correlation values increase whereas homogeneity decreases with image contrast for general images. There is no fixed variation pattern for medical images.

(d) Objective scores obtained for VIF, VIFP, IEM, IEMS$_{FR}$, EMEE, IEMS$_{BR}$, entropy and SD are highly consistent with subjective measures for natural as well as medical images. Hence these metrics can be used for measuring the contrast improvement for all types of images. A plot of the above metrics for contrast variations is shown in Fig.4.8

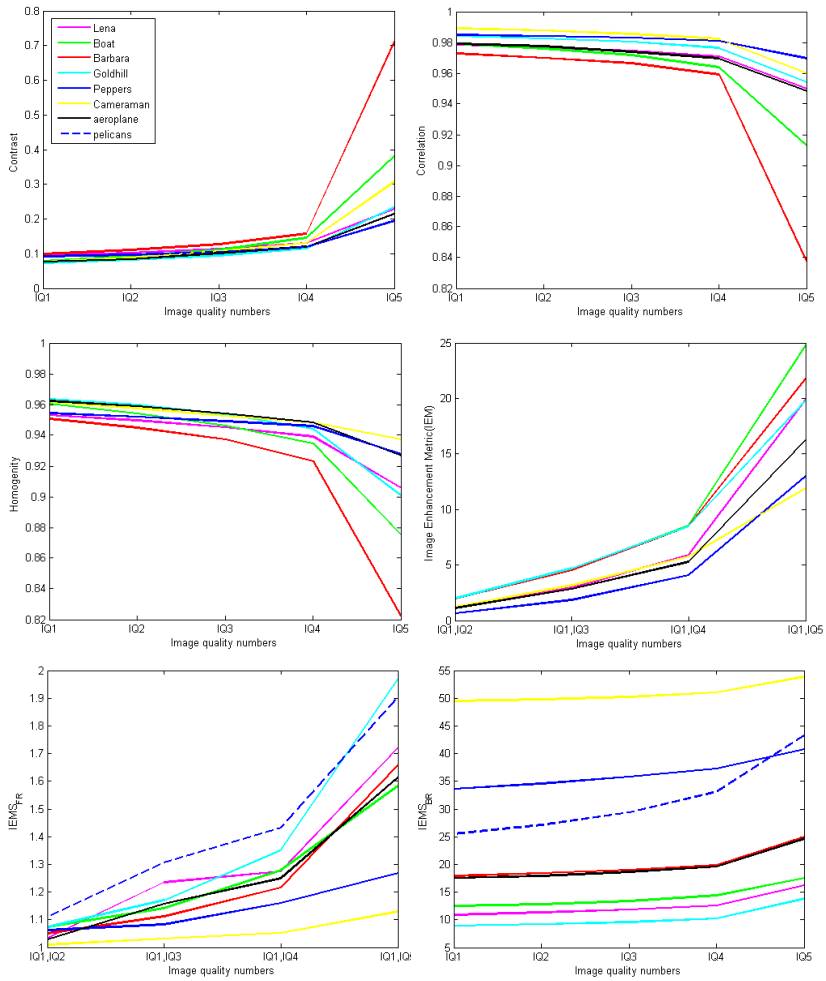

Fig. 4.8: Plot of useful parameters for increasing variations of contrast

3. Sharpness :

   (a) Scores obtained for PSNR, SNR, CNR, WSNR, VSNR, NQM, UQI, IFC, SSIM, MSSIM, FSIM, RFSIM, VIF, VIFP, AME, correlation and homogeneity generally decrease with increase in image sharpness.

(b) Values of IEM, IEMS$_{FR}$, IEMS$_{BR}$ and statistical contrast feature increase strictly with increase in image sharpness.

(c) Use of averaging filters affects contrast and brightness of images and hence there are variations for mean and SD.

(d) Objective scores obtained for IEM, IEMS$_{FR}$, IEMS$_{BR}$ and the statistical contrast, correlation and homogeneity features are highly consistent with subjective measures for medical and general images. A plot of the above metrics with sharpness variations is shown in Fig.4.9.

4. Combined Brightness, Contrast and Sharpness :

(a) Values of PSNR, SNR, CNR, WSNR, VSNR, NQM, UQI, IFC, SSIM, MSSIM, FSIM, RFSIM and homogeneity decrease with increase in image quality for medical as well as general images.

(b) MAE, AMBE, IEM, IEMS$_{FR}$, IEMS$_{BR}$, mean and SD give increasing values with increase in image quality.

(c) There is no fixed variation pattern for VIF, VIFP, EME, EMEE, AME, AMEE, SDME and the statistical features such as entropy, contrast and correlation.

(d) Objective scores obtained for IEM, IEMS$_{FR}$, IEMS$_{BR}$, mean, homogeneity and SD are highly consistent with subjective measures for natural as well as medical images. Hence these metrics can be used to measure a combination of brightness, contrast and sharpness improvements for all types of images. A plot of the above metrics for variations in the parameters is shown in Fig.4.10

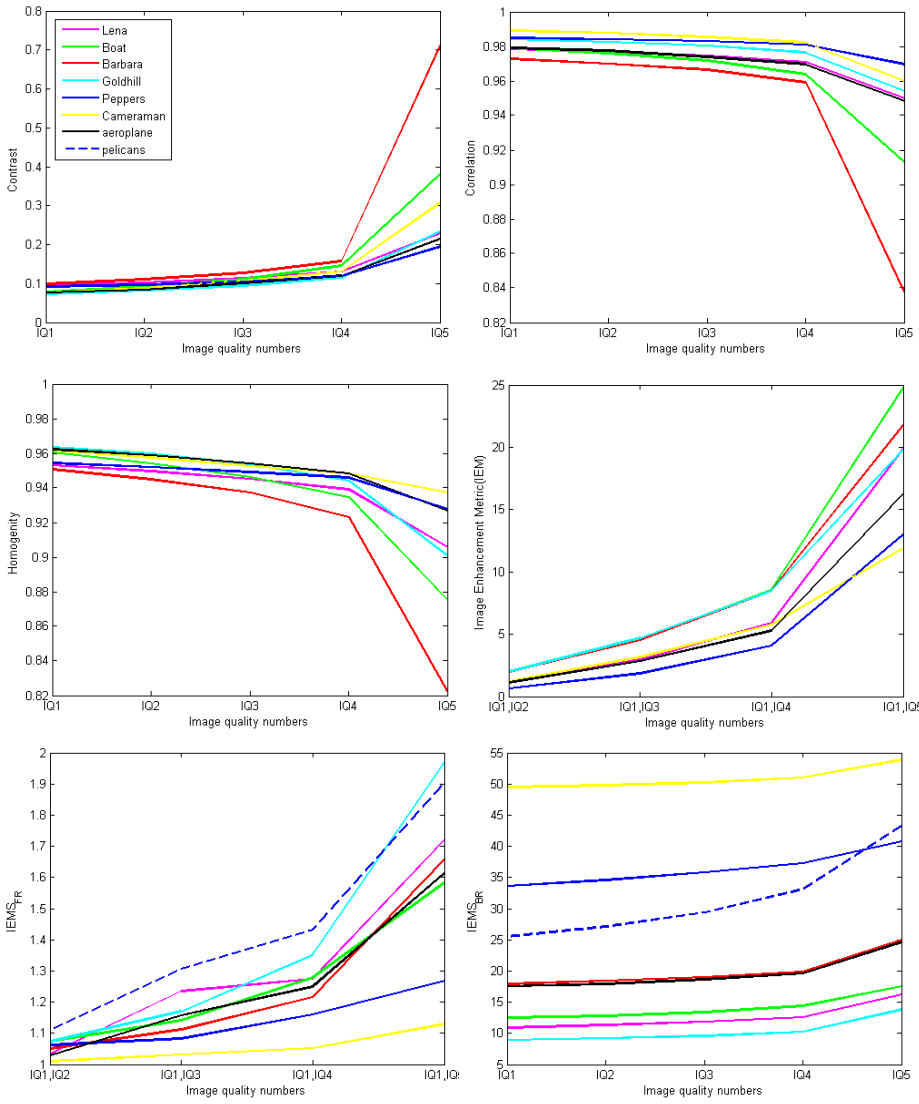

Fig. 4.9: Plot of useful parameters for increasing sharpness variations

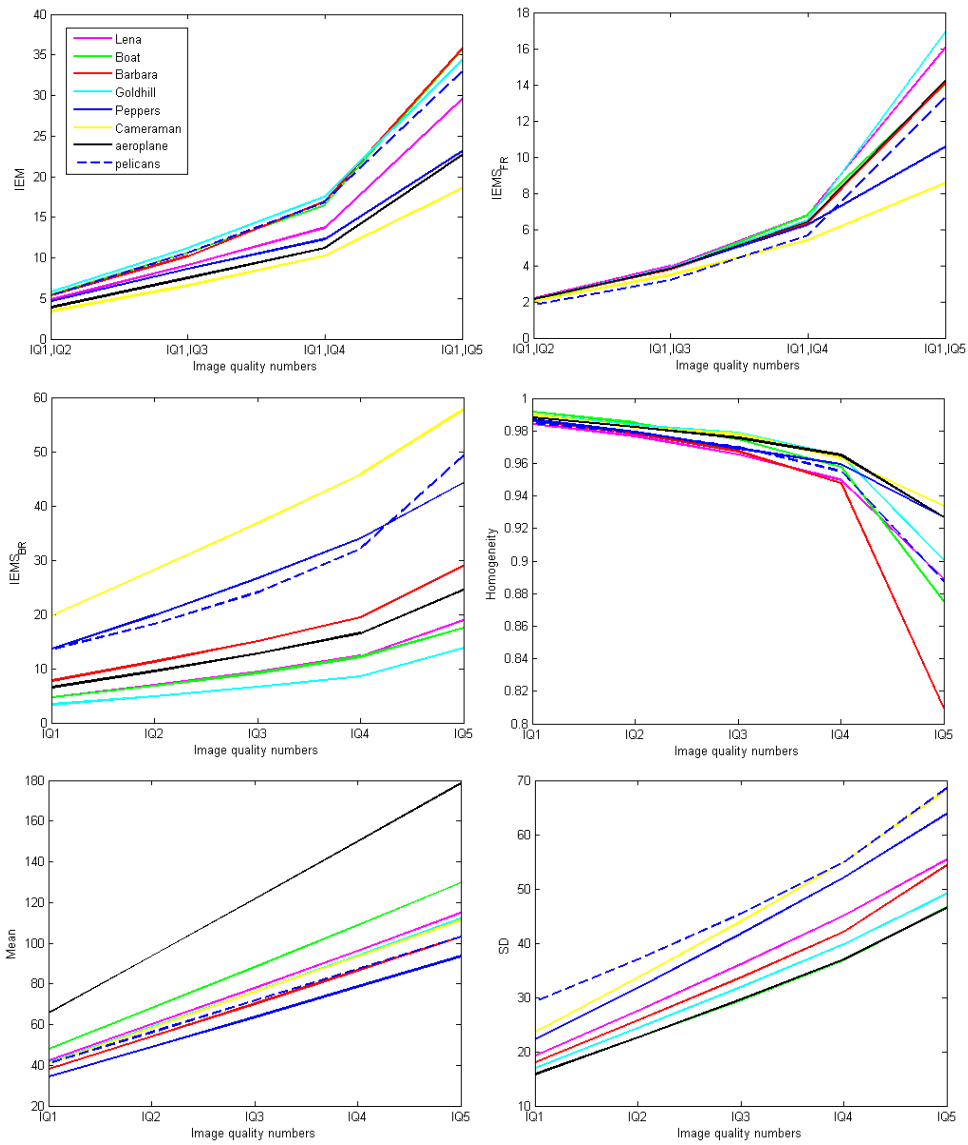

Fig. 4.10: Plot of useful parameters for increasing variations of brightness, sharpness and contrast

4.6 Identification of Useful Assessment Metrics

Useful variations in quantitative metrics for brightness, contrast, sharpness and their combination are considered for general and medical images separately and the metrics variations are tabulated in Table 4.10. The list of useful metrics for all types of images under study is given in Table 4.11 and the following observations are drawn from the table.

- AME can be used to measure brightness variations only.
- VIF, VIFP, EMEE and entropy can be used to measure contrast variations only.
- Statistical parameters like contrast and correlation can be used to measure sharpness only.
- Mean gives an indication of the brightness variations.
- SD gives a measure of the histogram spread and hence contrast.
- IEM, IEMS$_{FR}$, IEMS$_{BR}$ along with homogeneity, mean & SD can be used for enhancement which is a combination of brightness, contrast and sharpness improvements.

Metrics which are capable to assess variations such as contrast and sharpness of general as well as medical images is the proposed metrics, IEM, IEMS$_{FR}$ and IEMS$_{BR}$. Mean gives a measure of the brightness whereas SD accords a measure of contrast. So, in spatial domain image enhancement applications, IEM along with mean and SD can be used for contrast and sharpness measurements. Metrics such as IEMS$_{FR}$ and IEMS$_{BR}$, along with mean and SD (Mean and SD can be measured from SMRT coefficients as given in Eqs. 3.12 and 3.13) can be used for enhancement applications in the SMRT domain.

Table 4.10: Usefulness of assessment metrics and statistical features for image enhancement

Metrics	Brightness		Sharpness		Contrast		Combination	
	General	Medical	General	Medical	General	Medical	General	Medical
VIF	Constant	Constant	-	-	Yes	Yes	-	-
VIFP	Constant	Constant	-	-	Yes	Yes	-	-
IEM	Constant	Constant	Yes	Yes	Yes	Yes	Yes	Yes
$IEMS_{FR}$	Constant	Constant	Yes	Yes	Yes	Yes	Yes	Yes
EMEE	-	-	Yes	-	Yes	Yes	Yes	-
AME	Yes	Yes	-	-	-	-		
SDME	-	-	Yes	-	-	-	-	-
$IEMS_{BR}$	Constant	Constant	Yes	Yes	Yes	Yes	Yes	Yes
Entropy	Constant	Constant	-	-	Yes	Yes	-	-
Contrast	-	-	Yes	Yes	Yes	-	-	Yes
Correlation	-	-	Yes	Yes	-	-	-	-
Homogeneity	-	-	Yes	Yes	Yes	-	Yes	Yes
Mean	Yes	Yes	-	-	Constant	Constant	Yes	Yes
SD	Constant	Constant	-	-	Yes	Yes	Yes	Yes

Table 4.11: Usefulness of assessment metrics and statistical features for all types of images

Metrics	Brightness	Sharpness	Contrast	Combination
VIF	-	-	Yes	-
VIFP	-	-	Yes	-
IEM	-	Yes	Yes	Yes
$IEMS_{FR}$	-	Yes	Yes	Yes
EMEE	-	-	Yes	-
AME	Yes	-	-	-
$IEMS_{BR}$	-	Yes	Yes	Yes
Entropy	-	-	Yes	-
Contrast	-	Yes	-	-
Correlation	-	Yes	-	-
Homogeneity	-	Yes	-	Yes
Mean	Yes	-	-	Yes
SD	-	-	Yes	Yes

4.7 Validation

Validation of the useful metrics listed in Table 4.11 is an important step towards successful development of practical IQA metrics. Categorical Subjective Image Quality (CSIQ)[163] database of the

Computational Perception and Image Quality Lab is used for the validation of the above study for general images and to find the usefulness of the proposed metrics. It consists of 30 general images, each at four levels of contrast and five levels of sharpness variations. The images are natural images from animal, landscape, people, plants and urban categories. They are subjectively rated based on a linear displacement of the images across four calibrated LCD monitors placed side by side with equal viewing distance to the observer. Validation of brightness and combined changes in brightness, contrast and sharpness are done by generating 5 levels of the 30 original images from the CSIQ database.

Validation of medical images is done by deriving 5 brightness, contrast, sharpness and their combinations from 30 medical images of abdomen, brain, teeth, prostate, bone and breast. Total number of images used for testing and validation are shown in Table 4.12

Table 4.12: Number of images used for analysis

	Variations	Testing(8)	validation (30)
General	Brightness	5x8	5x30
	Contrast	5x8	4x30
	Sharpness	5x8	5x30
	All three	5x8	5x30
Medical	Brightness	5x8	5x30
	Contrast	5x8	5x30
	Sharpness	5x8	5x30
	All three	5x8	5x30
Total		320	1170

All metrics listed in Table 4.11 are used for validation and the results are shown in Table 4.13. On comparison, the validation results obtained are in excellent agreement with test results.

Table 4.13: Validation results of useful metrics and statistical features

Metrics	brightness	Sharpness	Contrast	Combination
VIF	True	-	True	-
VIFP	True	-	True	-
IEM	True	True	True	True
$IEMS_{FR}$	True	True	True	True
EMEE	-	-	True	-
AME	True	-	-	-
$IEMS_{BR}$	True	True	True	True
Entropy	True	-	True	-
Contrast	-	True	-	-
Correlation	-	True	-	-
Homogeneity	-	True	-	True
Mean	True	True	True	True
SD	True	True	True	True

4.8 Conclusion

Image Enhancement Metric (IEM) in the spatial domain and SMRT based FR and BR metrics, $IEMS_{FR}$ & $IEMS_{BR}$, are proposed. Study of 18 FR IQA (including the proposed metrics), 6 BR IQA (including the proposed metric) and 7 statistical feature metrics is performed for image enhancement applications. It has been observed that measures such as mean and AME can be used to assess the brightness alone and VIF, VIFP, EMEE, SD and entropy to judge contrast alone. The proposed IQA metrics can be used to evaluate improvements in contrast, sharpness and their combination for general and medical images. A validation is also done to substantiate the findings obtained from the analysis. All the above proposed metrics are computationally simple and can be used for all types of images.

Chapter 5

SMRT based Global Image Enhancement Techniques

5.1 Introduction

The important goal of image enhancement is to have the processed image more suitable than the original image for required task or purpose. It can be done in two ways - global enhancement and block level enhancement. Global enhancement method utilizes the entire image for intensity transformation and visual quality of low contrast image can be improved globally. In block level enhancement methods, image is divided into blocks and intensity transformation is applied on every block.

Most of the image enhancement techniques are performed in the spatial domain. Converting an image into transform domain offers additional capabilities that are very powerful, but requires some new way to interpret data.

The competence of SMRT in linear and nonlinear global image en-

hancement is investigated in this chapter. Visual appearance of an image can be significantly enhanced by brightness improvement and contrast stretching. Here the image brightness and contrast are improved by modifying DC and AC SMRT coefficients separately. Both techniques are compared with image enhancement using Histogram Equalization (HE), one of the well known global image enhancement techniques in spatial domain. The scope of SMRT in sharpness enhancement is also examined. Similar enhancement methods applied to wavelet transform coefficients are also verified.

The effectiveness of the above methods are quantitatively assessed using the existing metrics such as VIFP, SDME, EMEE and proposed metrics IEM, IEMS_{FR} and IEMS_{BR}.

5.2 Linear Enhancement Technique

Uniform scaling is the simplest linear contrast stretching method and this technique is applied in Linear Enhancement Technique (LET). The pixel values in the original and the modified images follow a linear relationship and distribute the pixel values linearly between the extremes of histogram range. Monochrome images of size $N \times N$ contain N^2 pixels, described by gray level intensities, whereas colour images of the same size contain 3 arrays of N^2 pixel level intensities corresponding to three components of colour scheme. So, gray-scale images and colour images are considered separately while discussing image enhancement techniques.

5.2.1 Gray-scale Images

The section deals with linear enhancement technique for gray-scale images based on SMRT discussed in chapter 3. The improvements

in brightness and contrast are investigated by applying scaling factors c_{dc} and c_{ac} on DC & AC SMRT coefficients respectively.

The brightness and contrast adjusted SMRT matrix can be expressed as

$$\tilde{S}(i,j) = \begin{cases} c_{dc}.S(i,j), & \text{if } i = j = 0 \\ c_{ac}.S(i,j), & \text{otherwise} \end{cases}$$

Experimental studies show that if c_{dc}>1, the histogram shifts in the increasing direction of intensity levels (right) and if it is less than one, the histogram shifts in the decreasing direction of intensity levels (left) without changing its shape and span. Hence, the brightness of the image can be increased as shown in Fig. 5.1, by scaling S(0,0), without any change in the contrast.

Experimental studies also show that the SD and contrast of an image can be changed by scaling AC SMRT coefficients while preserving the image mean. The histogram gets stretched or compressed when the scaling factor c_{ac} is greater or less than one and accordingly modifying the image contrast. Fig. 5.2 shows changes in contrast of the image and the corresponding histograms for different values of c_{ac}.

The histogram stretches and extends to both ends when c_{ac} is made higher and higher. The histogram gets split and depart to the two ends when this value is increased further. Finally it becomes a black and white image with values '0' and '255'.

The image mean or centre of the image histogram can be brought to the centre of histogram range ($2^{(n-1)}$ is the centre of histogram range for n bit image representation) by scaling $S(0,0)$ for maximum enhancement. Then, contrast can be maximized by scaling AC SMRT coefficients.

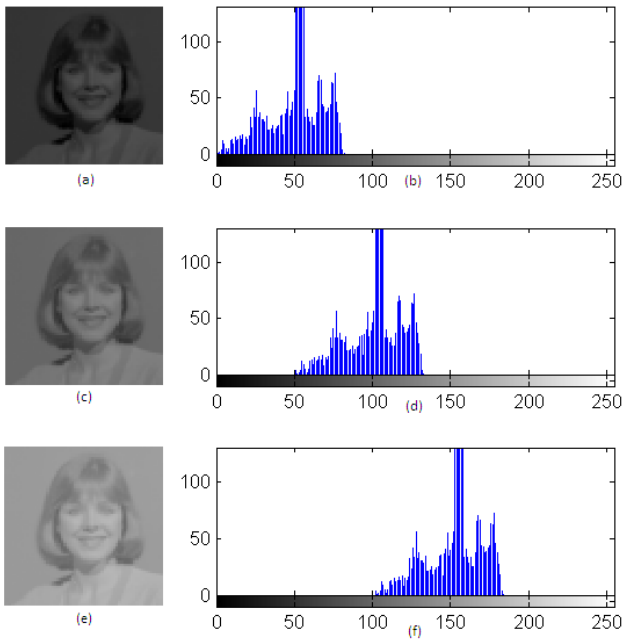

Fig. 5.1: Images and their histograms (a)&(b) Original (c)&(d) c_{dc}=2, c_{ac}=1 (e)&(f) c_{dc}=3, c_{ac}=1

5.2.1.a Brightness variations: DC SMRT coefficient

Scaling of DC SMRT coefficient, to improve brightness, can be done in two ways. In the first method, the scaling is done so as to bring the image mean to the centre of histogram range. The centre of image histogram is shifted to the centre of histogram range in the second method.

Modification of Image Mean Average value or mean, μ_s, of an image can be found from DC SMRT coefficient using Eq. 3.12. When c_{dc} is changed regularly, regular shifts in image mean is observed without any change in SD. The lower(r_l) and upper(r_h) val-

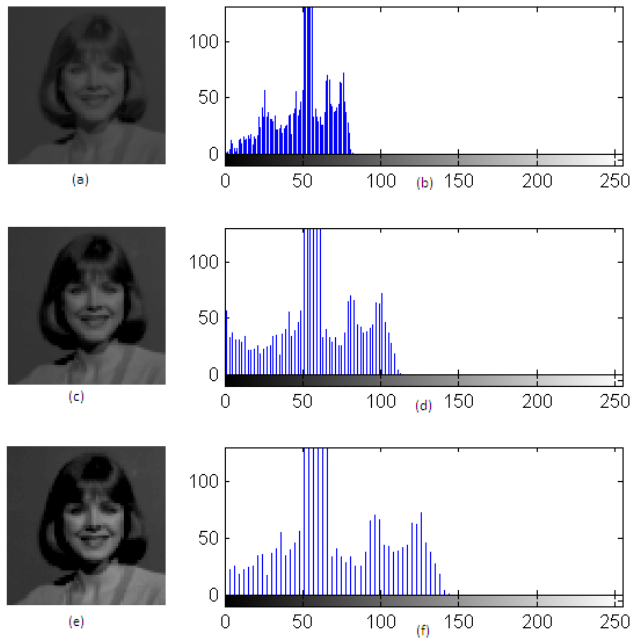

Fig. 5.2: Images and their histograms (a)&(b) Original (c)&(d) c_{dc}=1, c_{ac}=2 (e)&(f) c_{dc}=1, c_{ac}=3

ues of the image histogram also change in a linear manner. A plot of scaling factor versus μ_s, r_l and r_h values for *lena* image is shown in Fig. 5.3. The histogram span, $r_h - r_l$, is same for various c_{dc} values.

The shift in histogram to bring the image mean to the centre of histogram range ($2^{(n-1)}$) can be found from

$$r_{shift} = 2^{(n-1)} - \mu_s = \frac{\tilde{S}(0,0) - S(0,0)}{N^2} \tag{5.1}$$

Thus DC scaling factor,

$$c_{dc} = \frac{r_{shift} * N^2}{S(0,0)} + 1 \tag{5.2}$$

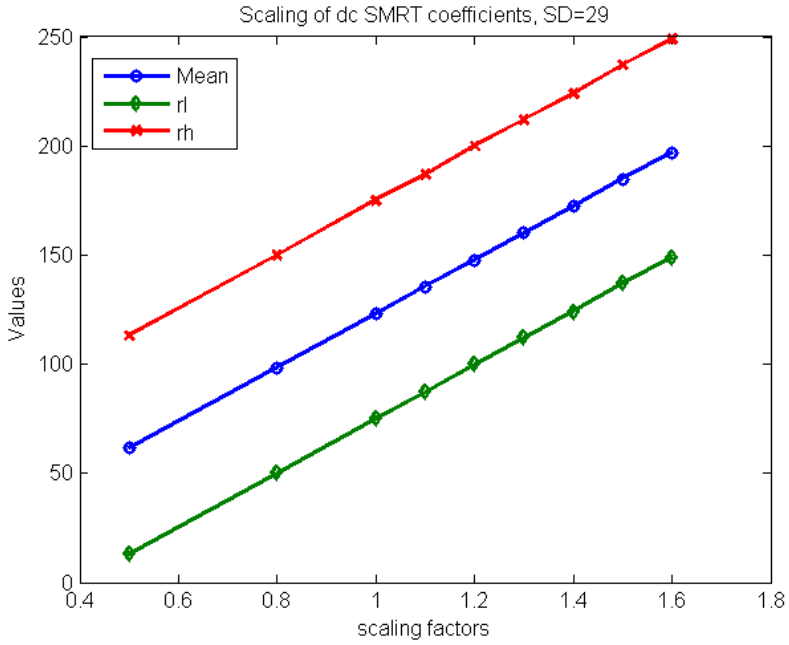

Fig. 5.3: Plot of mean, r_l and r_h of *lena* image for changes in c_{dc}

Shift of Image Histogram Centre The centre of image histogram, r_c, can be found from r_l and r_h values of the image histogram as given below.

$$r_c = (r_l + r_h)/2 \tag{5.3}$$

The histogram shift to change the image histogram centre to $2^{(n-1)}$ is

$$r_{shift} = 2^{(n-1)} - r_c \tag{5.4}$$

and c_{dc} can be found from equation(5.2).

So by scaling $S(0,0)$ alone, the image mean and hence brightness can be varied with no change in SD.

5.2.1.b Contrast variations: AC SMRT Coefficients

Image histogram can be stretched suitably by scaling AC SMRT coefficients. Fig. 5.4 shows a linear relationship between the scaling factor c_{ac} and the parameters SD, r_l and r_h for *lena* image. Histogram spread, $r_h - r_l$, also increases in a linear manner with increase in c_{ac}. A scaling factor which stretches the histogram to its ends gives the maximum contrast.

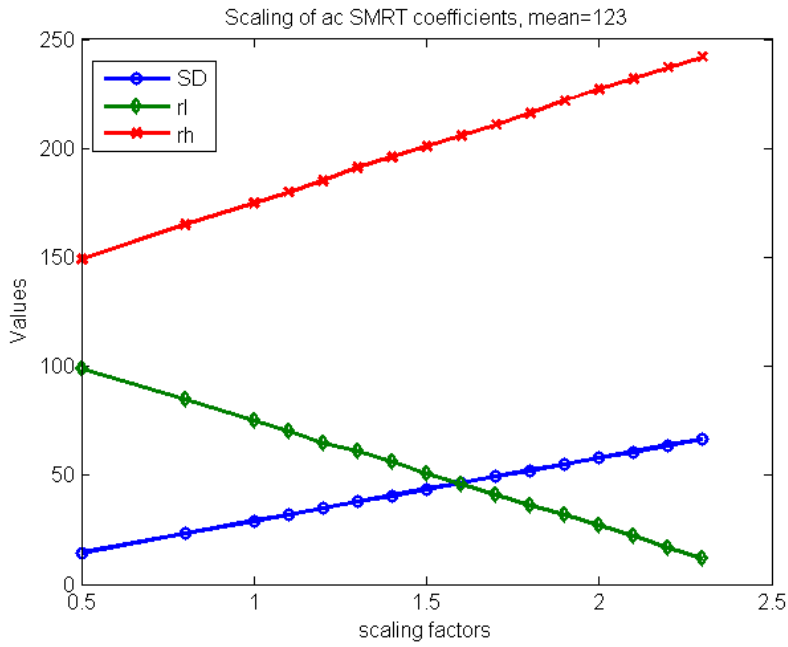

Fig. 5.4: Plot of SD, r_l and r_h of *lena* image for changes in c_{ac}

The shift in maximum pixel value, r_{hshift}, for 0.1 increase in scaling factor is calculated. The AC scaling factor is determined as

$$c_{ac} = \frac{2^n - (r_h + r_{shift})}{10 * r_{hshift}} + 1 \tag{5.5}$$

5.2.1.c Sharpness Variations

Image edges play an important role in improving visual quality. Sharpening techniques enhance the edges by improving borders and details. Transform based sharpness enhancement methods generally modify high frequency components.

The effect of scaling a selected set of SMRT coefficients is illustrated using examples. Fig. 5.5 shows the original and reconstructed images with all the diagonal blocks, except DC SMRT coefficient, scaled by 1.5. Here, quarter of image is seen to superimpose with the four quadrants. This effect is clearly visible in *cameraman* image.

Fig. 5.6 demonstrates the effect of scaling sequency packets on the diagonal of the SMRT matrix with a scaling factor 1.5. Here, as the scaling is restricted only to high sequency components, the images seem to appear sharp without distortion in the homogeneous regions. Best results are obtained when the SMRT coefficients with $c_1, c_2 \geq 16$ are scaled. The SMRT coefficients with $c_1, c_2 \geq 16$ are scaled using different scaling factors 1.5, 2, 2.5 and the original & reconstructed images of *lena* image are shown in Fig. 5.7. Distortion increases as the scaling factor is increased.

The above analysis shows that scaling the high sequency SMRT coefficients may not sharpen images. In SMRT, basis functions take values +1, -1 or 0, indicating that the pixel at the respective position is completely added, subtracted or not considered at all. So selective scaling of high sequency coefficients results in sharpness of edges and at the same time distortions can be seen at the homogeneous regions with artifacts more prominent as scaling factor is increased.

Fig. 5.5: (a)Original images (b)Reconstucted images by scaling uniformly all diagonal blocks having same row column sequency by a factor 1.5

5.2.2 Extension to Colour Images

The scope of the enhancement technique discussed in section 5.2.1 is investigated for colour images. Colour image can be enhanced either in the RGB space or it can be done in the perceptual colour spaces. Many colour spaces are defined and some of them are HSV, YCbCr, YUV, YIQ etc.

When humans see a colour, they interpret it by its luminance and chrominance components. However the RGB colour space does not correspond well to how humans interpret colours in such a way.

Fig. 5.6: (a)Original *lena* image, reconstructed image by scaling uniformly (b) $c_1, c_2 \geq 4$ (c)$c_1, c_2 \geq 8$ (d) $c_1, c_2 \geq 16$ by a factor 1.5

Fig. 5.7: (a)Original *lena* image (b) Reconstructed image by scaling uniformly $c_1, c_2 \geq 16$ by a factor (b) 1.5 (c) 2 (d) 2.5

Hence the processing of colour image requires a different colour space or colour model that intuitively describes human interpretation of colours. YCbCr colour space decouples the intensity component from the colour carrying chrominance component in a colour image. So YCbCr colour space, widely used in colour image processing, is chosen in this study.

The procedure for colour image enhancement is explained below. The RGB pixel values of an image are converted to YCbCr values first. The enhancement method used for gray-scale images is applied only to the luminance component (Y) while keeping Cb and Cr the same. This will retain the computational requirement of colour

image enhancement similar to that of gray-scale images. Inverse SMRT of the modified luminance component is found. Enhanced image in the YCbCr space is converted back to RGB space.

5.2.3 Results and Analysis

LET is applied to low contrast images or low contrast sub-images of general, mammogram, text and fingerprint images. The method scales DC and AC SMRT coefficients separately. Scaling of DC SMRT coefficient and uniform scaling of AC SMRT coefficients are performed to change the brightness and contrast of the images respectively and the variations in contrast and brightness are observed.

Histogram Equalization (HE), one of the fundamental techniques for global image processing, distributes gray levels uniformly over the dynamic range of gray levels. It produces an output image with a flattened histogram having uniform distribution and is used here for comparing the contrast improvement of the LET. The effect of scaling the image Wavelet Transform coefficients is also investigated to compare the significance of the proposed method.

5.2.3.a General Images

General images, possessing different histogram shapes, span etc. are selected for analysis. The proposed method is tested on several low contrast images holding different contrast levels. Three general images, *woman, lena, moon* and their enhanced images using HE, LET with respective histograms are shown in Figs. 5.8, 5.9 and 5.10. The *woman* is a low contrast, dark image whereas *lena* and *moon* are medium brightness images with medium contrast and low contrast respectively. c_{dc} and c_{ac} values, necessary for increasing the contrast levels, utilizing the maximum histogram range, are

specified in the respective figures. The c_{dc} value indicates a shift in histogram and c_{ac} value indicates the amount of contrast stretching. In all cases, linear stretching of the histogram to both ends utilizing the entire histogram range is observed.

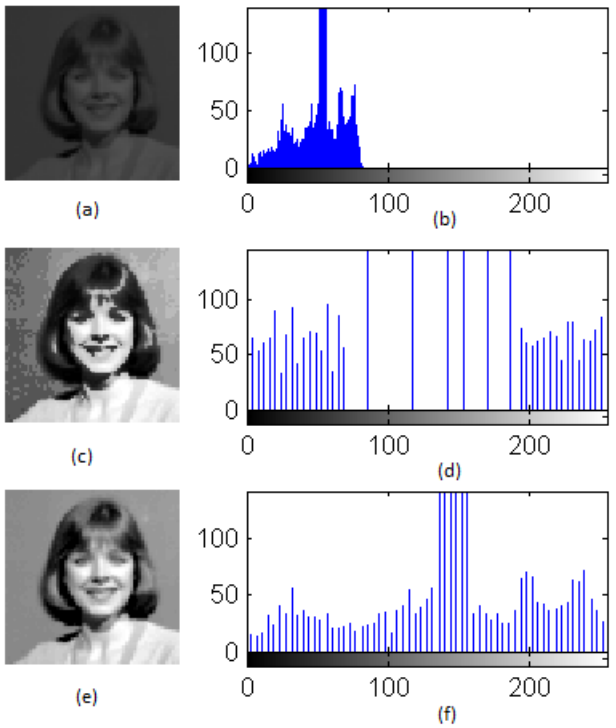

Fig. 5.8: Images and their histograms (a)&(b)Original(*woman*), Enhanced using (c)&(d)HE (e)&(f)LET (c_{dc}=2.66 and c_{ac}=4.15)

Fig. 5.11 shows the original *baboon, barbara, goldhill, peppers* images with the respective images of HE and LET based image enhancement techniques.

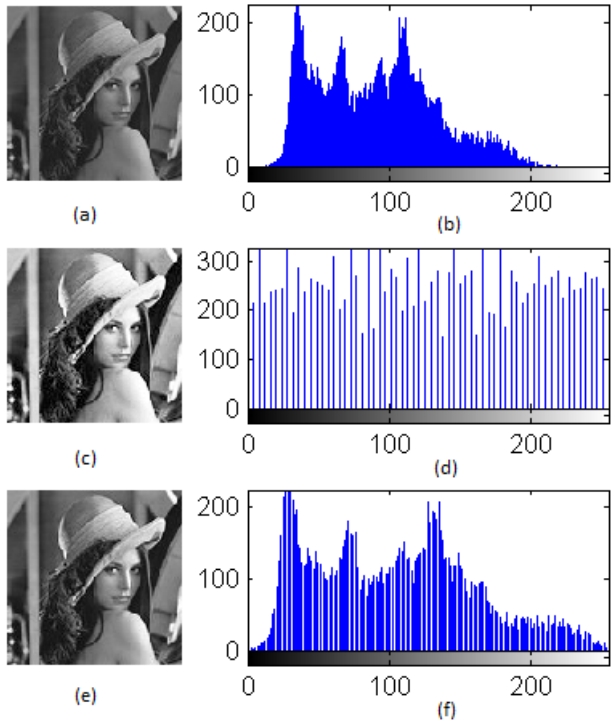

Fig. 5.9: Images and their histograms (a) & (b)Original(*lena*), Enhanced using (c)&(d)HE (e)&(f)LET (c_{dc}=1.16 and c_{ac}=1.38)

5.2.3.b Mammogram Images

Generally, for high contrast medical images, there is no further scope for enhancement by contrast stretching. But there may be certain objects of interest that are hidden as low contrast sub-images. In such cases, the global enhancement method can be used to view images locally.

Mammograms are usually not well defined and inspection of hidden objects are important in the early detection of breast cancer. The local regions under suspect is normally low in contrast. Enhancement of such low contrast image areas would help radiologists

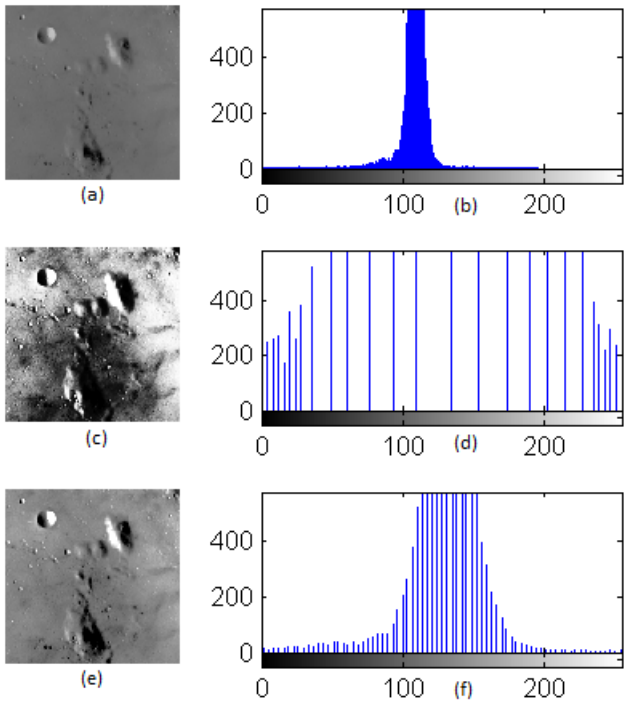

Fig. 5.10: Images and their histograms (a) & (b)Original(*moon*), Enhanced using (c)&(d)HE (e)&(f)LET (c_{dc}=1.18 and c_{ac}=2.01)

in interpreting data correctly and results in proper diagnosis. A mammogram image, *mdb002,* from Mini-MIAS digital mammography database [164] and a low contrast sub-image are shown in Fig. 5.12. The bright sub-image is enhanced using HE and LET. The enhanced images with their respective histograms are shown in Fig. 5.13. Comparison of the original and modified images using LET shows an increase in contrast, resulting in enhancement of calcification areas of mammogram sub-image.

More images from MIAS database are used to find the enhancement of low contrast areas. Sub-images containing calcifications, benign and malignant masses are identified and the proposed method is

Fig. 5.11: (a)Original images, Enhanced using (b)HE (c)LET

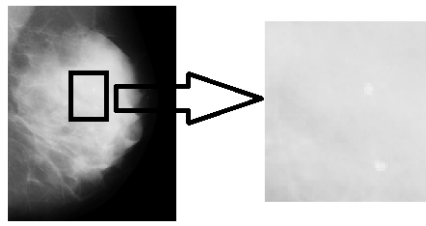

Fig. 5.12: Mammogram (*mdb002*) image and a low contrast sub-image

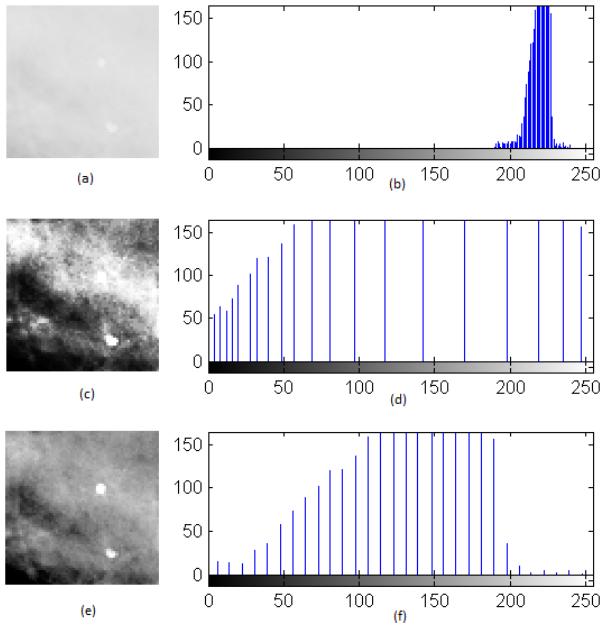

Fig. 5.13: Mammogram images and their histograms (a)Original, enhanced using (c)HE (e)LET (c_{dc}=0.60 and c_{ac}=8.34)

applied to these images. The original images, Histogram Equalized images and the enhanced images using LET are shown in Figs. 5.14, 5.15, 5.16, for calcification, benign and malignant masses respectively. It is observed that in all cases, the contrast of the foreground as well as background areas have improved resulting in overall enhancement.

5.2.3.c Comparison of Quantitative Measures

Subjective and objective evaluations of the existing and proposed method are useful to determine how efficient the proposed method is for enhancement. The HE and LET methods are compared using quantitative metrics. The improvement in contrast and visual

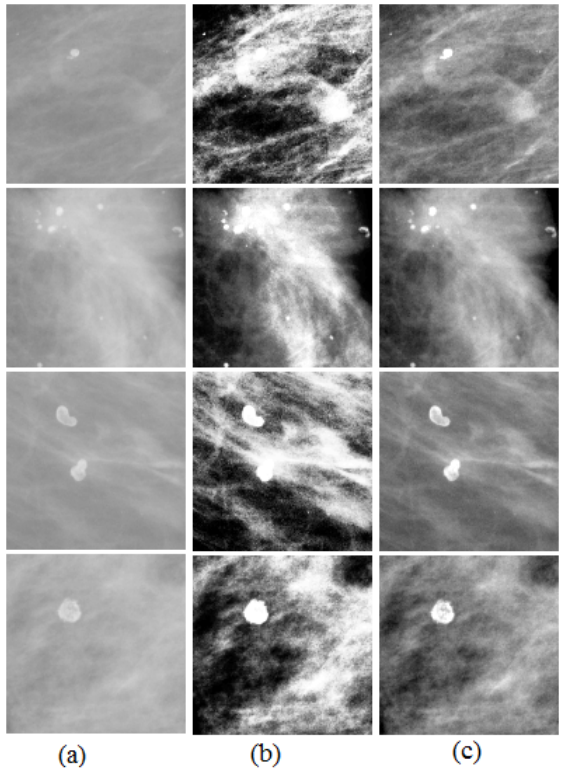

Fig. 5.14: Low contrast calcification areas of mammograms (a)Original images(*mdb009, 170, 204, 227*) Enhanced images using (b) HE (c) LET

quality of images can be verified using existing IQA metrics such as VIFP, EMEE, SDME and the proposed metrics such as IEM, IEMS_{FR}, IEMS_{BR}. Table 5.1 shows the existing metric values of HE and LET for general and mammogram images. Since SDME and EME are blind reference metrics, they are computed for original image also.

Table 5.1 shows that mean of Histogram Equalized image is constant at 128. Mean value falls above/below according to image histogram statistics for LET, since the value of c_{dc} is selected to shift

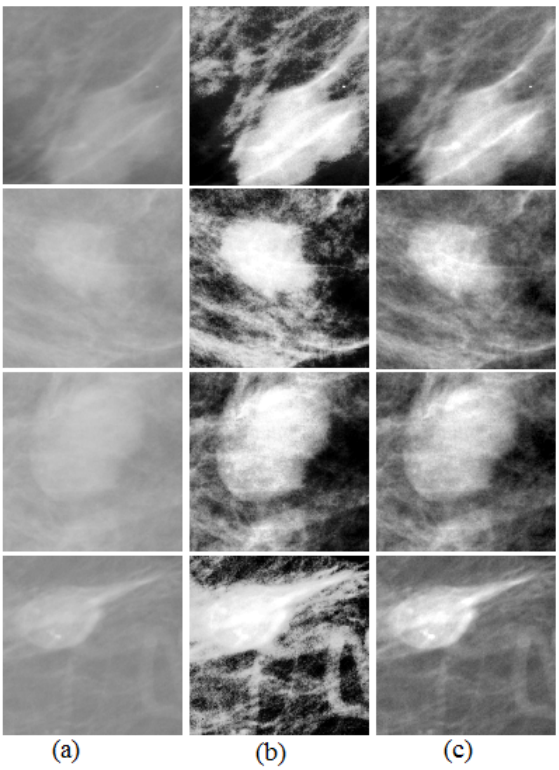

Fig. 5.15: Low contrast areas of mammograms containing benign tumours (a)Original images*(mdb005, 010, 019, 132*) Enhanced images using (b) HE (c) LET

the centre of image histogram to the centre of histogram range. SD of HE is also constant at 75 whereas for LET, its value is less than HE. For all images, VIFP and SDME values show that enhancement of LET is better compared to HE. For majority of the images, EMEE values are better for HE.

The values of IEM also show that LET is superior to HE as seen in Table 5.2. The SMRT metrics, IEMS_{FR} and IEMS_{BR} can be used to compare methods that use SMRT as the transform. However, comparison of the IEMS_{BR} metric of original and the enhanced

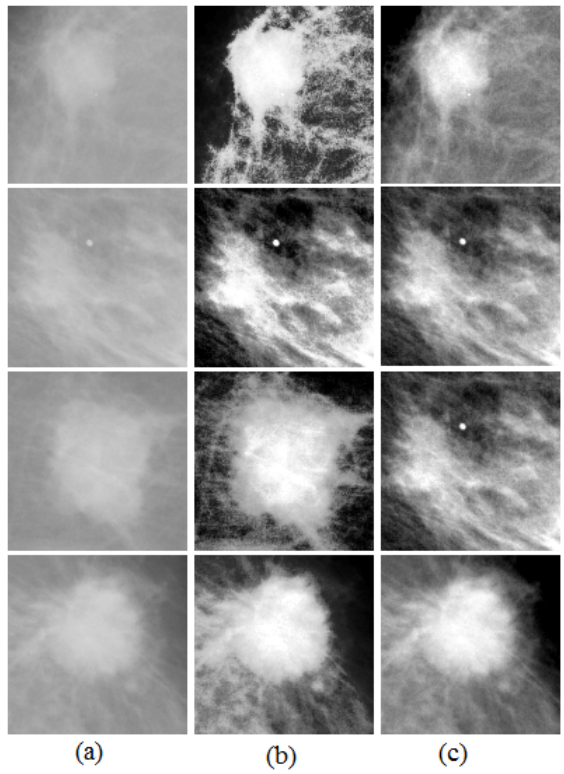

Fig. 5.16: Low contrast areas of mammograms containing malignant tumours (a)Original images(*mdb023, 058, 134, 202*) Enhanced images using (b) HE (c) LET

using LET shows that the values are better for the enhanced image.

5.2.3.d Wavelet Transform Scaling

Analysis similar to that in SMRT is performed by scaling the Wavelet Transform coefficients of images and found that there is blocking artifacts. Two level WT decomposition is done and different scaling factors are applied to approximation and detail coefficients. Scaling

Table 5.1: Comparison of Mean, SD, VIFP, EMEE, SDME of various images for HE and LET

Images	Mean			SD			VIFP		EMEE			SDME		
	Image	HE	LET	Image	HE	LET	HE	LET	Image	HE	LET	Image	HE	LET
baboon	131.9	127.4	132.9	25.4	**74.8**	58.8	0.82	**1.37**	0.35	**7.17**	5.38	77.82	52.11	**79.87**
barbara	115.1	127.7	125.1	28.7	**74.9**	59.6	0.84	**1.30**	0.36	4.89	**31.11**	77.16	56.50	**109.39**
goldhill	110.0	127.8	116.0	31.3	**74.9**	55.5	0.85	**1.25**	0.33	0.33	**1.15**	77.86	55.52	**100.56**
peppers	112.1	127.6	123.0	33.8	**74.8**	61.6	0.82	**1.24**	0.45	4.51	**6.47**	76.71	58.59	**118.36**
mdb009	154.3	127.5	120.8	7.9	**75.1**	33.8	0.53	**2.38**	0.04	**2.75**	0.33	97.63	57.49	**139.50**
mdb170	173.8	127.3	133.8	20.8	**74.9**	52.8	0.64	**1.71**	0.05	0.79	**1.49**	96.52	68.43	**162.11**
mdb204	160.0	127.7	109.5	10.3	**74.9**	27.8	0.45	**1.84**	0.04	**2.31**	0.19	96.81	61.82	**157.52**
mdb227	174.9	127.7	121.4	11.1	**74.8**	38.3	0.57	**2.05**	0.04	**1.69**	0.37	99.25	62.29	**143.81**
mdb005	140.0	127.3	131.0	16.6	**74.7**	54.7	0.55	**1.91**	0.05	**0.83**	0.34	97.31	63.70	**138.28**
mdb010	169.4	127.4	125.4	12.4	**74.9**	48.1	0.58	**2.12**	0.04	**1.59**	0.44	100.24	61.77	**132.78**
mdb019	172.9	127.6	127.9	14.3	**74.9**	58.9	0.75	**2.25**	0.04	0.97	**1.18**	100.14	66.29	**142.21**
mdb132	151.1	127.7	111.6	16.2	**74.9**	45.2	0.44	**1.78**	0.05	**4.30**	0.24	97.37	58.48	**145.22**
mdb023	164.1	127.4	141.6	15.2	**74.9**	52.9	0.45	**2.18**	0.04	**1.03**	0.34	100.61	57.28	**142.88**
mdb058	173.7	127.9	125.2	13.7	**74.8**	59.0	0.69	**2.18**	0.04	**1.69**	0.96	98.98	63.94	**139.04**
mdb134	162.9	127.6	120.4	19.5	**74.9**	61.3	0.59	**1.92**	0.04	**1.47**	0.27	98.09	63.88	**153.99**
mdb202	156.2	127.6	138.2	29.9	**74.7**	65.4	0.67	**1.54**	0.05	**0.34**	0.30	97.06	66.67	**155.47**
Average	151.4	127.6	125.2	19.2	**74.9**	52.1	0.64	**1.81**	0.13	2.29	**3.16**	93.10	60.92	**135.06**

Table 5.2: Comparison of IEM, IEMS$_{FR}$, IEMS$_{BR}$ of various images for HE and LET

Images	IEM		IEMS$_{FR}$	IEMS$_{BR}$	
	HE	LET	LET	Image	LET
baboon	16.46	**19.89**	0.19	33.40	**77.40**
barbara	14.49	**17.74**	0.23	44.55	**92.70**
goldhill	11.29	**17.74**	0.32	28.55	**50.59**
peppers	11.84	**15.86**	0.30	47.62	**86.83**
mdb009	28.84	**42.69**	0.06	9.68	**41.22**
mdb170	18.24	**25.43**	0.16	21.04	**53.31**
mdb204	19.83	**39.06**	0.14	11.87	**32.22**
mdb227	24.54	**35.88**	0.08	16.02	**55.21**
mdb005	23.33	**28.71**	0.09	16.78	**55.21**
mdb010	27.01	**33.93**	0.07	11.82	**45.94**
mdb019	27.85	**30.63**	0.06	13.06	**53.76**
mdb132	20.38	**36.63**	0.13	12.42	**34.54**
mdb023	23.97	**35.02**	0.08	11.97	**41.63**
mdb058	29.11	**33.07**	0.05	12.50	**53.96**
mdb134	22.80	**28.97**	0.10	17.80	**56.01**
mdb202	15.08	**18.24**	0.21	21.36	**46.77**
Average	20.94	**28.72**	0.14	20.65	**54.83**

the approximation coefficients shifts the mean value of the image histogram whereas scaling the detail coefficients stretches contrast. Fig. 5.17 shows a few images and the modified images using uniform scaling of SMRT and Wavelet Transform coefficients.

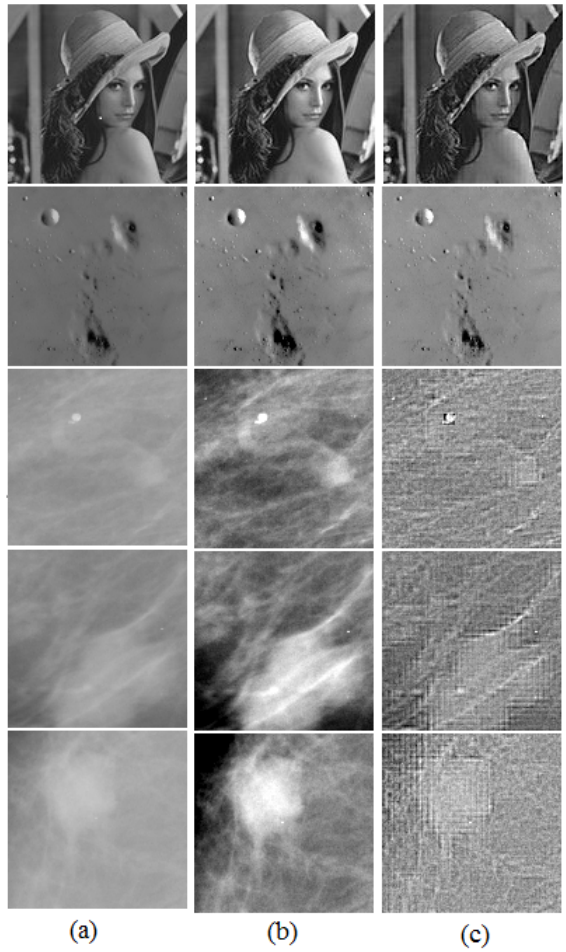

Fig. 5.17: (a) Original images *lena, Moon, mdb009, mdb005, mdb023*, Enhanced images using scaling of (b) SMRT (c) WT coefficients

The VIFP, EMEE, SDME and IEM metric values of the WT based

enhancement method are shown in Table 5.3. These values are compared with the corresponding values obtained for LET. All metrics except EMEE give better values for LET. The results show that EMEE cannot be considered as a measure of the image visual quality.

Table 5.3: Comparison of Mean, SD, VIFP, EMEE, SDME, IEM values for WT and SMRT scaling methods

Images	Mean		SD		VIFP		EMEE		SDME		IEM	
	WT	SMRT	WT	SMRT	WT	SMRT	WT	SMRT	WT	SMRT	WT	SMRT
lena	89.9	104.4	46.00	**57.3**	0.62	**1.12**	**6.59**	3.07	74.74	**99.91**	7.63	**11.75**
moon	139.9	126.6	18.18	**24.8**	1.03	**1.54**	0.60	**0.64**	114.50	**161.81**	13.60	**45.18**
mdb009	146.5	120.8	22.19	**33.8**	0.43	**2.38**	**0.61**	0.33	94.28	**139.50**	32.27	**42.69**
mdb005	133.0	131.0	26.13	**54.7**	0.32	**1.91**	**0.66**	0.34	91.45	**138.28**	20.54	**28.71**
mdb0023	155.9	141.6	25.52	**52.9**	0.39	**2.18**	**0.62**	0.34	93.15	**142.88**	34.88	**35.02**

5.2.3.e Fingerprints and Text Images

Extracting minutiae from fingerprint images is one of the most important steps in automatic fingerprint identification and classification. Most of the minutiae extraction methods are based on image binarization while others extract the minutiae directly from gray-scale images. The possibility of ridge contrast enhancement through the elimination of noises between ridges is explored by applying LET based on binarization of fingerprint images.

Image brightness is modified by shifting mean of the image to the centre of histogram range by scaling DC SMRT coefficient as explained in Section 5.2.1. When the AC SMRT coefficients are scaled using very high value scaling factor c_{ac}, the image gets binarized and as a consequence noise will also be eliminated.

Fig. 5.18 shows the effect of changing the scaling factors c_{dc} and c_{ac} original fingerprint image, the stages of enhancement with the respective histogram for various scaling constants, c_{dc} and c_{ac}. This binarization can be used as a preprocessing step for fingerprint pro-

cessing. Fig. 5.19(a) shows few fingerprint images and their binarization using (b) thresholding and (c) LET.

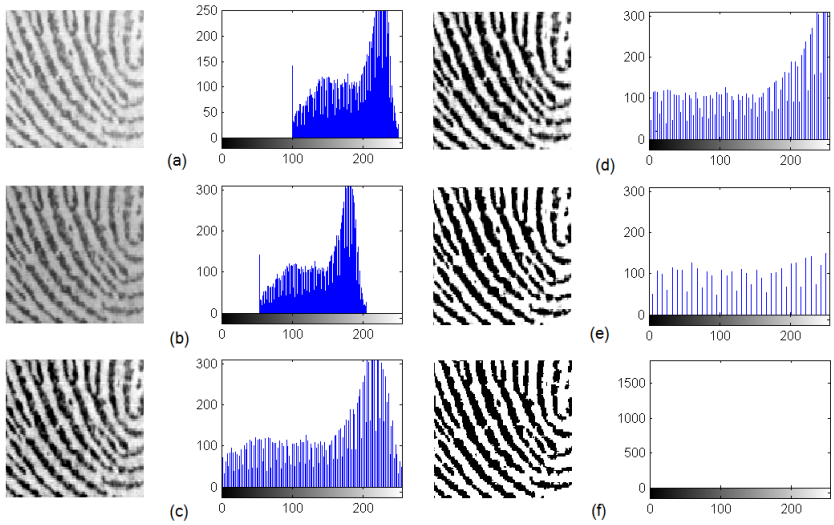

Fig. 5.18: Original and reconstructed fingerprint images and histograms (a) original (b) $c_{dc} = 0.86$, $c_{ac} = 1$ (c) $c_{dc} = 0.86$, $c_{ac} = 2$ (d) $c_{dc} = 0.86$, $c_{ac} = 3$ (e) $c_{dc} = 0.86$, $c_{ac} = 7$ (f) $c_{dc} = 0.86$, $c_{ac} = 1000$

Similar degradations are encountered in conversion of printed documents into electronic form. Besides text, scanned copies of numerous collection of mechanical and architectural drawings, property documents etc. often contain similar foreground and background degradations. Generally a cleaned background is derived by the application of thresholding, but often results in thinned and broken characters. But the application of the above technique enables to maintain stroke width of the characters, while removing background noise. Scanned, spoiled and tarnished text can thus be enhanced using the above technique. Fig. 5.20 shows an original spoiled document with the corresponding binirazed form from the application of simple thresholding and LET respectively.

Fig. 5.19: (a) Original fingerprint images, binarization using (b)Thresholding method (c) LET

5.2.3.f Application on Colour Images

The above method is applied on colour image considering both YCbCr space and RGB spaces. In the first representation, the method is applied to Y component alone whereas all the components of RGB space are applied with the method and the results are presented in Fig. 5.21. It shows that YCbCr representation applied with LET gives better quality image at lesser computational cost.

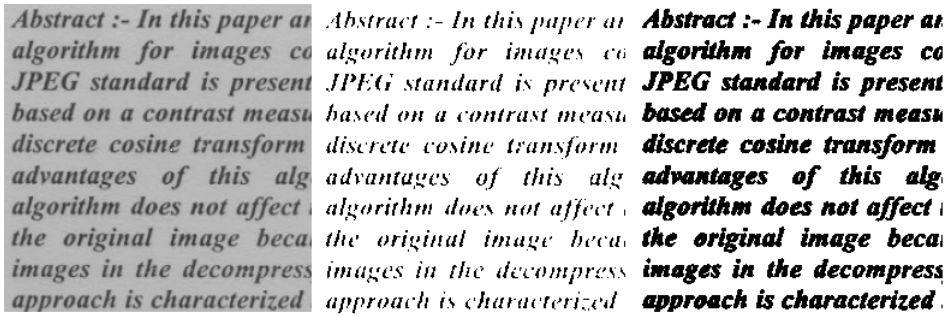

Fig. 5.20: (a) Original scanned document, binarization using (b) thresholding method (c) LET

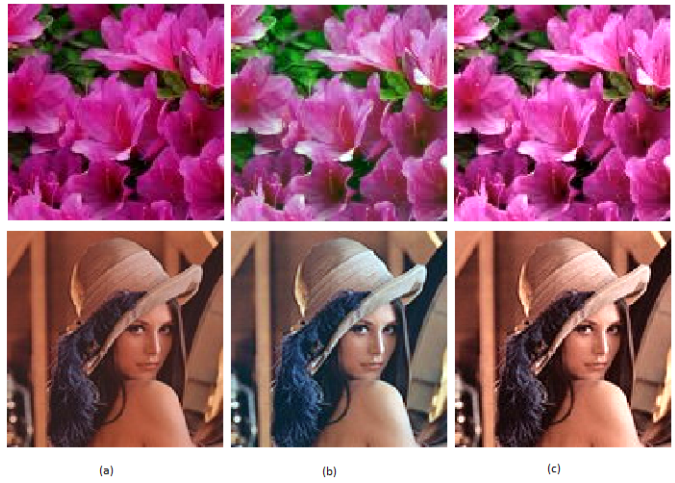

Fig. 5.21: Colour image enhancement using LET (a) Original image (b) RGB space (c) Y component of YCbCr space

Conclusion

A simple, linear, automatic, brightness and contrast enhancement method is presented. The image can be brightened or darkened by a simple scaling of DC SMRT coefficient. Dynamic range and thereby

contrast can be changed by properly scaling AC SMRT coefficients. Performance of the method is measured and compared with classical HE technique and WT scaling method. All metrics, except EMEE, show good performance for LET compared to others. Simulation results show that the resultant enhanced images using the proposed automatic linear enhancement method is better in contrast and brightness for monochrome and colour images. The proposed LET is also applied to fingerprint images & scanned documents that produce a binary image at a high value of c_{ac} with the benefit of noise removal. This method can give good performance for low contrast images quantitatively and qualitatively.

5.3 Nonlinear Enhancement Technique

Human Visual System (HVS) includes some nonlinear effects and hence nonlinear image processing techniques [165] have emerged as intensive topics for research. Therefore, to comply with the nonlinear characteristics of the HVS, nonlinear methods may be suitable. Scaling image data logarithmically is an example of nonlinear contrast stretch, in spatial domain.

Hence, a nonlinear Enhancement Technique (NLET) is proposed by which the SMRT coefficients are modified using nonlinear mapping techniques so as to include nonlinear feature of HVS in the image enhancement process.

5.3.1 Nonlinear Mapping Functions

Generally, nonlinear mapping functions are used in the spatial domain to modify pixel values nonlinearly. Similarly, nonlinear mapping functions can be used in the transform domain to nonlinearly modify the coefficients. Some of the nonlinear mapping functions

in the literature are alpha-rooting [39], Twicing function [39],[107], function proposed by Lee [109], Programmable-S-function [108] etc. The mathematical expressions and the respective plots are given in Appendix B.

Analysis of different mapping functions, used for image processing applications, reveals that enhancement is possible with nonlinear functions that expands the low valued transform coefficients. Considerable distortion is observed when the lower valued coefficients are compressed. Considering the above facts, two hyperbolic functions capable of expanding lower valued coefficients and compressing higher valued coefficients equally are proposed and presented here. They are inverse hyperbolic sine and hyperbolic tan functions, defined as

$$T(u,v) = \frac{sinh^{-1}(S(u,v))}{sinh^{-1}(1)} \tag{5.6}$$

$$T(u,v) = \frac{tanh(S(u,v))}{tanh(1)} \tag{5.7}$$

The values in the denominator of Eqs.5.6 & 5.7 are used for normalization of the functions. These functions can be applied recursively using the following equations for further expansion and compression.

$$T_k(u,v) = \frac{sinh^{-1}(T_{k-1}(u,v))}{sinh^{-1}(1)} \tag{5.8}$$

$$T_k(u,v) = \frac{tanh(T_{k-1}(u,v))}{tanh(1)} \tag{5.9}$$

where $T_0(u,v)$=$S(u,v)$ and $T_1(u,v) = T(u,v)$.

Plots of these functions are shown in Fig. 5.22 and Fig. 5.23 for various values of k. The significance of these functions compared to the nonlinear functions referred above are that the rate of expansion and compression are approximately equal and amplification at the origin is very small.

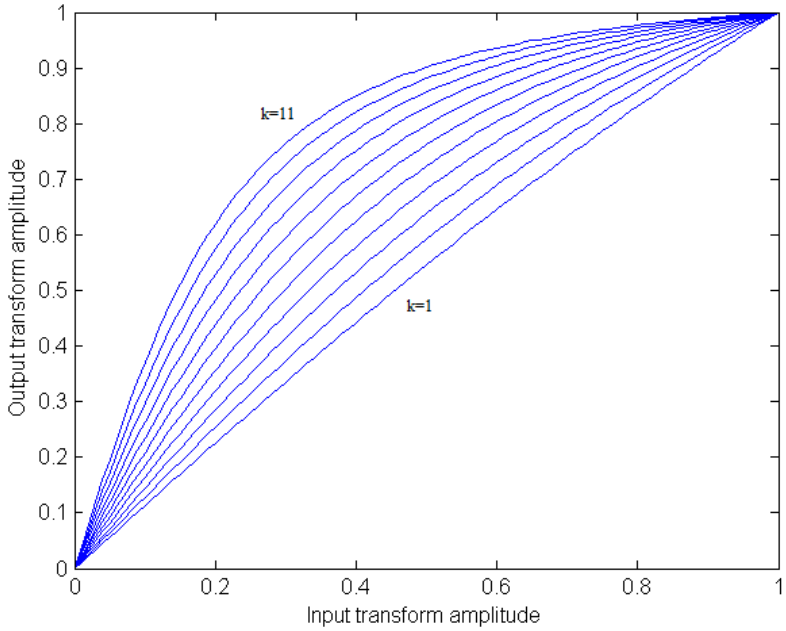

Fig. 5.22: A plot of $\sinh^{-1}$ function

NLET Algorithm

Image enhancement technique proposed in [39] was based on nonlinear functions applied in the compressed domain on DC coefficients of block level DCT to enhance brightness of the image. In this work, nonlinear functions are used to scale transform coefficients nonlinearly for global image enhancement. SMRT based enhancement will be computationally efficient due to the inherent simplicity in the number of computations compared to other transforms. The NLET operates in the SMRT domain and uses separate scaling factors for

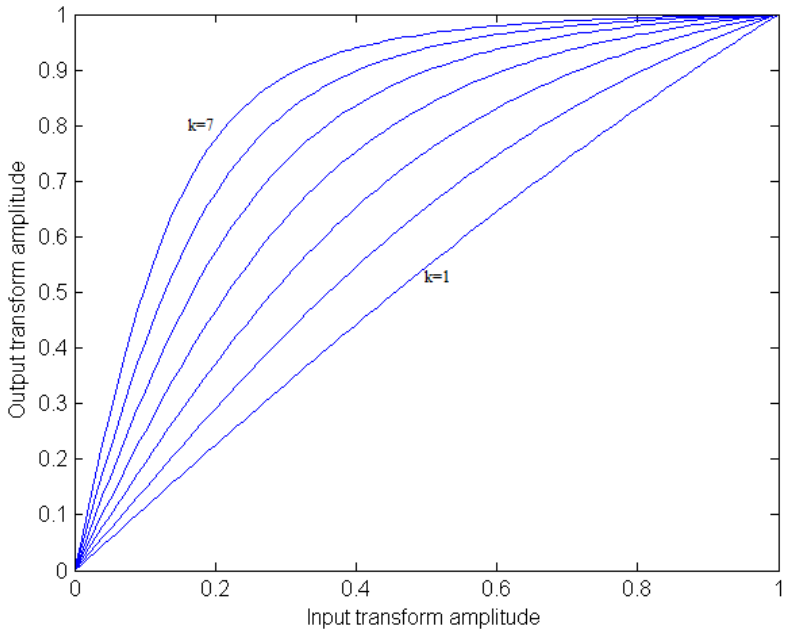

Fig. 5.23: A plot of tanh function

DC and AC coefficients.

First, the image is transformed into SMRT domain. DC coefficient is suitably scaled to adjust mean value to the centre of histogram range and hence brightness of the image is improved. The AC SMRT coefficients are normalized to the range [0,1] and modified using nonlinear mapping functions discussed in section 5.3.1.

Reasons for choosing alpha-rooting, twicing function, function proposed by Lee and programmable-S-functions are that they were used earlier in image processing applications and there is no single method by which every image can be enhanced. Hyperbolic tan and inverse hyperbolic sine functions, having symmetry at the rate of variation for low and high valued coefficients, are also employed

here for nonlinear mapping of SMRT coefficients. The objective is to observe the performance of the proposed algorithm with different choices of these mapping functions.

5.3.2 NLET Algorithm

1. Computed SMRT, S, of the input image $x(n_1, n_2), 0 \leq n_1, n_2 \leq N-1$.
2. DC SMRT coefficient is made zero retaining a copy of it as $dc = S(0,0)$
3. S is normalized.
   - $s = \text{Max}(|S(s_1, s_2)|,\ 0 \leq s_1, s_2 \leq N-1$
   - S^+ and S^- are obtained as

$$S^+(s_1, s_2) = \begin{cases} S(s_1, s_2), & S(s_1, s_2) \geq 0 \\ 0, & \text{otherwise} \end{cases} \tag{5.10}$$

   and

$$S^-(s_1, s_2) = \begin{cases} |S(s_1, s_2)|, & S(s_1, s_2) < 0 \\ 0, & \text{otherwise} \end{cases} \tag{5.11}$$

   - $S_n^+ = S^+/s$ and $S_n^- = S^-/s$
4. S_n^+ and S_n^- are modified as T_n^+ and T_n^- using the existing mapping functions and the proposed hyperbolic functions.
5. Denormalized SMRT coefficients as $T^+ = T_n^+ s$ and $T^- = T_n^- s$.
6. SMRT is modified as $T = T^+ - T^-$
7. DC SMRT coefficient is modified as in Eq. (5.2), $T(0,0) = \frac{r_{shift} N^2}{dc} + 1$, where $r_{shift} = 128 - \frac{dc}{N^2}$

8. Inverse SMRT is computed.

5.3.3 Results and Analysis

Experimental results of the proposed image enhancement algorithm using different mapping functions, described in section 5.3.1, are presented for general images & low contrast mammogram sub-images discussed in sections 5.2.3 & 5.2.3 and compared with the results of HE. Nonlinear stretching of the histogram is observed when the parameters of the mapping functions are varied. These parameters have been chosen empirically for maximum contrast and varied until histogram utilizes the full dynamic range.

General Images

General images possessing different histogram shapes, span etc. are used for analysis using different mapping functions. As an example, *lena* image and its enhanced versions using alpha-rooting, twicing function, function proposed by Lee, Programmable-S-function, hyperbolic tan, inverse hyperbolic sine mapping functions respectively are shown in the first row in Fig. 5.24 and a zoomed portion of these images in the same order in the second row. The figure shows that contrast is improved in all cases. However, artifacts can be seen in Fig. 5.24(b) and over-enhancement in figs. 5.24(c) and (e). Good results are achieved for enhancement using function proposed by Lee, inverse hyperbolic sine and hyperbolic tan functions as shown in Figs. 5.24(d), 5.24(f) and 5.24(g) respectively.

Mammogram Images

Low contrast areas of mammogram images are considered for analysis. Fig. 5.25 shows a mammogram image, *mdb028*, and a portion

Fig. 5.24: Original *lena* image and its enhanced versions using mapping functions in the order, below the zoomed portion of the images in the same order

of it containing the benign mass. Fig. 5.26 (a)&(b) shows the original *mdb028* sub-image, (c)&(d) Histogram Equalized version, the enhanced versions using different mapping functions with (e)&(f) alpha-rooting, (g)&(h) twicing function, (i)&(j) Programmable- S-function, (k)&(l) function proposed by Lee, (m) &(n)Hyperbolic tan, (o)&(p) Inverse hyperbolic sine mapping functions and the corresponding histograms are shown. Similarly, Fig. 5.27 shows the original and enhanced images corresponding to low contrast mammogram (*mdb005*) sub-image.

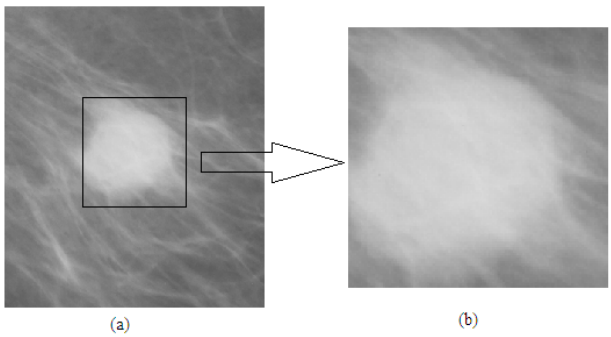

Fig. 5.25: Mammogram (*mdb028*) image and its low contrast sub-image

The NLET is applied to calcification, benign and malignant areas

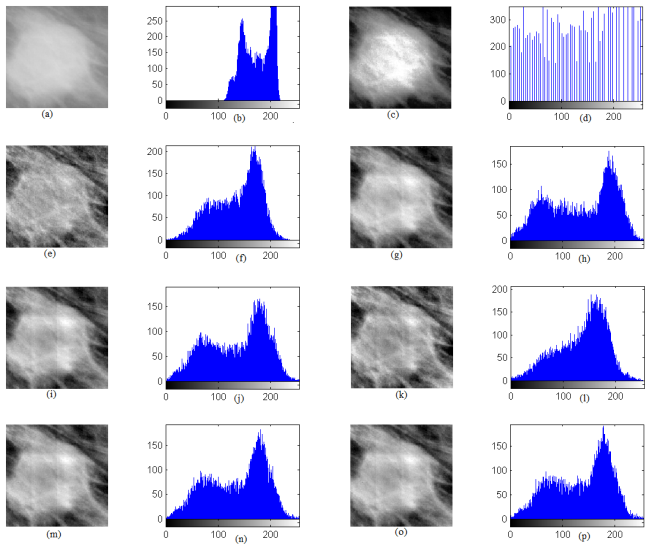

Fig. 5.26: Original and enhanced *mdb028* images and their histograms

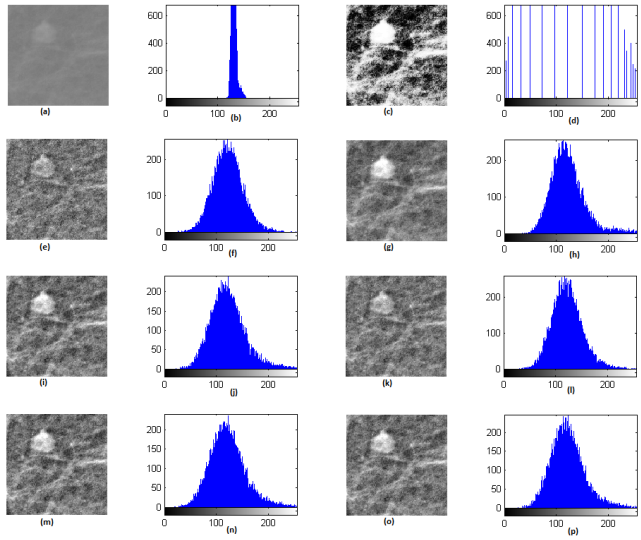

Fig. 5.27: Original and enhanced *mdb005* images and their histograms

of mammograms from MIAS database and the original & enhanced images using various mapping techniques are shown in Figs. 5.28, 5.29 and 5.30 respectively.

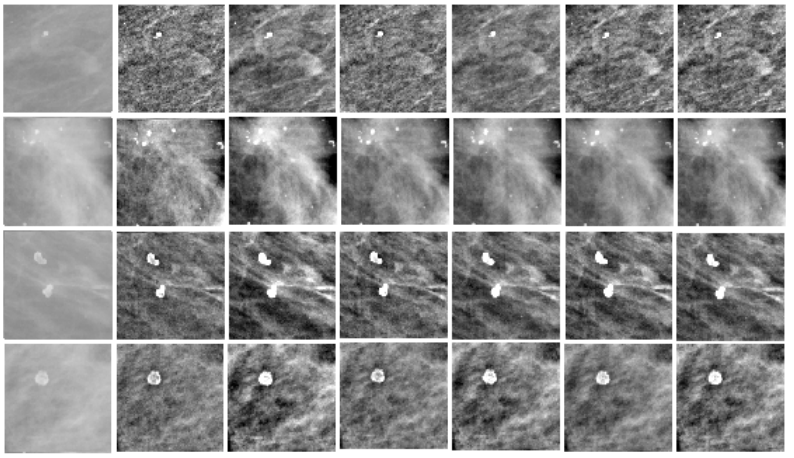

Fig. 5.28: Original mammogram sub-images (*mdb009,mdb170, mdb204, mdb227*) containing calcifications in the first column and enhanced images using NLET with different mapping functions in remaining columns

Analysis of the above results shows that NLET processing gives better distinction between background and calcification areas are more prominent in mammogram sub-images containing calcification.

Quantitative Analysis

The IQA metrics and general & mammogram images, as mentioned in section 5.2.3 are considered for analysis. The metric values are tabulated for the 16 images considered with six mapping functions. Since it is difficult to show the metric values corresponding to all images in 16 tables, one image each from different categories is considered here for convenience. Tables 5.4, 5.5, 5.6 and 5.7 list met-

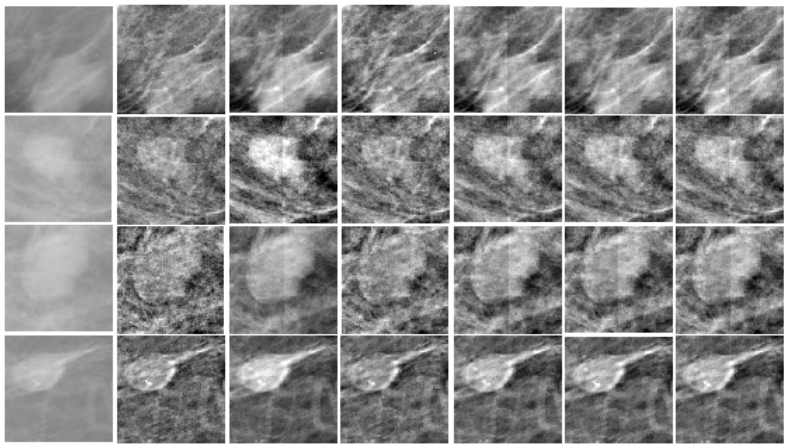

Fig. 5.29: Original mammogram sub-images (*mdb005,mdb010, mdb019, mdb132*) containing benign masses in the first column and enhanced images using NLET with different mapping functions in remaining columns

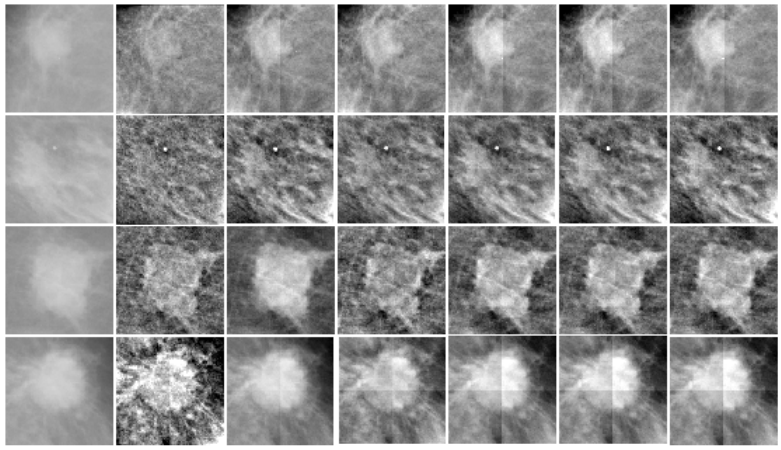

Fig. 5.30: Original mammogram sub-images (*mdb023, mdb058, mdb134, mdb202*) containing malignant masses in the first column and enhanced images using NLET with different mapping functions in remaining columns

ric values corresponding to *lena* (general), *mdb204* (calcification), *mdb132* (benign) and *mdb023* (malignant) respectively.

Table 5.4: Comparison of Mean, SD, VIFP, EMEE, SDME of *lena* image for various mapping functions

Mapping functions	Mean	SD	VIFP	EMEE	SDME	IEM	$IEMS_{FR}$	$IEMS_{BR}$
Alpha-rooting	104.4	56.2	0.68	5.45	65.03	11.41	**0.535**	78.63
Twicing function	104.4	**77.8**	0.86	7.25	55.94	10.96	0.271	110.44
Function proposed by Lee	104.4	55.8	0.70	6.68	66.37	9.19	0.511	80.45
Programmable-S-function	104.4	76.3	0.70	**9.50**	56.83	**12.42**	0.269	**110.99**
Inverse hyperbolic sine	104.4	57.4	**0.89**	4.33	**66.50**	7.46	0.488	82.32
Hyperbolic tan	104.4	66.4	0.80	7.42	62.86	10.50	0.356	96.43

Table 5.5: Comparison of Mean, SD, VIFP, EMEE, SDME of *mdb 204* image for various mapping functions

Mapping functions	Mean	SD	VIFP	EMEE	SDME	IEM	$IEMS_{FR}$	$IEMS_{BR}$
Alpha-rooting	109.5	32.7	0.56	0.63	67.78	38.07	**0.085**	40.67
Twicing function	109.5	**56.8**	**1.09**	**1.38**	64.86	39.55	0.026	**73.03**
Function proposed by Lee	109.5	40.1	0.58	0.94	66.94	**39.56**	0.054	51.25
Programmable-S-function	109.5	44.3	0.91	0.73	**69.80**	36.07	0.042	58.05
Inverse hyperbolic sine	109.5	47.0	0.80	0.90	66.33	38.66	0.037	61.72
Hyperbolic tan	109.5	44.4	0.86	0.72	69.03	36.80	0.041	58.49

Table 5.6: Comparison of Mean, SD, VIFP, EMEE, SDME of scaling *mdb 132* image for various mapping functions

Mapping functions	Mean	SD	VIFP	EMEE	SDME	IEM	$IEMS_{FR}$	$IEMS_{BR}$
Alpha-rooting	111.6	35.3	0.48	**0.77**	67.26	**37.91**	**0.094**	40.443
Twicing function	111.6	**44.8**	**1.15**	0.37	**75.64**	26.83	0.082	43.404
Function proposed by Lee	111.6	33.5	0.53	0.65	70.48	34.42	0.086	42.314
Programmable-S-function	111.6	40.5	0.76	0.54	73.94	30.83	0.066	48.309
Inverse hyperbolic sine	111.6	40.0	0.73	0.55	72.45	31.82	0.067	47.988
Hyperbolic tan	111.6	40.6	0.73	0.57	72.82	31.77	0.065	**48.809**

Table 5.7: Comparison of Mean, SD, VIFP, EMEE, SDME of *mdb 023* image for various mapping functions

Mapping functions	Mean	SD	VIFP	EMEE	SDME	IEM	$IEMS_{FR}$	$IEMS_{BR}$
Alpha-rooting	141.6	23.7	0.49	0.26	79.74	**31.32**	**0.168**	29.183
Twicing function	141.6	31.3	0.84	0.28	**81.72**	26.44	0.097	38.370
Function proposed by Lee	141.6	32.5	0.75	0.29	80.32	29.81	0.082	41.929
Programmable-S-function	141.6	39.8	**1.07**	0.26	80.60	27.05	0.076	43.436
Inverse hyperbolic sine	141.6	**42.0**	0.96	**0.43**	79.52	29.76	0.059	**49.247**
Hyperbolic tan	141.6	38.9	1.03	0.30	81.54	26.96	0.075	43.784

Table 5.4 shows that the EMEE, IEM and IEMS$_{BR}$ values of Twicing function and Programmable-S-functions give high values and according to Fig. 5.24 the modified images are over-enhanced indicating that these metrics give a measure of contrast. VIFP and SDME values are highest for inverse hyperbolic sine and Fig. 5.24 indicates that they give a measure of visual quality.

On comparison of the metric values for various images using different mapping functions, no mapping function can be judged as superior to other mapping functions. A metric value superior for one image using a particular mapping function may show inferior values for another image. Hence average of the metric values of the 16 images are calculated for finding a suitable mapping function for enhancement. Table. 5.8 shows the average of the metric values of the 16 images considered and they are plotted in Fig. 5.31. The plots also show that no mapping function can be identified suitable for all images.

Table 5.8: Comparison of average values of metrics for various mapping functions

Mapping functions	VIFP	EMEE	SDME	IEM	IEMS$_{FR}$	IEMS$_{BR}$
Alpha-rooting	0.486	1.289	68.81	**37.40**	**0.140**	49.91
Twicing function	**1.066**	1.213	**74.58**	28.68	0.106	60.73
Function proposed by Lee	0.578	1.233	72.69	33.27	0.137	52.55
Programmable-S-function	0.838	**1.327**	74.35	30.26	0.093	61.65
Inverse hyperbolic sine	0.821	0.977	74.56	30.09	0.121	58.45
Hyperbolic tan	0.769	1.304	72.72	32.48	0.089	**65.04**

The normalized metric values of the average of all images for the mapping functions considered are shown in Table 5.9 and plotted in Fig. 5.32. The comparison plots are formed to find the best mapping function applicable to different images. A comparison of metric values for all images, using different mapping functions, is done and a better mapping function that suits most of the images under consideration for most of the metrics is the twicing function. So for comparison, mapping with twicing function is considered for remaining part of this work for analysis.

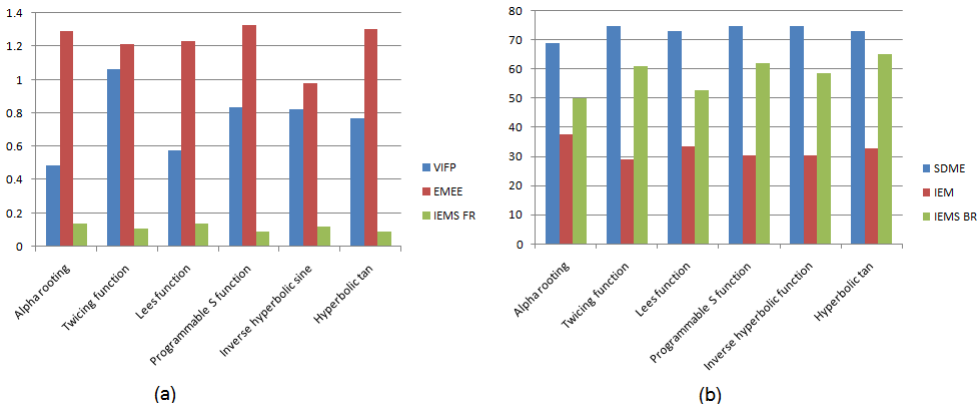

Fig. 5.31: (a) Plots of average values of VIFP, EMEE, IEMS$_{FR}$ (b) Plots of average values of SDME, IEM, IEMS$_{BR}$

Table 5.9: Comparison of normalized average values of metrics in percentage for various mapping functions

Images	VIFP	EMEE	SDME	IEM	IEMS$_{FR}$	IEMS$_{BR}$
Alpha-rooting	46	97	92	**100**	**100**	77
Twicing function	**100**	91	**100**	77	76	93
Function proposed by Lee	54	93	97	89	98	81
Programmable-S-function	79	**100**	**100**	81	66	95
Inverse hyperbolic sine	77	74	**100**	80	86	90
Hyperbolic tan	72	98	98	87	64	**100**

Enhanced general images using twicing function is shown in Fig. 5.33.

Application to Colour Images

The proposed algorithm is applied to the luminance component of the YCbCr space of colour images. The enhanced *lena* image using inverse hyperbolic sine and hyperbolic tan functions along with original images are shown in Fig. 5.34.

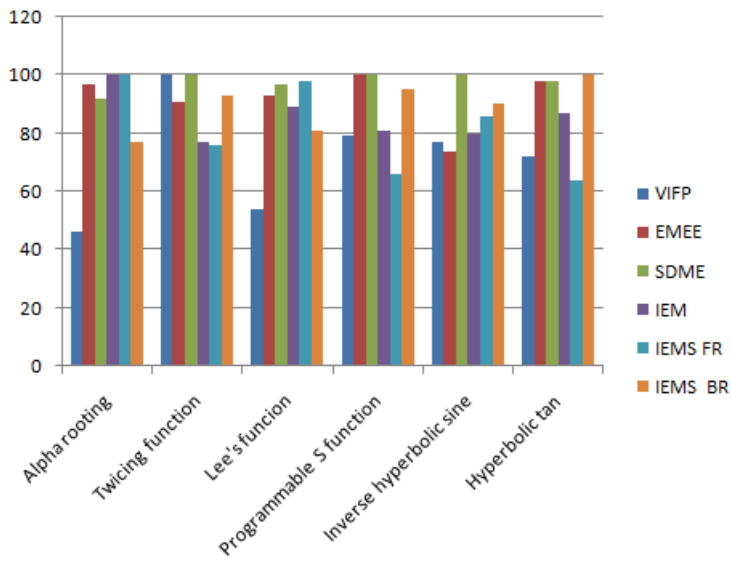

Fig. 5.32: Plots of normalized average values of VIFP, EMEE, SDME, IEM, IEMS$_{FR}$, IEMS$_{BR}$

5.4 Conclusion

The chapter presents a simple, global, transform based approach to enhance low contrast images through linear and nonlinear modification of AC SMRT coefficients. In both cases, DC SMRT coefficient value is scaled to bring the mean of image histogram to the centre of histogram range. In the linear method, AC SMRT coefficients are scaled uniformly to improve the contrast to optimum levels. The scaling factors are selected automatically to utilize the full dynamic range of the histogram. In nonlinear method, the transform coefficients are modified using nonlinear mapping techniques. Nonlinear scaling of AC SMRT coefficients is done using nonlinear mapping functions. Simple hyperbolic mapping functions with symmetry are also proposed to expand / compress coefficients at low / high values respectively. Both techniques are compared with image enhance-

Fig. 5.33: (a)Original images, enhanced versions using (b)LET (c) NLET using twicing function

ment using HE in terms of quantitative assessment metrics.

The proposed LET and NLET methods are applied to general and mammogram images. Simulation results show that the resultant enhanced images using the proposed methods are better in contrast and brightness. These methods can give good performance for low contrast images quantitatively and qualitatively. The LET method, applied to fingerprint images and scanned documents, produces a thresholded binary image when the c_{ac} is made much higher. The calcification areas of mammogram images are enhanced better by

Fig. 5.34: Original *lena* colour image(a) and enhanced images using NLET (b) inverse hyperbolic sine (c) hyperbolic tan functions

NLET method. Though, the six nonlinear functions considered perform almost in a similar manner for different types of images examined, twicing function seems to be better than other functions.

LET and NLET are applied to colour images also by modifying the Y component of YCbCr representation. Results of enhancement reveals that LET is more suitable in terms of quality and computational simplicity.

Chapter 6

SMRT based Block Level Fuzzy Enhancement Techniques

6.1 Introduction

Global enhancement techniques are based on modification of intensity values of all the pixels in the image. This may cause over-enhancement of bright and dark areas of the image. On the other hand, image can be divided into non-overlapping image blocks and application of enhancement techniques on these blocks can reduce problems associated with global enhancement techniques. Block level enhancement techniques usually introduce blocking artifacts and need to be minimized.

Fuzzy techniques offer flexible framework for the development of image enhancement algorithms. They are nonlinear, knowledge-based and robust. The potential of fuzzy set theory with respect to image enhancement is not yet investigated in comparison with other established methods. Recently, fuzzy theory has been used to develop new techniques for contrast improvement. A higher con-

trast can be achieved by darkening the gray levels in the lower gray level and brightening the ones in the upper gray level in a nonlinear manner. Fuzzy techniques in spatial domain offer different tools of fuzzy set theory to adjust the image contrast, namely Fuzziness minimization, Equalization using fuzzy expected value, Histogram hyperbolization, α-enhancement, rule based approach, fuzzy relations etc. An examination of fuzzy methods in transform domain may be investigated to develop better enhancement techniques.

Two well-known contrast enhancement techniques are employed in the current chapter to modify SMRT coefficients- Fuzziness minimization based on intensification operator and the fuzzy rule based contrast enhancement method.

6.2 Intensification Operator based Enhancement using SMRT

Fuzzy set theory has been applied to develop new methods for image enhancement to maximize the dynamic range by reducing image fuzziness. This processing usually implies the use of a nonlinear function. A possible mathematical form of such a function is the intensification operator (Appendix B).

Intensification operator (INT) is used to reduce the fuzziness of the image that results in an increase of image contrast. INT operator is used usually in the spatial domain and the idea can be extended to transform domain applications.

6.2.1 Intensification Operator in Spatial Domain

Fuzzy image enhancement in spatial domain is based on gray level mapping from a gray plane into a fuzzy plane using a membership

transformation. Gray levels of the image can be assigned a membership value depending on the gray level intensity of each pixel. An INT operator applied on this fuzzy set will increase/decrease the membership values above/below the set threshold value. Defuzzification of the modified membership values produces enhanced image.

Mathematical formulation of fuzzy intensification based image enhancement adopted in this work is summarized below. A digital image with gray level values, r in the range [0,255], is assigned a membership value in accordance with a piecewise linear membership function $B(r)$ between r_{min} & r_{max} and used to describe the linguistic concept of "brightness of gray levels" is shown in Fig 6.1. If the pixel gray level has a membership value less than 0.5, it is more likely to be dark than bright, else bright than dark.

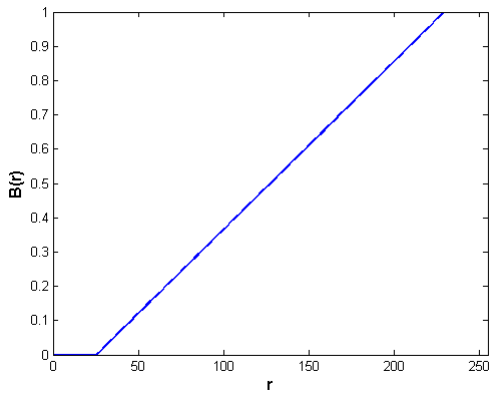

Fig. 6.1: Piecewise linear membership function

$B(r)$ is expressed mathematically as

$$B(r) = \begin{cases} 0, & 0 \leq r \leq r_{min} \\ a.r + b, & r_{min} < r < r_{max} \\ 1, & r_{max} \leq r \leq 255 \end{cases} \tag{6.1}$$

The slope and intercept, represented by a and b respectively, are calculated as

$$a = \frac{1}{(r_{max} - r_{min})} \tag{6.2}$$

$$b = 1 - a.r_{max} \tag{6.3}$$

A simple way to achieve contrast enhancement by reducing the fuzziness of the set is to apply fuzzy INT operator, as defined in Eq. 1.12, on the membership function of the fuzzy set. A flexible INT operator can be defined as in Eq. 6.4, where $B(r)$ represents the membership value of the pixel r and $B(r_t)$ represents the flexible threshold.

$$\text{INT(B(r))} = \begin{cases} \frac{B^2(r)}{B(r_t)}, & 0 \leq B(r) \leq B(r_t) \\ 1 - \frac{(1-B(r))^2}{1-B(r_t)}, & B(r_t) < B(r) \leq 1 \end{cases} \tag{6.4}$$

This operation reduces the fuzziness by increasing/decreasing the value of $B(r)$ that is above/below the threshold value, $B(r_t)$. Fuzziness can be reduced further by increasing the power of $B(r)$ as

$$\text{INT(B(r))} = \begin{cases} \frac{B^p(r)}{B^{(p-1)}(r_t)}, & 0 \leq B(r) \leq B(r_t) \\ 1 - \frac{(1-B(r))^p}{(1-B^{(p-1)}(r_t))}, & B(r_t) < B(r) \leq 1 \end{cases} \tag{6.5}$$

Result of the INT operator for the piecewise linear function $B(r)$ would be the modified membership function $B'(r) = \text{INT}(B(r))$ as shown in Fig. 6.2 for various values of p. Fuzziness decreases with increase in value of p.

6.2.2 Intensification Operator in SMRT Domain

Basic gray level transformation using fuzzy INT operator, Eq. 6.4, can be reformulated to suit the transform domain. Within the

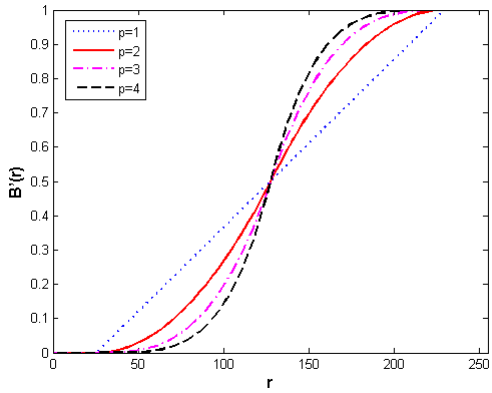

Fig. 6.2: Fuzzy Intensification operator plot for different p

maximum and minimum limits, fuzzification in the spatial domain is completely described by $B(r) = a.r + b$. Hence Eq. (6.4) can be modified by combining the fuzzification and intensification operations together to yield

$$B'(r) = \begin{cases} \frac{(a.r+b)^2}{B(r_t)} & , r_{min} \leq a.r + b \leq B(r_t) \\ 1 - \frac{(1-a.r-b)^2}{1-B(r_t))} & , B(r_t) < a.r + b \leq r_{max} \end{cases} \tag{6.6}$$

Defuzzification operation is also combined with Eq. 6.6 and the resulting gray level values, r' can be obtained from $B'(r) = a.r' + b$ as

$$r' = \frac{B'(r) - b}{a} \tag{6.7}$$

$$r' = \begin{cases} \frac{b}{B(r_t)}[\frac{a}{b}.r^2 + 2.r + \frac{b-B(r_t)}{a}] & , \frac{r_{min}-b}{a} \leq r \leq \frac{B(r_t)-b}{a} \\ \frac{b-1}{B(r_t)-1}[\frac{a}{b-1}.r^2 + 2.r + \frac{b-B(r_t)}{a}] & , \frac{B(r_t)-b}{a} < r \leq \frac{r_{max}-b}{a} \end{cases} \tag{6.8}$$

For transform domain applications, Eq. 6.8 can be used for modification of transform coefficients by reducing the fuzziness.

In the transform domain, an approximate image histogram can be constructed from the block mean values given by DC SMRT coefficients, $S^B(0,0)$ as explained in section 3.3.2. Hence Eq. (6.2) & (6.3) can be modified in terms of block DC SMRT coefficients as

$$a = \frac{1}{(s^B_{max} - s^B_{min})} \quad \& \quad b = 1 - a.s^B_{max}, \tag{6.9}$$

where $s^B_{min} = \min\{\frac{S^B(0,0)}{N^2}\}$, $s^B_{max} = \max\{\frac{S^B(0,0)}{N^2}\}$. The threshold value, $s_t = \frac{B(r_t)-b}{a}$, is fixed as $s^B_{max} < s_t < s^B_{min}$.

6.2.3 Fuzzy Image Enhancement in SMRT Domain

SMRT based fuzzy image enhancement technique, using the INT operator (FIOS) in Eq. (6.8), can be described by the following equations. Let S^B and S^B_{sq} be the SMRT matrices corresponding to 8×8 block of pixel values and squared pixel values respectively. The modified transform coefficients of the enhanced image are

$$S^B_{mod}(i,j) = k_1.[k_2.S^B_{sq}(i,j) + k_3.S^B(i,j)], \text{ for } i,j = 0,1,2,...,7 \tag{6.10}$$

$$S^B_{mod}(0,0) = S^B_{mod}(0,0) + k_1.k_4 \tag{6.11}$$

where $k_3 = 2$, $k_4 = \frac{b-B(r_t)}{a}$

- Case(i) if $\frac{S^B(0,0)}{N^2} < s_t$, then $k_1 = \frac{b}{B(r_t)}$ & $k_2 = \frac{a}{b}$

- Case(ii) if $\frac{S^B(0,0)}{N^2} \geq s_t$, then $k_1 = \frac{b-1}{B(r_t)-1}$ & $k_2 = \frac{a}{b-1}$

Here, comparison of block mean values is done with the threshold (s_t) and can be made adaptive, depending on image characteristics.

FIOS Algorithm

The different steps to perform FIOS are

- Image is divided into non-overlapping blocks of size 8×8 and the corresponding SMRT matrices, S^B and S^B_{sq} are obtained.
- Approximate image histogram is constructed from the block mean values (section 3.3.2).
- s^B_{min} & s^B_{max} of the histogram are used to find the parameters a & b using Eq. (6.9).
- $s_t \in (s^B_{min}, s^B_{max})$ is chosen based on the image characteristics.
- For each block,
  - k_1, k_2, k_3, k_4 are computed from the values of $\frac{S^B(0,0)}{N^2}$ & s_t.
  - SMRT coefficients are modified using Eqs.(6.10) and (6.11).
  - Inverse SMRT is computed.

6.3 Rule based Enhancement using SMRT

The fuzzy rule based approach is a powerful and universal method for many image processing tasks. A fuzzy rule based model operates on an *if* $\rightarrow$ *then* principle, where *if* corresponds to fuzzy inputs and *then* corresponds to some fuzzy consequences.

6.3.1 Fuzzy Rule based Technique in Spatial Domain

Fuzzy image enhancement is basically a question of whether a pixel should become brighter or darker than it already is. In fuzzy theory, gray level intensity (r) of an image can be described by three linguistic terms *Dark*, *Gray* and *Bright*, represented by trapezoidal and triangular membership functions as shown in Fig. 6.3(a). The corresponding linguistic output variables (r_o) are *Black*, *Midgray* and *White*. When Takagi-Sugeno fuzzy rule based system is used, outputs can be represented as fuzzy singletons denoted by r_o^b for *black*, r_o^g for *mid gray* and r_o^w for *white* as shown in Fig. 6.3(b).

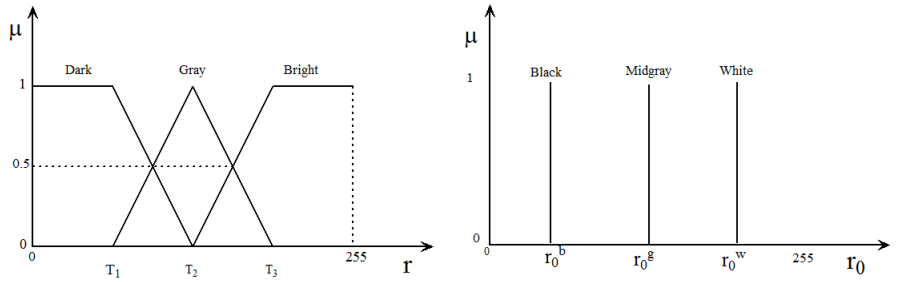

Fig. 6.3: Membership functions for fuzzy rule based contrast enhancement

The important steps for fuzzy rule based enhancement are:

- Initialization of the parameters.
- Fuzzification of gray levels.
- Inference procedure to evaluate appropriate rules
  (For example, if r & r_o denote input and output variables,
  - Rule 1: If r is *dark* then $r_o = r_o^b$ is *black*

  - Rule 2: If r is *gray* then $r_o = r_o^g$ is *midgray*
  - Rule 3: If r is *bright* then $r_o = r_o^w$ is *white*)

- Defuzzification of the output using three singletons, r_o^b, r_o^g & r_o^w as shown in Fig. 6.3(b) (eg. $r_o^b = r_{min}$, $r_o^g = r_{mean}$, $r_o^w = r_{max}$).

$$r' = \frac{\mu_{dark}(r).r_o^b + \mu_{gray}(r).r_o^g + \mu_{bright}(r).r_o^w}{\mu_{dark}(r) + \mu_{gray}(r) + \mu_{bright}(r)} \tag{6.12}$$

Trapezoidal function, $f : r[0, 255] \rightarrow [0, 1]$, is selected to represent the input fuzzy set membership functions generally and is shown in Fig. 6.4. The dynamic range of r for 8-bit image representation is [0,255].

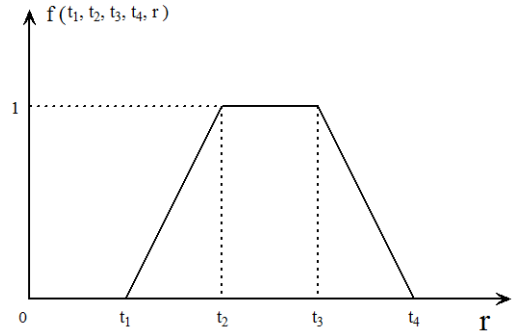

Fig. 6.4: Trapezoidal function for representing the input membership functions

The function f can be represented mathematically as

$$f(t_1, t_2, t_3, t_4, r) = \begin{cases} 0, & \text{if } 0 \leq r < t_1 \\ \frac{r-t_1}{t_2-t_1}, & \text{if } t_1 \leq r < t_2 \\ 1, & \text{if } t_2 \leq r < t_3 \\ \frac{t_4-r}{t_4-t_3}, & \text{if } t_3 \leq r < t_4 \\ 0, & \text{if } t_4 \leq r \leq 255 \end{cases} \tag{6.13}$$

Hence, the input membership function, μ, for *dark*, *gray* and *bright*, as shown in Fig. 6.3(a), can be expressed mathematically in terms of f as

$$\begin{aligned} \mu_{dark}(r) &= f(0, 0, T_1, T_2, r) \\ \mu_{gray}(r) &= f(T_1, T_2, T_2, T_3, r) \\ \mu_{bright}(r) &= f(T_2, T_3, 255, 255, r) \end{aligned} \tag{6.14}$$

The modified gray level values (r') corresponding to gray level values (r) can be obtained from Eq. 6.12 where $\mu_{dark}(r) + \mu_{gray}(r) + \mu_{bright}(r) = 1$.

6.3.2 Fuzzy Rule based Technique in SMRT Domain

Improvements in brightness and contrast can be achieved by separately modifying the block level DC and AC SMRT coefficients respectively. Two constants, necessary for multiplication and addition (v_m^z and v_a^z, $z \in \{dark, gray, bright\}$), can be found from the parameters t_1, t_2, t_3, t_4 and average brightness of each block ($\mu_s^B 2$). Average brightness of each block can be found from DC SMRT coefficient ($S^B(0,0)$) as $\mu_s^B = \frac{S^B(0,0)}{N^2}$.

$v_m^z = f'(t_1, t_2, t_3, t_4, \mu_s^B)$ & $v_a^z = f"(t_1, t_2, t_3, t_4, \mu_s^B)$ can be expressed as

$$f' = \begin{cases} 0, & 0 \leq \mu_s^B < t_1 \\ \frac{1}{t_2 - t_1}, & t_1 \leq \mu_s^B < t_2 \\ 1, & t_2 \leq \mu_s^B < t_3 \\ \frac{-1}{t_4 - t_3}, & t_3 \leq \mu_s^B < t_4 \\ 0, & t_4 \leq \mu_s^B \leq 255 \end{cases} \tag{6.15}$$

$$f" = \begin{cases} 0, & 0 \leq \mu_s^B < t_1 \\ \frac{-t_1}{t_2 - t_1}, & t_1 \leq \mu_s^B < t_2 \\ 1, & t_2 \leq \mu_s^B < t_3 \\ \frac{t_4}{t_4 - t_3}, & t_3 \leq \mu_s^B < t_4 \\ 0, & t_4 \leq \mu_s^B \leq 255 \end{cases} \tag{6.16}$$

$$\begin{aligned} v_m^{dark} &= f'(0, 0, T_1, T_2, \mu_s^B) \\ v_m^{gray} &= f'(T_1, T_2, T_2, T_3, \mu_s^B) \\ v_m^{bright} &= f'(T_2, T_3, 255, 255, \mu_s^B) \end{aligned} \tag{6.17}$$

$$\begin{aligned} v_a^{dark} &= f"(0, 0, T_1, T_2, \mu_s^B) \\ v_a^{gray} &= f"(T_1, T_2, T_2, T_3, \mu_s^B)) \\ v_a^{bright} &= f"(T_2, T_3, 255, 255, \mu_s^B) \end{aligned} \tag{6.18}$$

The value of μ_s^B in each block falls in any of the 5 ranges given in Eqs. 6.15 & 6.16. Comparison with DC SMRT coefficient alone is performed for each of the 8×8 image blocks. Thus for each block, SMRT coefficients are to be multiplied with v_m^z and DC SMRT coefficient is to be added with v_a^z, where $z \in \{dark, gray, bright\}$.

Let M^z, $z \in \{dark, gray, bright\}$ be the matrices of modified membership values of the 8×8 block of the SMRT coefficients, S^B. These values can be computed as

$$\begin{aligned} M^z &= v_m^z . S^B \\ M^z(0,0) &= M^z(0,0) + v_a^z \end{aligned} \tag{6.19}$$

The fuzzy rule based contrast enhancement method in spatial domain, as given in Eq. 6.12, reformulated in the SMRT domain can be described by

$$S_{mod} = M^{dark} . r_o^b + M^{gray} . r_o^g + M^{bright} . r_o^w \tag{6.20}$$

where S_{mod} is the modified SMRT blocks.

FRBS Algorithm

- Image is divided into non-overlapping blocks of size 8×8 and the corresponding SMRT matrices, S^B are obtained.
- Approximate image histogram is constructed from the block mean values (section 3.3.2).
- r_{min}, r_{mean} & r_{max} of the histogram are found and the values are assigned to r_o^b, r_o^g & r_o^w.
- For each block,
  - Average brightness μ_s^B is computed from S^B.
  - v_m^z, v_a^z, $z \in \{dark, gray, bright\}$ are found using Eqs. 6.17 & 6.18.
  - Membership matrices, M^z, $z \in \{dark, gray, bright\}$ are found using Eq. 6.19.
  - SMRT coefficients are modified using Eq. 6.20.
  - Inverse SMRT is computed.

6.4 Results and Analysis

General and mammogram images are used to investigate the effectiveness of the fuzzy techniques for image enhancement. The fuzzy intensification operator based algorithm (FIOS) and fuzzy rule based technique (FRBS) implemented in SMRT domain for image enhancement are applied to images that are low in contrast. Fuzzy INT operator based image enhancement in the spatial domain (FIOP) [166], is used to compare the effectiveness of the proposed method.

The FIOS algorithm, explained in section 6.2.3, is applied by varying threshold, s_t, and the corresponding image histograms are observed. The membership values below/above the threshold are changed to a lower/higher value. Hence, a compression of membership values appears to the left of the threshold and an expansion to the right. Most of the membership values change to a higher value when s_t is small and the image appears to be bright. On application of the correct threshold, the image appears to be enhanced with edges more pronounced. The effect of changing threshold values on *baboon* and mammogram *(mdb028)* images are shown in Figs. 6.5 and 6.6 along with the respective histograms. Simulation results show that the image mean can give better enhancement and hence threshold value is fixed as the image mean.

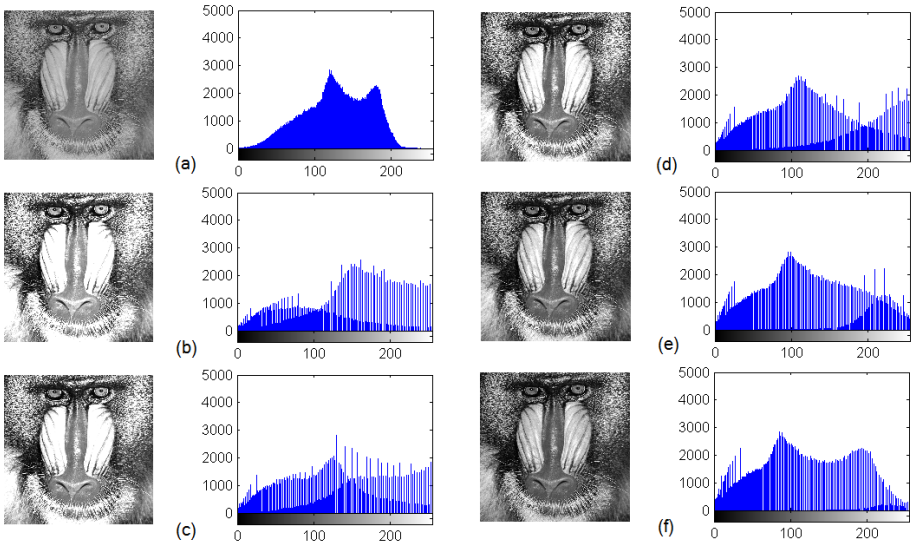

Fig. 6.5: Images and their histograms (a) Original *baboon* image (b) to (f) Enhanced images using FIOS for thresholds $B(s_t) = 0.4, 0.5, 0.6, 0.7, 0.8$

FRBS method is also applied to the images and the original and enhanced images with their corresponding histograms are shown

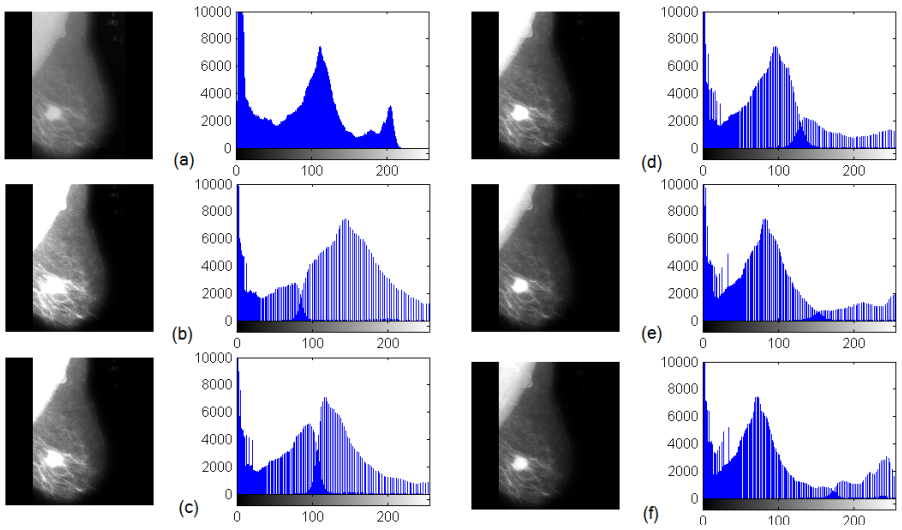

Fig. 6.6: Mammogram(*mdb028*) images and their histograms (a) Original image (b) to (f)Enhanced images using FIOS for different thresholds $B(s_t) = 0.4, 0.5, 0.6, 0.7, 0.8$

in Fig. 6.7. The histograms show an improvement in contrast and brightness for all images.

The FIOP, FIOS & FRBS methods are applied to general and mammogram images used in sections 5.2.3 & 5.3.3. The enhanced general images using the three methods are shown in Fig. 6.8. Enhanced images of calcification, benign and malignant areas of mammograms taken from MIAS database are shown in Figs. 6.9, 6.10 and 6.11 respectively. Subjective evaluation of the results shows that there is enhancement using both methods, but better enhancement for FRBS method.

Tables 6.1 and 6.2 show the metric values obtained for the general and mammogram images for the existing and proposed metrics respectively. The images considered have mean values ranging from 110 to 175 and SD ranging from 8 to 34 indicating dark to bright images and low contrast to medium contrast images respectively.

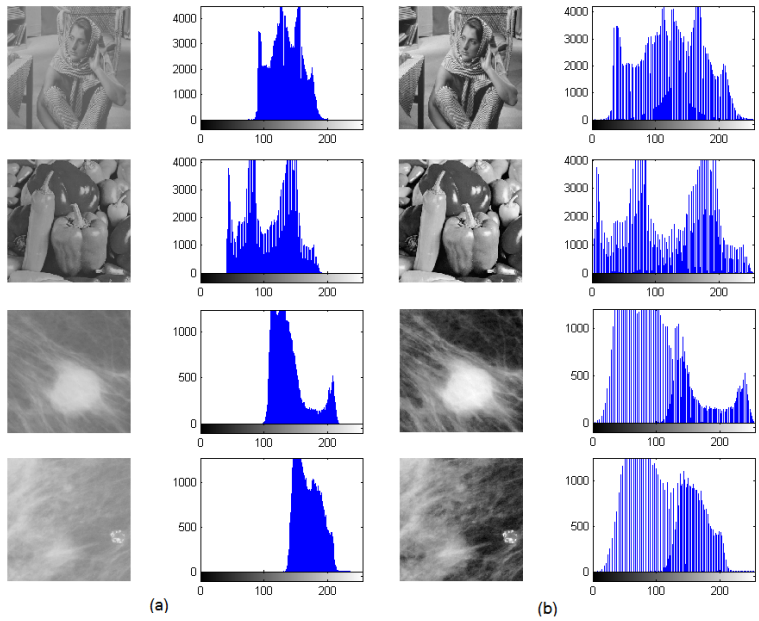

Fig. 6.7: Images (*barbara, peppers, mdb028, mdb119*) and their histograms (a) Original (b) Enhanced for FRBS method

Average of statistical parameters such as mean and SD values of the 16 images shows that FRBS method keeps the brightness level to mid histogram range and SD to the maximum for most of the images. VIFP and SDME of all images show good values for FRBS method. EMEE of all images except *peppers* shows good values for FRBS method. Table 6.2 shows that all the proposed metric values give good results for FRBS for most of the images. The average values of all metrics, taken on 16 images, show good results for FRBS method.

Fig. 6.12 shows a plot of the normalized average values of the metrics in percentage. This plot also shows that average values of the metrics considered give good metric values for FRBS method.

Fig. 6.8: (a) Original images, Enhanced images using (b) FIOP, (c) FIOS, (d) FRBS methods

Table 6.1: Comparison of Mean, SD, VIFP, EMEE, SDME of various images for FIOP, FIOS and FRBS

Images	Mean				SD				VIFP			EMEE				SDME			
	Image	FIOP	FIOS	FRBS	Image	FIOP	FIOS	FRBS	FIOP	FIOS	FRBS	Image	FIOP	FIOS	FRBS	Image	FIOP	FIOS	FRBS
baboon	131.9	130.5	136.3	132.7	25.4	43.1	**49.9**	43.5	1.06	1.02	**1.11**	0.35	0.981	1.08	**1.58**	77.8	69.4	67.8	**80.3**
barbara	115.1	114.6	121.9	127.4	28.7	47.9	**57.3**	50.9	1.02	0.94	**1.22**	0.36	1.073	1.19	**1.73**	77.2	77.1	74.6	**102.5**
house	110.0	110.1	118.6	123.7	31.3	50.5	**69.8**	55.3	1.09	1.01	**1.11**	0.33	0.864	0.99	**1.76**	77.9	73.8	72.0	**85.3**
peppers	112.1	111.1	122.0	126.4	33.8	55.6	**67.8**	54.1	0.97	0.87	**1.12**	0.45	1.529	**1.73**	1.64	76.7	78.4	76.6	**108.7**
mdb009	154.3	152.5	153.9	117.2	7.9	14.9	16.1	**32.0**	1.55	1.63	**1.72**	0.04	0.088	0.09	**0.47**	97.6	104.9	104.1	**131.5**
mdb170	173.8	168.4	175.7	131.6	20.8	36.8	**40.2**	37.3	1.36	1.44	**1.45**	0.05	0.089	0.10	**0.13**	96.5	108.6	107.6	**124.0**
mdb204	160.0	158.7	160.0	115.0	10.3	18.4	21.5	**37.5**	1.45	1.50	**1.52**	0.04	0.080	0.09	**0.49**	96.8	108.4	107.4	**136.5**
mdb227	174.9	171.9	174.9	127.0	11.1	20.6	22.2	**30.1**	1.47	1.56	**1.82**	0.04	0.082	0.09	**0.26**	99.3	107.2	106.8	**132.0**
mdb005	140.0	139.0	141.4	130.3	16.6	29.7	33.1	**41.7**	1.42	1.51	**1.65**	0.05	0.106	0.11	**0.23**	97.3	102.9	101.1	**131.6**
mdb010	169.4	168.2	169.6	127.1	12.4	22.5	25.2	**41.8**	1.46	1.56	**1.99**	0.04	0.084	0.09	**0.31**	100.2	105.3	104.2	**126.3**
mdb019	172.9	171.3	173.4	129.1	14.3	26.2	28.6	**52.0**	1.46	1.59	**2.12**	0.04	0.074	0.08	**0.43**	100.1	108.6	107.6	**134.9**
mdb132	151.1	153.1	152.2	116.8	16.2	27.3	35.2	**39.7**	1.36	1.50	**1.57**	0.05	0.093	0.10	**0.43**	97.4	105.3	103.2	**129.3**
mdb023	164.1	161.6	165.1	136.8	15.2	26.5	28.7	**36.7**	1.54	1.64	**1.66**	0.04	0.078	0.08	**0.16**	100.6	106.9	106.2	**132.7**
mdb058	173.7	171.2	174.0	125.5	13.7	25.3	27.4	**53.6**	1.44	1.55	**2.06**	0.04	0.084	0.09	**0.55**	99.0	107.0	106.1	**125.6**
mdb134	162.9	164.9	164.6	118.4	19.5	33.3	40.5	**61.2**	1.35	1.55	**1.75**	0.04	0.075	0.08	**0.48**	98.1	109.8	107.1	**133.2**
mdb202	156.2	152.8	161.6	137.0	29.9	48.9	**58.0**	53.2	1.27	1.33	**1.34**	0.05	0.099	0.11	**0.13**	97.1	106.9	104.3	**147.9**
Average	151.4	150.0	154.1	126.4	19.2	33.0	38.8	**45.0**	1.33	1.39	**1.58**	0.13	0.340	0.38	**0.67**	93.1	98.8	97.3	**122.6**

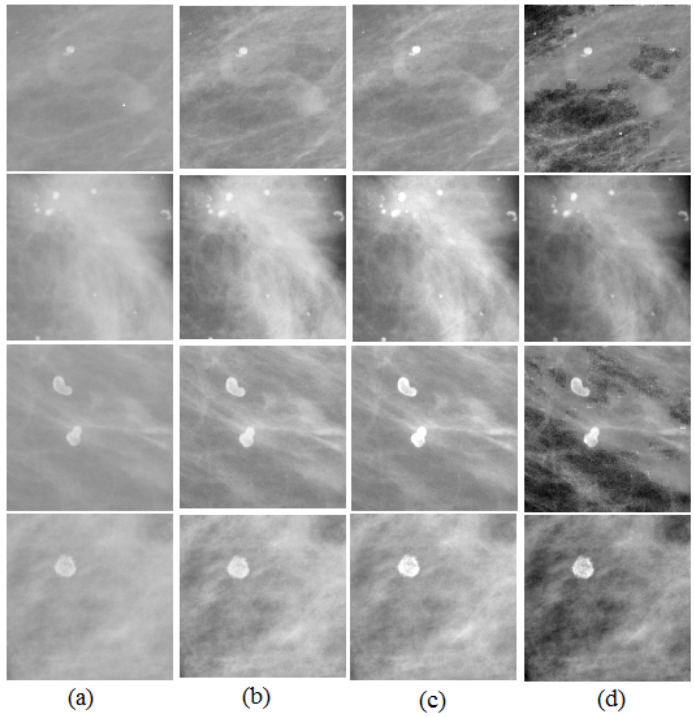

Fig. 6.9: (a) Original mammogram sub-images containing calcifications, Enhanced images using (b) FIOP, (c) FIOS, (d) FRBS methods

Conclusion

A flexible fuzzy INT operator based image enhancement based on SMRT (FIOS) is proposed first. The algorithm hence derived is tested on both general and mammogram images. The results are compared with that of the fuzzy INT operator based enhancement technique in the spatial domain (FIOP). All metric values are good for FIOS compared to FIOP. The FIOS algorithm requires SMRT of both image blocks and image pixel squared blocks and the computational complexity is thus increased. So, this puts a limit to the FIOS algorithm.

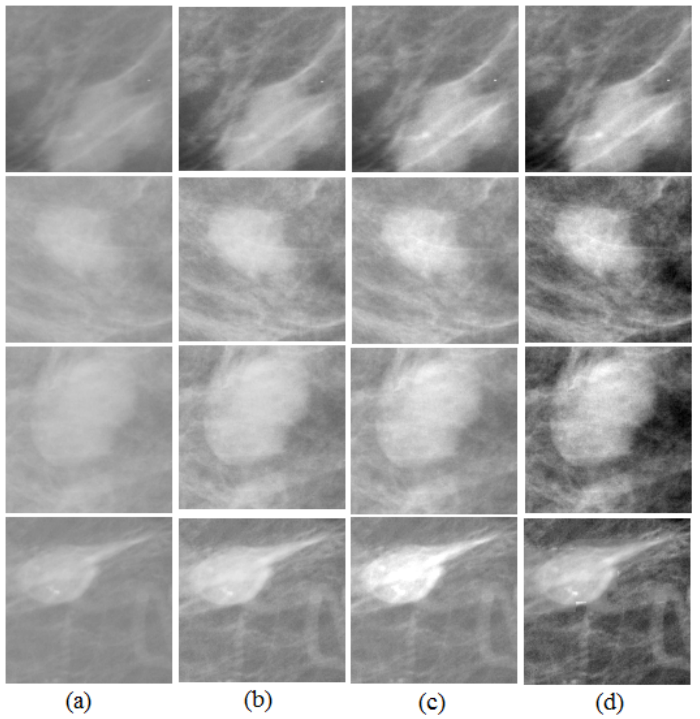

Fig. 6.10: (a) Original mammogram sub-images containing benign masses, Enhanced images using (b) FIOP, (c) FIOS, (d) FRBS methods

The usefulness of the fuzzy rule based algorithm is investigated. Fuzzy rule based algorithm overcomes the drawback of FIOS as it requires the SMRT of the image blocks only. Subjective evaluation of the enhanced images shows that there is better enhancement for FRBS compared to FIOP and FIOS. Comparison of the IQA metric values for the different methods also substantiates this. A comparison of the methods considered for global and block level image enhancement will be useful in finding a method suitable for all images.

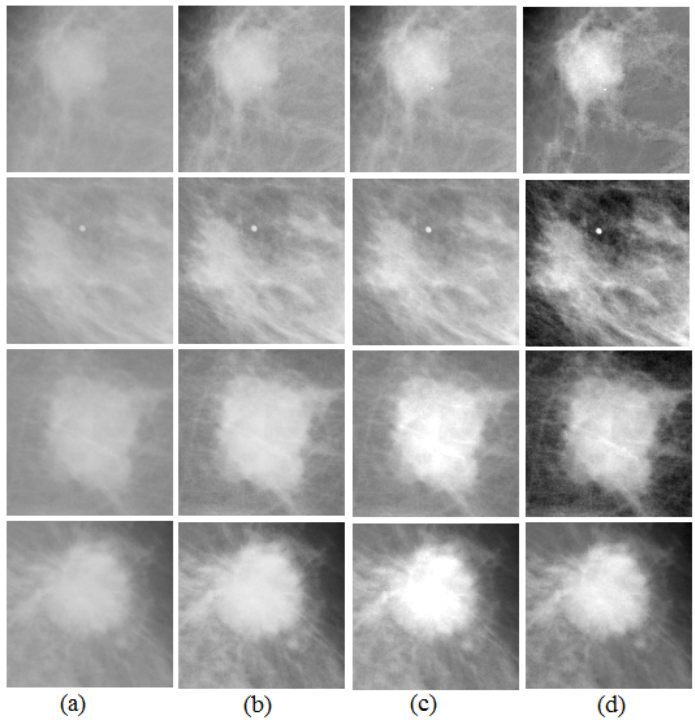

Fig. 6.11: (a) Original mammogram sub-images containing malignant masses, Enhanced images using (b) FIOP, (c) FIOS, (d) FRBS methods

6.5 Comparison of Global and Block Level Enhancement Methods

The results of the global (LET, NLET) and block level (FIOS, FRBS) methods of image enhancement are compared quantitatively using the metrics VIFP, EMEE, SDME and IEM. It is not reasonable to compare the SMRT based metrics for global and block level methods, as their approaches are different. Hence, these metrics are not considered for the analysis in this section. The values of these metrics for 16 images and the average values of the metrics for different methods are tabulated in Table 6.3 for comparison.

Table 6.2: Comparison of IEM, IEMS$_{FR}$, IEMS$_{BR}$ of various images for FIOP, FIOS and FRBS

Images	IEM			IEMS$_{FR}$		IEMS$_{BR}$		
	FIOP	FIOS	FRBS	FIOS	FRBS	Image	FIOS	FRBS
baboon	10.29	**13.51**	10.61	**32.48**	27.88	13.62	**26.61**	22.96
barbara	9.47	**12.83**	11.43	**32.44**	22.13	12.35	**24.36**	22.00
house	9.44	11.40	**12.05**	32.50	**41.20**	10.06	18.83	**19.97**
peppers	8.23	**12.03**	9.27	**32.16**	27.10	14.54	**29.97**	23.28
mdb009	12.79	13.84	**24.93**	32.13	**69.01**	2.98	6.28	**11.67**
mdb170	10.73	11.58	**12.16**	**32.32**	29.90	3.32	**6.84**	6.15
mdb204	12.52	13.65	**26.27**	32.20	**72.16**	3.29	7.06	**11.92**
mdb227	12.26	13.73	**19.83**	32.06	**43.15**	2.94	5.98	**7.89**
mdb005	11.64	13.65	**18.06**	32.37	**39.84**	2.96	6.00	**7.36**
mdb010	11.91	13.71	**24.47**	32.08	**54.38**	2.76	5.50	**9.38**
mdb019	11.44	13.67	**25.67**	32.09	**58.01**	2.49	4.94	**9.01**
mdb132	11.63	13.15	**23.10**	32.24	**54.78**	2.94	6.16	**9.13**
mdb023	12.16	13.67	**18.58**	32.14	**45.63**	2.45	4.89	**6.93**
mdb058	11.57	13.70	**27.20**	32.12	**62.65**	3.24	6.51	**12.79**
mdb134	10.35	13.36	**24.18**	32.20	**55.37**	2.52	5.06	**8.71**
mdb202	9.28	11.60	**11.61**	**32.64**	29.86	2.97	**5.93**	5.43
Average	10.98	13.07	**18.71**	32.26	**45.82**	5.34	10.68	**12.16**

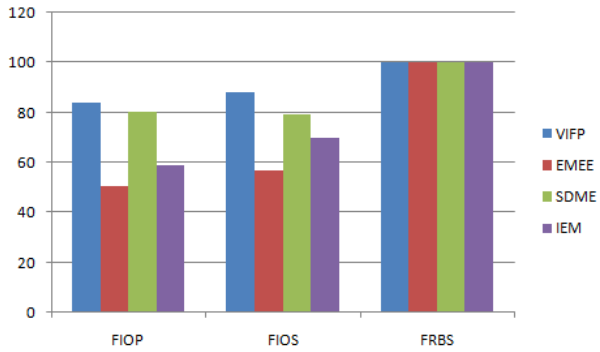

Fig. 6.12: Normalised plots of average values of the metrics for FIOP, FIOS and FRBS methods

VIFP and SDME values show that LET is superior to other methods. Average values on 16 images also show that LET is superior. FRBS shows good metric values among block level techniques.

A plot of the normalized mean values in percentage is shown in Fig. 6.13. This plot also substantiates that LET and FRBS can be considered as better methods for global and block level enhance-

Table 6.3: Comparison of spatial domain metrics IEM, VIFP, EMEE, SDME of various images for LET, NLET, FIOS and FRBS methods

Images	VIFP				EMEE				SDME				IEM			
	LET	NLET	FIOS	FRBS	LET	NLET	FIOS	FRBS	LET	NLET	FIOS	FRBS	LET	NLET	FIOS	FRBS
baboon	**1.37**	1.08	1.02	1.11	**5.38**	3.28	1.08	1.58	79.87	64.90	67.82	**80.28**	**16.46**	13.52	13.51	10.61
barbara	**1.30**	1.01	0.94	1.22	**31.11**	2.31	1.19	1.73	**109.39**	69.86	74.64	102.47	**14.49**	13.71	12.83	11.43
house	**1.25**	1.06	1.01	1.11	1.15	1.75	0.99	**1.76**	**100.56**	68.04	72.02	85.25	11.29	**13.55**	11.40	12.05
peppers	**1.24**	0.57	0.87	1.12	**6.47**	3.24	1.73	1.64	**118.36**	70.49	76.62	108.65	11.84	**14.98**	12.03	9.27
mdb009	**2.28**	0.69	1.63	1.72	0.33	**1.04**	0.09	0.47	**139.50**	63.73	104.12	131.52	42.69	**44.00**	13.84	24.93
mdb170	**1.71**	0.95	1.44	1.45	**1.49**	0.26	0.10	0.13	**162.11**	83.11	107.61	124.00	**25.43**	21.28	11.58	12.16
mdb204	**1.84**	0.86	1.50	1.52	0.19	**0.72**	0.09	0.49	**157.52**	69.03	107.38	136.45	**39.06**	36.80	13.65	26.27
mdb227	**2.05**	0.93	1.56	1.82	0.37	**0.45**	0.09	0.26	**143.81**	75.01	106.77	132.02	**35.88**	31.57	13.73	19.83
mdb005	**1.91**	0.73	1.51	1.65	0.34	**0.73**	0.11	0.23	**138.28**	75.77	101.14	131.61	28.71	**31.91**	13.65	18.06
mdb010	**2.12**	0.80	1.56	1.99	0.44	**0.97**	0.09	0.31	**132.78**	70.05	104.22	126.31	**33.93**	31.77	13.71	24.47
mdb019	**2.25**	0.79	1.59	2.12	**1.18**	0.69	0.08	0.43	**142.21**	71.27	107.61	134.90	**30.63**	26.96	13.67	25.67
mdb132	**1.78**	0.73	1.50	1.57	0.24	**0.57**	0.10	0.43	**145.22**	72.82	103.17	129.27	**36.63**	31.77	13.15	23.10
mdb023	**2.18**	1.03	1.64	1.66	**0.34**	0.30	0.08	0.16	**142.88**	81.54	106.15	132.72	**35.02**	26.96	13.67	18.58
mdb058	**2.18**	0.75	1.55	2.06	**0.96**	0.84	0.09	0.55	**139.04**	69.86	106.10	125.61	33.07	**37.14**	13.70	27.20
mdb134	**1.92**	0.52	1.55	1.75	0.27	**0.76**	0.08	0.48	**153.99**	70.58	107.13	133.21	28.97	**37.17**	13.36	24.18
mdb202	**1.54**	0.74	1.33	1.34	**0.30**	0.28	0.11	0.13	**155.47**	81.87	104.26	147.89	18.24	**21.89**	11.60	11.61
Average	**2.02**	0.83	1.39	1.58	0.79/3.16	**1.14**	0.38	0.67	**148.91**	72.37	97.30	122.64	**32.82**	27.19	13.07	18.71

ment respectively. But comparison of the SMRT based metrics for global and block level methods separately also shows that LET and FRBS are better methods.

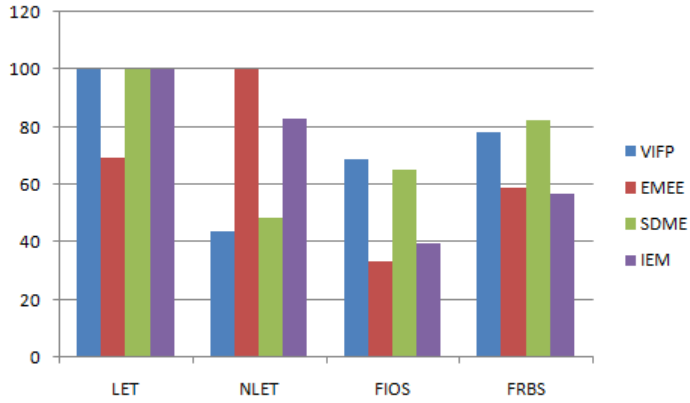

Fig. 6.13: Normalised plots of average values of the metrics for LET, NLET, FIOS and FRBS methods

A method that incorporates the goodness of linear and nonlinear techniques, ie. LET and FRBS, can be a better solution for image enhancement techniques.

6.6 Global Fuzzy Rule based Linear Enhancement in SMRT Domain

A fuzzy rule based modification on the whole image followed by LET integrates the goodness of both the methods. An investigation is carried out in this direction and the following algorithm is developed.

GFLS Algorithm

The different steps for GFLS method:

- SMRT of the whole image is found
- FRBS is applied to the SMRT of the whole image
- Automatic linear scaling method, LET, is applied
- ISMRT of the whole image is found

The new method is applied to general and mammogram images and the results obtained are displayed. Fig. 6.14 shows general images and the corresponding enhanced images. Enhanced images of calcification, benign and malignant portions of mammogram images are shown in Fig. 6.15.

The quantitative metric values obtained for the 16 images are shown in Table 6.4. The average values of the metrics for 16 images calculated for the new method and compared with LET, NLET, FIOS and FRBS methods are given in Table 6.5. The normalized plot of average values of metric values obtained for the five proposed methods is shown in Fig. 6.16.

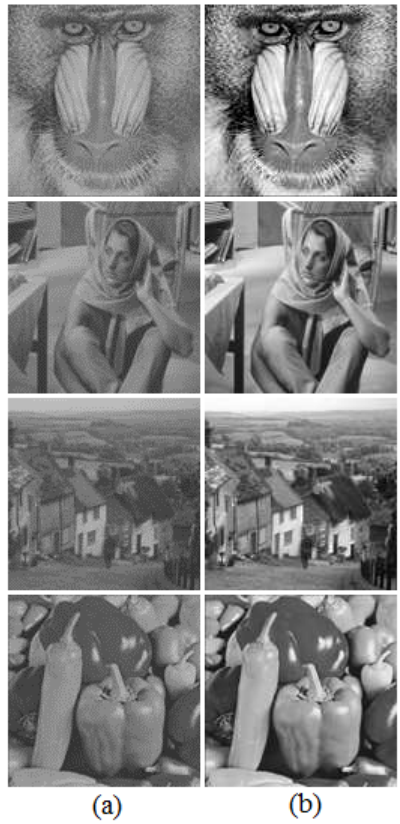

Fig. 6.14: (a)Original images (b) Enhanced images using GFLS method

Subjective Analysis

Subjective ratings of the enhanced images (HE, LET, NLET, FIOP, FIOS, FRBS, GLFS) are carried out using MOS. The general and mammogram images used for the MOS analysis are shown in Figs. 6.17 & 6.18. The judgments from 10 observers are taken using an image quality scale from 1 to 5 where 1 is *bad*, 2 *poor*, 3 *fair*, 4 *good*, 5 *excellent* and the mean of the opinion score is calculated. The MOS values obtained for the seven methods are given in Table 6.6 and the highest two values are highlighted for comparison. The table

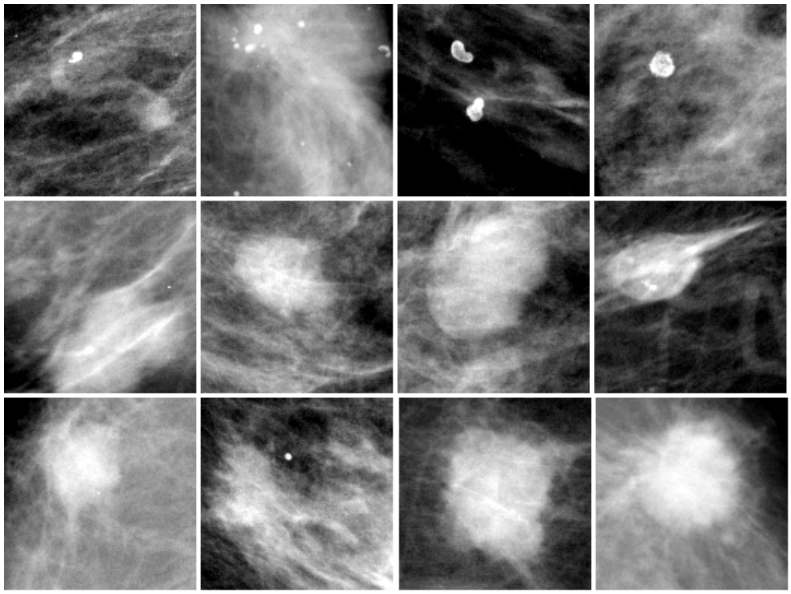

Fig. 6.15: Enhanced images using GFLS method, Row 1- Calcification sub-images, Row 2- Benign areas, Row 3 -Malignant areas

Table 6.4: Mean, SD, VIFP, EMEE, SDME, IEM, IEMS$_{FR}$, IEMS$_{BR}$ values of various images for GFLS method

Images	Mean	SD	VIFP	EMEE	SDME	IEM	IEMS$_{FR}$	IEMS$_{BR}$
baboon	137.80	56.43	1.35	27.71	76.49	15.80	4.95	74.30
barbara	122.71	60.71	1.31	5.83	109.17	14.86	4.49	94.38
house	103.86	60.27	1.29	2.74	95.37	12.85	3.71	54.99
peppers	119.86	63.09	1.25	80.20	115.77	12.23	3.49	88.96
mdb009	86.62	42.27	2.61	1.182	127.99	33.02	28.46	51.62
mdb170	139.74	50.20	1.67	0.514	164.94	17.28	5.81	50.70
mdb204	21.68	44.53	2.26	1.670	165.53	19.83	18.86	51.55
mdb227	111.02	41.22	2.11	0.577	139.96	26.07	13.78	59.48
mdb005	136.10	52.49	1.88	1.367	138.49	22.59	9.95	52.96
mdb010	118.91	50.54	2.17	0.518	129.63	27.87	16.64	48.22
mdb019	127.56	59.10	2.25	8.631	142.34	27.93	17.04	53.90
mdb132	65.10	59.77	2.00	2.279	125.17	25.53	13.53	45.67
mdb023	149.85	49.12	2.11	0.230	145.57	22.65	10.42	38.63
mdb058	117.60	62.43	2.23	4.958	135.75	30.17	20.85	57.10
mdb134	107.53	67.16	2.00	0.732	148.13	24.59	11.87	61.33
mdb202	142.37	63.11	1.52	0.539	157.39	14.60	4.46	45.12
Average	115.38	51.56	2.07	1.95	149.01	23.26	15.55	57.67

shows that LET and GFLS methods give the best Mean Opinion

Table 6.5: Comparison of spatial domain metrics VIFP, SDME and IEM of various images for LET, NLET, FIOS, FRBS and GFLS methods

Images	VIFP					SDME					IEM				
	LET	NLET	FIOS	FRBS	GFLS	LET	NLET	FIOS	FRBS	GFLS	LET	NLET	FIOS	FRBS	GFLS
baboon	**1.37**	1.08	1.02	1.11	1.35	79.87	64.90	67.82	**80.28**	76.49	**16.46**	13.52	13.51	10.61	15.80
barbara	1.30	1.01	0.94	1.22	**1.31**	**109.39**	69.86	74.64	102.47	109.17	14.49	13.71	12.83	11.43	**14.86**
house	1.25	1.06	1.01	1.11	**1.29**	**100.56**	68.04	72.02	85.25	95.37	11.29	**13.55**	11.40	12.05	12.85
peppers	1.24	0.57	0.87	1.12	**1.25**	**118.36**	70.49	76.62	108.65	115.77	11.84	**14.98**	12.03	9.27	12.23
mdb009	2.28	0.69	1.63	1.72	**2.61**	**139.50**	63.73	104.12	131.52	127.99	42.69	**44.00**	13.84	24.93	33.02
mdb170	**1.71**	0.95	1.44	1.45	1.67	162.11	83.11	107.61	124.00	**164.94**	**25.43**	21.28	11.58	12.16	17.28
mdb204	1.84	0.86	1.50	1.52	**2.26**	157.52	69.03	107.38	136.45	**165.53**	**39.06**	36.80	13.65	26.27	19.83
mdb227	2.05	0.93	1.56	1.82	**2.11**	**143.81**	75.01	106.77	132.02	139.96	**35.88**	31.57	13.73	19.83	26.07
mdb005	**1.91**	0.73	1.51	1.65	1.88	138.28	75.77	101.14	131.61	**138.49**	28.71	**31.91**	13.65	18.06	22.59
mdb010	2.12	0.80	1.56	1.99	**2.17**	**132.78**	70.05	104.22	126.31	129.63	**33.93**	31.77	13.71	24.47	27.87
mdb019	**2.25**	0.79	1.59	2.12	**2.25**	142.21	71.27	107.61	134.90	**142.34**	**30.63**	26.96	13.67	25.67	27.93
mdb132	1.78	0.73	1.50	1.57	**2.00**	**145.22**	72.82	103.17	129.27	125.17	**36.63**	31.77	13.15	23.10	25.53
mdb023	**2.18**	1.03	1.64	1.66	2.11	142.88	81.54	106.15	132.72	**145.57**	**35.02**	26.96	13.67	18.58	22.65
mdb058	2.18	0.75	1.55	2.06	**2.23**	**139.04**	69.86	106.10	125.61	135.75	33.07	**37.14**	13.70	27.20	30.17
mdb134	1.92	0.52	1.55	1.75	**2.00**	**153.99**	70.58	107.13	133.21	148.13	28.97	**37.17**	13.36	24.18	24.59
mdb202	**1.54**	0.74	1.33	1.34	1.52	155.47	81.87	104.26	147.89	**157.39**	18.24	**21.89**	11.60	11.61	14.60
Average	2.02	0.83	1.39	1.58	**2.07**	148.91	72.37	97.30	122.64	**149.01**	**32.82**	27.19	13.07	18.71	23.26

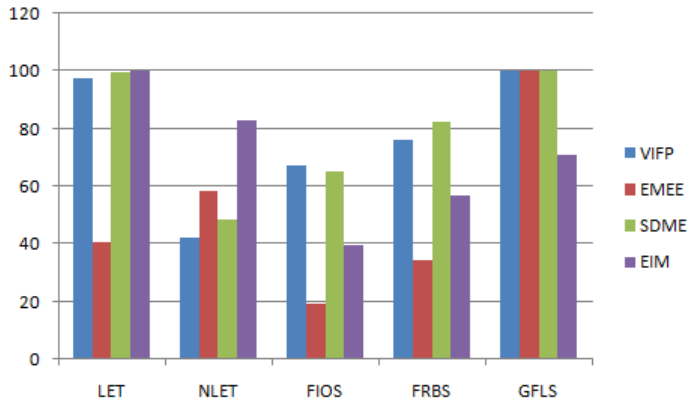

Fig. 6.16: Normalised plots of average values of the metrics for FIOP, FIOS, FRBS and GFLS methods

Scores compared to other methods.

6.7 Conclusion

Block level fuzzy enhancement techniques in the SMRT domain are proposed in the current chapter. Flexible fuzzy INT operator based

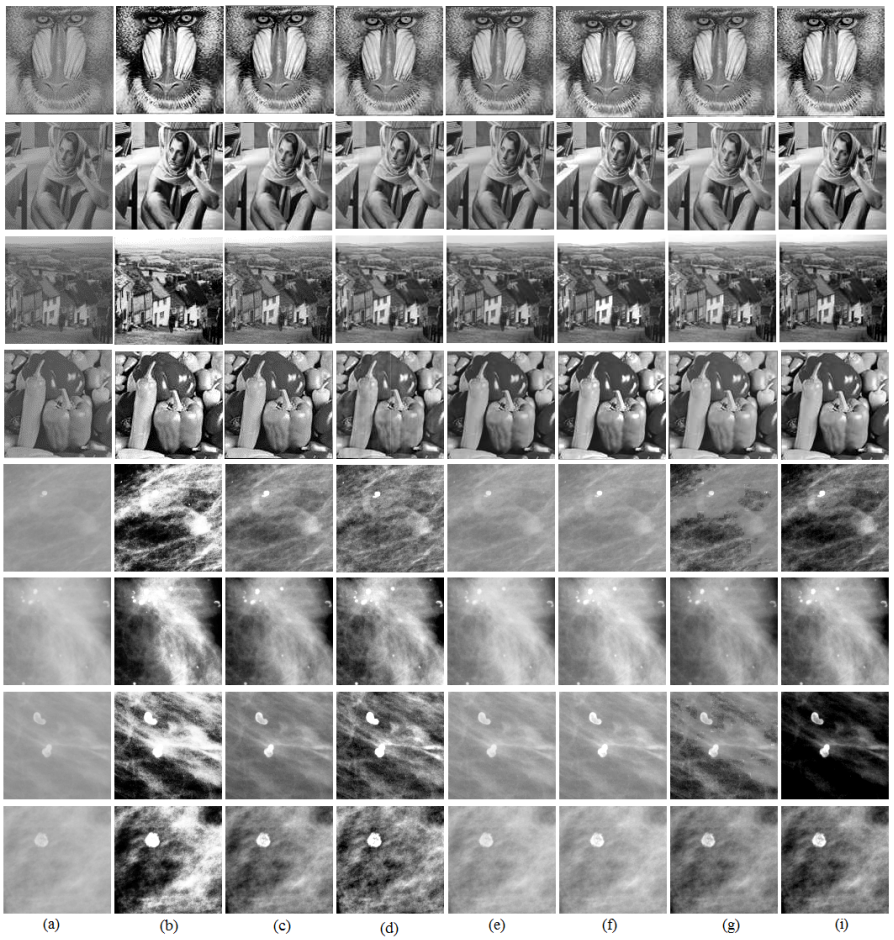

Fig. 6.17: (a)Original images and enhanced images using (b)HE (c)LET (d)NLET (e)FIOP (f)FIOS (g)FRBS (h)GFLS methods

and fuzzy rule based image enhancement algorithms are proposed. The algorithm hence derived is tested on both general and mammogram images. The results are compared with that of the fuzzy INT operator based enhancement technique in the spatial domain (FIOP). Majority of the metric values are good for FRBS compared to the other two methods.

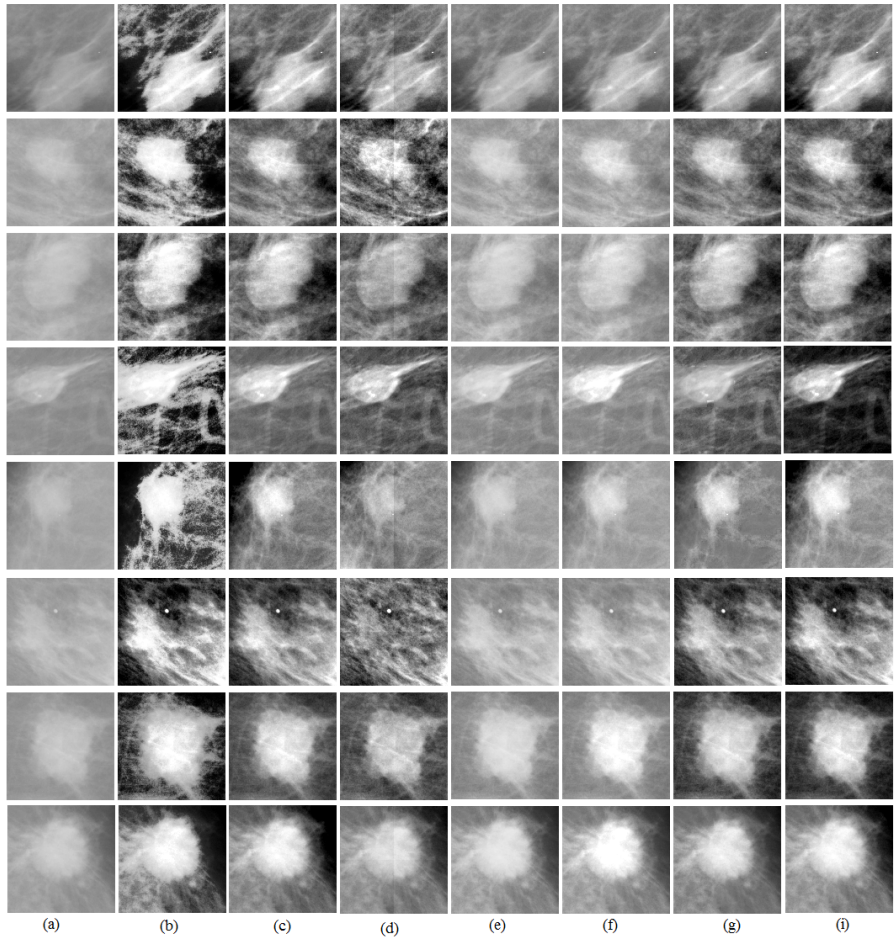

Fig. 6.18: (a)Original images and enhanced images using (b)HE (c)LET (d)NLET (e)FIOP (f)FIOS (g)FRBS (h)GFLS methods

A comparison of global and block level enhancement methods are done to find the best enhancement methods proposed. LET and FRBS excel among the global and block level methods respectively. A global method of enhancement is considered where the image is transformed using Fuzzy rule based algorithm followed by linear scaling technique. Promising quantitative results are obtained

Table 6.6: MOS for various image enhancement techniques

Images	Mean Opinion Score (MOS)						
	HE	LET	NLET	FIOP	FIOS	FRBS	GFLS
baboon	2.7	**4.2**	3.7	3.1	4.1	3.7	**4.3**
barbara	3.0	**4.1**	3.6	2.9	3.4	**3.9**	**4.1**
house	3.2	**4.3**	3.8	2.9	3.0	**4.0**	**4.3**
peppers	1.4	**4.2**	3.9	4.0	**4.2**	**4.2**	**4.6**
mdb009	1.4	**3.4**	**4.4**	2.7	2.8	3.3	**4.4**
mdb170	2.4	**4.2**	**4.1**	3.0	3.2	3.5	4.0
mdb204	1.7	3.8	**4.4**	3.0	3.4	4.0	**4.5**
mdb227	2.8	**4.4**	**4.4**	2.7	2.9	**4.0**	**4.4**
mdb005	2.3	**4.2**	3.9	3.2	3.8	3.8	**4.3**
mdb010	2.0	**4.5**	**3.9**	2.8	3.0	3.8	**4.5**
mdb019	2.3	**4.5**	3.0	3.2	3.2	3.6	**4.4**
mdb132	1.4	**4.5**	4.2	3.4	3.5	4.0	**4.7**
mdb023	1.7	**4.4**	2.9	3.0	3.2	4.2	**4.5**
mdb058	2.4	**4.5**	2.6	2.7	2.9	4.4	**4.6**
mdb134	1.8	**4.5**	3.8	2.7	2.8	**4.1**	**4.5**
mdb202	2.7	**4.3**	3.7	3.5	3.5	4.1	**4.2**

for the GFLS method. Subjective evaluation also points to the fact that Global fuzzy rule based linear image enhancement in the SMRT domain performs best enhancement among the methods developed. Quantitative and qualitative analysis of the various approaches developed for image enhancement show that the performance values of LET is very close to that of GFLS method. Considering the computational simplicity of LET compared with GFLS, LET is an equally competent enhancement technique.

Chapter 7

Conclusion

The chapter presents the summary of investigations carried out and the conclusions drawn therein. Important contributions of this work and future scope are also discussed.

7.1 Summary and Conclusion

The essence of the research work is incorporated in chapters 3 to 6 for which the work is introduced through chapter 1 and the status of the related works in the literature are discussed in chapter 2. Development of a stand-alone, sequency ordered transform, SMRT, is presented in chapter 3. Analysis of existing and proposed metrics for image enhancement is discussed in chapter 4. Chapters 5 & 6 explain different linear and nonlinear techniques of image enhancement using global and block level methods respectively. Hybrid technique of image enhancement is also presented in chapter 6.

7.1.1 Development of SMRT

The former researchers of the research team modified the 2-D DFT computation and derived a new transform MRT that involves only real additions rather than complex multiplications. But MRT is a highly redundant transform with a size of $\frac{N^3}{2}$ coefficients for an $N \times N$ data. Subsequently, it is modified as UMRT by removing the redundant coefficients and arranging in the form of an $N \times N$ matrix. The arrangement of UMRT matrix poses problem in various applications due to scattered arrangement of connected coefficients. So, a new sequency ordered arrangement of the unique MRT coefficients, named SMRT, is proposed in the present work. SMRT placement, basis functions, forward and inverse algorithms are discussed. Some of its properties such as linearity, orthogonality, energy compaction, energy conservation etc. are outlined. The computation of statistical parameters from SMRT coefficients, its use in pattern analysis and template matching, are discussed. SMRT, with its unique sequency ordered basis images, finds applications in many human vision and computer vision image processing applications. The scope of SMRT in lossless text compression is also investigated and compared with DCT & WT. Finally, SMRT is developed as a stand-alone transform.

7.1.2 Development and Analysis of Image Quality Metrics

Even though there are numerous IQA metrics present in the literature, no specific comparative evaluation was noticed in identifying a suitable metric to assess enhanced images. Thus an investigation of the various IQA metrics available in the literature to identify the best suited one is performed. Subsequently Image Enhancement Metric (IEM) in the spatial domain and SMRT based FR & BR metrics (IEMS_{FR} & IEMS_{BR}) are proposed. Study of 18

FR IQA (including the proposed metrics), 6 BR IQA (including the proposed metric) and 7 statistical feature metrics is conducted for image enhancement applications. Useful metrics for evaluating improvements in brightness, contrast, sharpness and their combination suitable for general and medical images are identified. It has been observed that measures such as AME & mean can be used to assess the brightness alone; VIF, VIFP, EMEE & SD for finding contrast alone; statistical measures such as contrast, correlation & homogeneity to assess sharpness alone and homogeneity, mean & SD to assess a combination of brightness, contrast and sharpness. The proposed IQA metrics are found to be useful for measuring the above mentioned parameters except brightness. A validation is also done to substantiate the findings obtained from the analysis. All the above proposed metrics are computationally simple and can be used for all types of images to quantify enhancement.

7.1.3 Global Image Enhancement Techniques

Brightness of an image can be modified very easily by properly scaling the single DC SMRT coefficient alone. Linear and nonlinear approaches are developed for scaling AC SMRT coefficients to improve contrast. In the linear method, AC SMRT coefficients are scaled uniformly to improve the contrast to optimum levels. The scaling factors are selected automatically to utilize the full dynamic range of the histogram. In the nonlinear method, AC SMRT coefficients are modified using six nonlinear mapping techniques that includes two simple hyperbolic mapping functions that are proposed with symmetry in modifying coefficients at low and high values.

The proposed methods are applied to general & mammogram images and the enhanced images are assessed quantitatively. Existing and proposed quantitative measures such as VIFP, SDME, EMEE, IEM, SMRT_{FR}, SMRT_{BR} are used to quantify the effectiveness of the developed methods. Both techniques are compared with HE.

LET enhances all types of images well. NLET seems to be more appropriate to enhance calcifications in mammograms.

The LET method, applied to fingerprint images and scanned documents, produces a binary image when the c_{ac} is made much higher. Both methods are applied to luminance component of YCbCr image space keeping Cb and Cr unchanged for colour image enhancement.

7.1.4 Block Level Image Enhancement Techniques

Fuzzy intensification operator based and fuzzy rule based image enhancement techniques in the SMRT domain are proposed. The algorithm hence derived is tested on both general and medical images. The results are compared with that of the fuzzy INT operator based enhancement technique in the spatial domain. IQA metrics are used to quantitatively assess the enhanced image quality. Experimental results show that the FRBS algorithm works well quantitatively and qualitatively in both general and medical images.

A comparison of global and block level enhancement methods is done to find the best of the four methods proposed. LET and FRBS excel among the global and block level methods respectively. A combination of these two methods cannot be recommended when computational complexity is considered, since global and block level methods require the inverse transform to be applied after the first step. So global method of enhancement is considered for fuzzy rule based and a combination of fuzzy rule based followed by LET is applied in the global scenario. Promising results are obtained for the new method.

7.2 Research Contributions

1. Development of a sequency ordered, orthogonal, integer-to-integer transform, called SMRT for $N \times N$ data, N a power of 2.
2. Identification of scope of SMRT for lossless text compression.
3. Development and analysis of IQA metrics in spatial domain and SMRT domain.
4. Development of global enhancement algorithms in the SMRT domain
   (a) Scaling of DC SMRT coefficient to improve brightness.
   (b) Uniform scaling or nonlinear mapping of AC SMRT coefficients to improve contrast.
5. Development of a linear and global enhancement technique in SMRT domain for enhancing fingerprint and scanned text documents.
6. Development of fuzzy techniques for block level enhancement in the SMRT domain
   (a) Fuzzy intensification operator based enhancement.
   (b) Fuzzy rule based enhancement
7. Development of global enhancement technique using fuzzy rule based and uniform scaling of SMRT coefficients.

7.3 Scope for Future Work

Few possible areas and suggestions for future study are presented.

1. The importance of SMRT for sequency domain representation of 1-D and 2-D signals and systems can be explored.
2. SMRT is developed for $N \times N$ data, for N a power of 2. In practical applications, SMRT for rectangular data matrix $M \times N$ for any M, N is often required and an attempt can be made in this direction.
3. Section 3.3 describes few properties of SMRT. Further properties of SMRT can be investigated.
4. Each SMRT coefficient value is computed based on N^2 comparisons. A direct basis image generation will reduce the computation time further.
5. Comparison of time-sequency localization of SMRT with time-frequency localization of Wavelet Transform can be explored.
6. Extraction of directional features of SMRT in evaluating the structural information can be explored and compared with other directional transforms that have emerged recently.
7. Group patterns and combined group patterns can be used for direction analysis and can be used for extracting features for fingerprint identification systems.
8. The scope of SMRT for edge enhancement, denoising, image filtering etc. can be examined.
9. The usefulness of SMRT based enhancement techniques to compressed images can be verified.

List of Publications

International Journals

- V. L. Jaya and R. Gopikakumari, Automatic Enhancement of Low Contrast Images using SMRT, *International Journal of Scientific and Engineering Research*, vol.4, Issue 9, pp.1510-1515, Sept.2013.
- V. L. Jaya and R. Gopikakumari, IEM: A New Image Enhancement Metric for Contrast and Sharpness Measurements, *International Journal of Computer Applications,*vol.79, Issue 9, pp. 1-9, Oct.2013.
- B. Manju, V.L. Jaya, K.Meenakshy, R.Gopikakumari, 8x8 SMRT based Texture Descriptors, *Lecture Notes in Software Engineering*, vol.3, No.4, pp.295-298, Nov. 2015.
- V. L. Jaya and R. Gopikakumari, Enhancement of Mammogram Images in SMRT Domain using Nonlinear Mapping Functions, *International Journal of Biomedical Engineering and Technology*, Accepted for publication.
- V. L. Jaya and R. Gopikakumari, N×N SMRT for N a power of 2 : Properties and Applications, communicated to IEEE Trans. on Signal Processing

International Conferences

- V. L. Jaya, B. Preetha and R. Gopikakumari, "SMRT: A new placement approach of 2-D unique MRT coefficients for N a power of 2," in *Annual IEEE India Conference (INDICON)*, pp. 233 - 237, Dec. 2012.
(http://ieeexplore.ieee.org/iel5/6410222/6420575/06420621.pdf?arnumber=6420621)

- V. L. Jaya and R. Gopikakumari, Fuzzy Intensification Operator based image enhancement in the SMRT domain, *International Conference on Signal and Speech Processing,* ICSSP 2014. pp. 214-220, Aug. 21-23, 2014. (http://www.elsevierst.com/ConferenceBookdetail.php?pid=90)
- V. L. Jaya and R. Gopikakumari, Fuzzy rule based enhancement in the SMRT domain for low contrast images, *Procedia Computer Science, Proceedings of the International Conference on Information and Communication Technologies (ICICT)*, vol.46, pp.1747-1753, 2015. (http://www.sciencedirect.com/science/article/pii/S1877050915001891)

National Conference

- V. L. Jaya and R. Gopikakumari, N x N Sequency based MRT, N a power of 2, 24^{th} *Swadeshi Science Congress, National Seminar*, pp. 372-377, 2014.

Bibliography

[1] S. E. Umbaugh, *Digital Image Processing and Analysis: Human and Computer Vision Applications with CVIP tools, Second Edition*. Taylor & Francis, 2010.

[2] Y. Zhou, K. Panetta, and S. S. Agaian, "Human visual system based mammogram enhancement and analysis," in *International Conference on Image Processing Theory Tools and Applications (IPTA)*, pp. 229–234, 2010.

[3] J. G. Proakis and D. G. Manolakis, *Digital Signal Processing: Principles, Algorithms and Applications*. Pearson Education, 2007.

[4] R. E. Blauhut, *Fast Algorithms for Digital Signal Processing*. Addison-Wesley Publishing Co., New York, 1985.

[5] E. O. Brigham, *The Fast Fourier Transform and its Applications*. Prentice-Hall Inc., Englewood Cliffs, New Jersy, 1988.

[6] D. Elliott and K. Rao, *Fast Transforms: Algorithms, Analysis, Applications*. Academic Press, New York, 1982.

[7] N. Ahmed, T. Natarajan, and K. R. Rao, "Discrete cosine transform," *IEEE Trans. on Computers*, vol. C-23, no. 1, pp. 90–93, Jan. 1974.

[8] B. J. Fino and V. Algazi, "Unified matrix treatment of the fast walsh-hadamard transform," *IEEE Trans. on computers*, vol. C-25, no. 11, pp. 1142–1146, Nov. 1976.

[9] S. S. Agaian, *Hadamard Matrices and their Applications*. Springer-Verlag Berlin Heidelberg, 1985.

[10] R. Baghaie and V. Dimitrov, "Computing Haar Transform using Algebraic Integers," in *Thirty-Fourth Asilomar Conference on Signals, Systems and Computers*, pp. 438–442, Oct. 2000.

[11] A. K. Jain, "A fast Karhunen-Loeve Transform for finite discrete images," in *Proceedings of National Electronics Conference*, (Chicago), pp. 323–328, Oct. 1974.

[12] S. G. Mallat, "A theory for multiresolution signal decomposition: The wavelet representation," *IEEE Transactions on Pattern analysis and machine intelligence*, vol. 11, no. 7, pp. 674–693, July 1989.

[13] I. Daubechies, "The wavelet transform, time-frequency localization and signal analysis," *IEEE Transactions on Information Theory*, vol. 36, no. 5, pp. 961–1005, Sept. 1990.

[14] G. Strang and T. Nguyen, *Wavelets and Filter Banks*. Wellesley-Cambridge Press, 1996.

[15] E. Le Pennec and S. Mallat, "Sparse geometric image representation with bandelets," *IEEE Trans. Image Processing*, vol. 14, no. 4, pp. 423–438, Apr. 2005.

[16] E. J. Candes and D. L. Donoho, "New tight frames of curvelets and optimal representations of objects with piece-

wise c^2 singularities," *Commun. on Pure Appl. Math.*, vol. 57, no. 2, pp. 219–266, 2002.

[17] M. N. Do and M. Vetterli, *Contourlets, in Beyond Wavelets*. Academic Press, 2003.

[18] P. Feng, Y. Pan, B. Wei, W. Jin, and M. Deling, "Enhancing retinal image by the contourlet transform," *Pattern Recognition Letters*, vol. 28, no. 4, pp. 516–522, March 2007.

[19] V. P. Shah, N. H. Younan, and R. L. King, "An efficient pan-sharpening method via combined adaptive PCA approach and contourlets," *IEEE Trans. on Geoscience and Remote Sensing*, vol. 46, no. 5, pp. 1323–1335, 2008.

[20] M. M. Eltoukhy, I. Faye, and B. B. Samir, "Breast cancer diagnosis in digital mammogram using multiscale curvelet transform," *Computerized Medical Imaging and Graphics*, vol. 34, no. 4, pp. 269–276, 2010.

[21] G. G. Bhutada, R. S. Anand, and S. C. Saxena, "Edge preserved image enhancement using adaptive fusion of images denoised by wavelet and curvelet transform," *Digital Signal Processing*, vol. 21, no. 1, pp. 118–130, 2011.

[22] D. Labate, W. Lim, G. Kutyniok, and G. Weiss, "Sparse multidimensional representation using shearlets," *Proceedings of the SPIE*, vol. 5914, pp. 254–262, 2005.

[23] K. Guo, D. Labate, W. Lim, G. Weiss, and W. E., "Wavelets with composite dilations and their MRA properties," *Applied and Computational Harmonic Analysis*, vol. 20, no. 2, pp. 202–236, 2006.

[24] K. Guo and D. Labate, "Optimally sparse multidimensional representation using shearlets," *SIAM J Math. Anal.*, vol. 39, no. 1, pp. 298–318, 2007.

[25] V. Velisavljevi, P. L. Dragotti, and M. Vetterli, "Directional wavelet transforms and frames," in *Proc. IEEE Inf. Conf. Image Processing*, pp. 589–592, June 2002.

[26] V. Velisavljevi, B. Beferull-Lozano, M. Vetterli, and P. L. Dragotti, "Discrete multi-directional wavelet bases," in *Int.IEEE Conf. Image Processing*, pp. 1025–1028, Sept. 2003.

[27] V. Velisavljevic, B. Beferull-Lozano, M. Vetterli, and P. Dragotti, "Directionlets: anisotropic multidirectional representation with separable filtering," *IEEE Transactions on Image Processing*, vol. 15, no. 7, pp. 1916–1933, 2006.

[28] V. Velisavljevic, "Low-complexity iris coding and recognition based on directionlets," *IEEE Trans. on Information Forensics and Security*, vol. 4, no. 3, pp. 410–417, 2009.

[29] S. Anand, S. Jeeva, and T. Thivya, "Edge detection using skewed and elongated basis functions," *International Journal of Applied Information Systems*, vol. 1, no. 4, pp. 28–34, 2012.

[30] R. Gopikakumari, *Investigations on the Development of an ANN Model and Visual Manipulation Approach for 2-D DFT Computation in Image Processing*. Ph.D dissertation, Cochin University of Science and Technology, Kochi, 1998.

[31] C. R. Rajesh and R. Gopikakumari, "A new transform for 2-D signal representation(MRT) and some of its properties," in *IEEE international conference on signal processing and communications (SPCOM)*, pp. 363–367, Dec. 2004. (http://ieeexplore.ieee.org/iel5/9869/31229/01458423.pdf).

[32] C. R. Rajesh, *Development of a New Transform: MRT*. Ph.D dissertation, Cochin University of Science and Technology, Kochi, 2009.

[33] V. Bhadran, *Development and Implementation of Visual Approach and Parallel Distributed Architecture for*

2-D DFT and UMRT Computation. Ph.D dissertation, Cochin University of Science and Technology, Kochi, 2009.

[34] R. C. Gonzalez and R. E. Woods, *Digital Image Processing.* Addison Wesley, 1992.

[35] S. Aghagolzadeh and O. Ersoy, "Transform image enhancement," *Optical Engineering*, vol. 31, no. 3, pp. 614–626, 1992.

[36] A. Grigoryan and S. Agaian, "Transform-based image enhancement algorithms with performance measure," *Advances in Imaging and Electron Physics*, vol. 130, pp. 165–242, 2004.

[37] K. Narasimhan, C. R. Sudarshan, and N. Raju, "A comparison of contrast enhancement techniques in poor illuminated gray level and colour images," *International Journal of Computer Applications*, vol. 25, no. 2, pp. 17–25, 2011.

[38] S. Sulochana and R. Vidya, "Satellite image contrast enhancement using multiwavelets and singular value decomposition (SVD)," *International Journal of Computer Applications*, vol. 35, no. 7, pp. 1–5, 2011.

[39] S. K. Mitra and T. H. Yu, "Transform amplitude sharpening: A new method of image enhancement," *Computer Vision, Graphics, and Image Processing*, vol. 40, no. 2, pp. 205–218, 1987.

[40] E. Kerre and M. Nachtegael, *Fuzzy techniques in image processing.* Physica-Verlag HD, 2000.

[41] D. B. Judd, "Hue, saturation and lightness of surface colours with chromatic illumination," *Journal of Research of the National Bureau of Standards*, vol. 24, pp. 294–330, March 1940.

[42] H. Lee, R. Ramotowski, and R. Gaensslen, *Advances in fingerprint technology, Second Edition.* CRC Press, 2001.

[43] Z. Wang and A. Bovik, *Modern image quality assessment*. Morgan & Claypool Publishers, New York, 2006.

[44] A. Ali, . Al-zuky, S. S. Salema, and H. A. Anwar, "Study the quality of image enhancement by using retinex technique which capture by different lighting (sun and tungsten)," *International Journal of Computer Applications*, vol. 73, pp. 31–38, July 2013. Published by Foundation of Computer Science, New York, USA.

[45] P. Ankita, S. Sarbjeet, and P. Ankur, "Review : On performance metrics for quantitative evaluation of contrast enhancement in mammograms," *International Journal of Computer Applications*, vol. 75, pp. 40–45, August 2013. Foundation of Computer Science, New York, USA.

[46] ITU-T Recommendation, P.800 (08/96), "Methods for subjective determination of transmission quality," 1996.

[47] J. W. Cooley, P. W. A. Lewis, and P. D. Welch, "Historical notes on the fast fourier transform," *IEEE Trans. on Audio Electroacoustics*, vol. AU 15, no. 2, pp. 76–79, June 1967.

[48] J. Walsh, E. Saff, and T. Rivlin, *Joseph L. Walsh: Selected Papers*. Springer, New York, 2000.

[49] M. Wojtas, "On Hadamard's inequality for the determinants of order non-divisible by 4," *Colloq. Math.*, vol. 12, pp. 73–83, 1964.

[50] W. Pratt, J. Kane, and H. C. Andrews, "Hadamard transform image coding," *Proc.of the IEEE*, vol. 57, pp. 58–68, Jan. 1969.

[51] H. F. Harmuth, *Transmission of information by Orthogonal functions*. Springer-Verlag, New York, 1969.

[52] H. C. Andrews and K. Casparie, *Orthogonal Transformations*. Computer Techniques in Image Processing, Academic Press, New York, 1970.

[53] D. Mackenzie, *Wavelets: Seeing the forest and trees*. National Academy of Sciences, Washington, DC, 2001.

[54] A. Grossman and J. Morlet, "Decomposition of hardy functions into square integrable wavelets of constant shape," *SIAM J. Math. Anal.*, pp. 723–736, 1984.

[55] S. Mallat, "A compact multiresolution representation: The wavelet model," *Proc. IEEE Computer Society Workshop on Computer Vision*, pp. 2–7, 1987.

[56] C. E. Heil and D. F. Walnut, "Continuous and discrete wavelet transforms," *SIAM J. Numer. Anal.*, pp. 628–666, 1989.

[57] R. A. DeVore and B. J. Lucier, "Wavelets," *Acta Numerica*, pp. 1–56, 1991.

[58] O. Rioul and M. Vetterli, "Wavelet and signal processing," *IEEE Signal processing magazine*, pp. 14–38, 1991.

[59] R. S. Strichartz, "How to make wavelets," *Amer. Math. Soc. (N.S)*, pp. 539–556, 1993.

[60] G. Strang, "Wavelet transforms versus fourier transforms," *Bull. Amer. Math. Soc. (N.S)*, vol. 28, pp. 288–305, 1993.

[61] M. N. Do and M. Vetterli, "Pyramidal directional filter banks and curvelets," in *Proc. of IEEE International Conference on Image Processing (ICIP)*, pp. 158–161, Oct. 2001.

[62] M. N. Do and M. Vetterli, "The contourlet transform: An efficient directional multiresolution image representation," *IEEE Transactions on Image Processing*, vol. 14, no. 12, pp. 2091–2106, Dec. 2005.

[63] C. R. Rajesh, M. S. AnishKumar, and R. Gopikakumari, "An invertible transform for image representation and its application to image compression," in *Proceedings of the Int. Symposium on Signal Processing and its Applications(ISSPA)*, pp. 1–4, 2007. (http://ieeexplore.ieee.org/iel5/6410222/6420575/06420621.pdf?arnumber=45555

[64] V. Bhadran, C. R. Rajesh, and R. Gopikakumari, "Visual representation of 2-D DFT in terms of 2x2 data: A pattern analysis," in *Proceedings of International Conference on Computing, Communication and Networking (ICCCN)*, pp. 1–9, Dec. 2008. (ieeexplore.ieee.org/iel5/4783155/4787659/04787762.pdf).

[65] B. Preetha, V. Bhadran, and R. Gopikakumari, "A new algorithm to compute forward and inverse 2-D UMRT for N-a power of 2," in *Second Int. Conference on Power, Signals, Control and Computation (EPSICON)*, pp. 1–5, Jan. 2012. (http://ieeexplore.ieee.org/xpl/articleDetails.jsp?arnumber=6175226).

[66] K. Meenakshy, *Development and Implementation of a CAD System to Predict the Fragmentation of Renal Stones Based on Texture Analysis of CT Images*. Ph.D dissertation, Cochin University of Science and Technology, Kochi, 2010.

[67] M. S. Anishkumar, C. R. Rajesh, and R. Gopikakumari, "A new image compression and decompression technique based on 8x8 MRT," *Int. Journal on Graphics, Vision and Image Processing*, vol. 6, no. 1, pp. 51–53, July 2006.

[68] M. S. Anishkumar, B. Preetha, and R. Gopikakumari, "UMRT based adaptive block size transform coder for images using quad-tree partitioning," *Int. Journal of Scientific & Engineering Research*, vol. 4, no. 12, pp. 1170–1176, Dec. 2013.

[69] E. Hall, R. Kruger, S. Dwyer, D. Hall, R. Mclaren, and G. Lodwick, "A survey of preprocessing and feature extraction techniques for radiographic images," *IEEE Trans. on Computers*, vol. 20, no. 9, pp. 1032–1044, 1971.

[70] R. A. Hummel, "Histogram modification techiques," in *Technical report, Computer Science Centre*, (Maryland University College Park), pp. 209–224, Sept. 1974.

[71] P. E. Trahanias and A. N. Venetsanopoulos, "Colour image enhancement through 3-d histogram equalization," in *International conference on image, speech, and signal analysis*, (Maryland University College Park), pp. 545–548, 1992.

[72] R. H. Sherrier and G. A. Johnson, "Regionally adaptive histogram equalization of the chest," *IEEE Trans .Med. Imaging*, vol. 6, no. 1, pp. 1–7, 1987.

[73] S. M. Pizer and E. P. Amburn, "Adaptive histogram equalization and its variations," *Computer Vision, Graph, Image Process*, vol. 39, pp. 355–368, 1987.

[74] T. L. Ji, M. K. Sundareshan, and H. Roehrig, "Adaptive image contrast enhancement based on human visual properties," *IEEE Trans. on medical imaging*, vol. 13, no. 4, pp. 573–586, Dec.,1994.

[75] Y. T. Kim, "Contrast enhancement using brightness preserving bi-histogram equalization," *IEEE Trans. Consumer Electronics*, vol. 43, no. 1, pp. 1–8, Feb., 1997.

[76] K. Wongsritong, K. Kittayaruasiriwat, F. Cheevasuvit, K. Dejhan, and A. Somboonkaew, "Contrast enhancement using multipeak histogram equalization with brightness preserving," in *IEEE Asia-Pacific Conference on Circuits and System (APCCAS)*, (Maryland university College Park), pp. 455–458, Nov. 1998.

[77] Y. Wang, Q. Chen, and Z. Bao-Min, "Image enhancement based on equal area dualistic sub-image histogram equalization method," *IEEE Trans. Consumer Electronics*, vol. 45, no. 1, pp. 68–75, Feb. 1999.

[78] S.-D. Chen and A. R. Ramli, "Contrast enhancement using recursive mean-separate histogram equalization for scalable brightness preservation," *IEEE Trans. Consumer Electronics*, vol. 49, no. 4, pp. 1301–1309, Nov. 2003.

[79] C. Wang and Zhongfue., "Brightness preserving histogram equalization with maximum entropy: a variational perspective," *IEEE Trans. Consumer Electronics*, vol. 51, no. 4, pp. 1326–1324, Nov. 2005.

[80] S.-D. Chen and A. R. Ramli, "Minimum mean brightness error bi-histogram equalization in contrast enhancement," *IEEE Trans. Consumer Electronics*, vol. 49, no. 4, pp. 1310 – 1319, 2003.

[81] K. S. Sim, C. P. Tso, and Y. Y. Tan, "Recursive sub-image histogram equalization applied to gray scale images," *Pattern Recognition Letters*, vol. 28, no. 10, pp. 1209–1221, 2007.

[82] M. Abdullah-Al-Wadud, M. Hasanul Kabir, M. Ali Akber Dewan, and O. Chae, "A dynamic histogram equalization for image contrast enhancement," *IEEE Trans. Consumer Electronics*, vol. 53, no. 2, pp. 593–600, May 2007.

[83] I. Haidi and N. S. P. Kong, "Brightness preserving dynamic histogram equalization for image contrast enhancement," *IEEE Trans. Consumer Electronics*, vol. 53, no. 4, Nov., 2007.

[84] M. Kim and M. G. Chung, "Recursively separated and weighted histogram equalization for brightness preservation and contrast enhancement," *IEEE Trans. Consumer Electronics*, vol. 54, no. 3, pp. 1389–1397, Aug., 2008.

[85] P. Rajavel, "Image dependent brightness preserving histogram equalization'," *IEEE Trans. Consumer Electronics*, vol. 56, no. 2, May2010.

[86] R. Chauhan and S. S. Bhadoria, "An improved image contrast enhancement based on histogram equalization and brightness preserving weight clustering histogram equalization," in *International Conference on Communication Systems and Network Technologies*, (Katra, Jammu), pp. 597–600, June 2011.

[87] M. Sundaram, K. Ramar, N. Arumugham, and G. Prabin, "Histogram based contrast enhancement for mammogram images," in *Proceedings of 2011 International Conference on Signal Processing, Communication, Computing and Networking Technologies (ICSCCN)*, pp. 842–846, July 2011.

[88] S. Debashis and K. P. Sankar, "Automatic exact histogram specification for contrast enhancement and visual system based quantitative evaluation," *IEEE Trans. on image processing*, vol. 10, no. 5, May 2011.

[89] A. Sarrafzadeh, F. Rezazadeh, and J. Shanbehzadeh, "Brightness preserving fuzzy dynamic histogram equalization," in *Proceedings of the International Multiconference of Engineers and Computer Scientists (IMECS)*, (Hong Kong), Jan. 2013.

[90] K. Thangavel, R. Manavalan, and I. Laurence Aroquiaraj, "Removal of speckle noise from ultrasound medical image based on special filters: Comparative study," *ICGST-GVIP Journal*, vol. 9, no. 3, June 2009.

[91] S. K. Mitra and H. Li, "A new class of nonlinear filters for image enhancement," in *International Conference on Acoustics, Speech, and Signal Processing (ICASS)*, pp. 2525–2528, July 1991.

[92] Polesel, A. Ramponi, and G. Mathews, "Image enhancement via adaptive unsharp masking," *IEEE Trans. on Image Processing*, vol. 9, no. 3, pp. 505–510, 2002.

[93] K. A. Panetta, Z. Yicong, S. S. Agaian, and H. Jia, "Nonlinear unsharp masking for mammogram enhancement," *IEEE Trans. on information technology in biomedicine*, vol. 15, pp. 918–928, Nov, 2011.

[94] T. Xiurong, "The application of adaptive unsharp mask algorithm in medical image enhancement," in *Cross Strait Quad-Regional Radio Science and Wireless Technology Conference (CSQRWC)*, pp. 1368–1370, 2011.

[95] L. A. Zadeh, "Fuzzy sets," *Information and control*, vol. 8, pp. 338–353, 1965.

[96] S. Pal and R. King, "Image enhancement using fuzzy set," *Electronics letters*, vol. 16, no. 10, pp. 376–378, 1980.

[97] S. Pal and R. King, "Image enhancement using smoothing with fuzzy sets," *IEEE Trans. on System, Man and Cybernetics*, vol. 11, no. 7, pp. 494–501, 1981.

[98] H. Li and H. S. Yang, "Fast and reliable image enhancement using fuzzy relaxation technique," *IEEE Trans. System man Cybernet*, vol. 9, no. 5, pp. 1276–1281, 1989.

[99] S. M. Zhou and Q. Can, "Convergence analysis and performance improvement of a fuzzy relaxation algorithm for image contrast enhancement," in *Technical Report*, (Department of Computer Science, University of Essex), 2003.

[100] S. M. Zhou and Q. Can, "A new fuzzy relaxation algorithm for image contrast enhancement," in *Proceedings of the 3rd International Symposium on Image and Signal Processing and Analysis*, pp. 11–16, 2003.

[101] H. D. Cheng and H. Xu, "A novel fuzzy logic approach to contrast enhancement," *Pattern recognition*, vol. 33, pp. 809–819, 2000.

[102] K. Hasikin and N. A. Mat Isa, "Enhancement of the low contrast image using fuzzy set theory," in *14th International Conference on Modeling and Simulation*, (Cambridge), pp. 371–376, March 2012.

[103] T. Chaira, "Medical image enhancement using intuitionistic fuzzy set," in *First International conference on Recent Advances in Information Technology(RAIT)*, (Dhanbad), pp. 54–57, March 2012.

[104] H. C. Andrews, A. G. Tescher, and K. P. Kruger, "Image processing by digital computer," *IEEE Spectrum*, vol. 9, pp. 20–32, 1972.

[105] A. Jain, "Advances in mathematical models for image processing," *Proc. of the IEEE*, vol. 69, no. 5, May 1981.

[106] R. Arun, S. N. Madhu, R. Vrinthavani, and R. Tatavarti, "An alpha rooting based hybrid technique for image enhancement," *On line publication in IAENG,*, pp. 155–158, Aug. 2011.

[107] M. Amore, S. K. Mitra, M. Carli, and J. S. McElvain, "Image enhancement in the compressed domain," in *International symposium on Signals, Circuits and Systems (ISSCS)*, (Lasi), pp. 1–4, July 2007.

[108] T. De, "A simple programmable s-function for digital image processing," in *Proc. 4th IEEE Region 10 Int.Conf.(TENCON)*, (Bombay), pp. 573–576, Nov. 1989.

[109] S. Lee, "An efficient content-based image enhancement in the compressed domain using retinex theory," *IEEE Trans. on*

Circuits and Systems for Video Technology, vol. 17, no. 2, pp. 199–213, Feb. 2007.

[110] J. Tang, E. Peli, and S. Acton, "Image enhancement using a contrast measure in the compressed domain," *IEEE Signal Processing Letters*, vol. 10, pp. 289–292, Oct. 2003.

[111] J. Mukherjee and S. K. Mitra, "Enhancement of colour images by scaling the DCT coefficients," *IEEE Trans. Image Processing*, vol. 10, pp. 1783–1794, Oct. 2008.

[112] E. H. Land, "The retinex theory of colour vision," *Scientific American*, pp. 108–128, 1977.

[113] Z. Rahman, D. J. Jobson, and G. A. Woodell, "A multiscale retinex for bridging the gap between colour images and the human observation of scenes," *IEEE Trans. on Image Processing*, vol. 6, no. 7, pp. 965–976, 1977.

[114] D. J. Jobson, Z. Rahman, and G. A. Woodell, "Properties and performance of a centre/surround retinex," *IEEE Trans. on Image Processing*, vol. 6, no. 3, pp. 451–462, 1977.

[115] N. Hess-Nielsen and M. V. Wickerhauser, "Wavelets and time-frequency analysis," *Proc. of the IEEE*, vol. 84, pp. 523–540, Apr. 1996.

[116] J. Lu, D. Healy, and J. B. Weaver, "Contrast enhancement of medical images using multi-scale edge representation," *Opt. Eng.*, vol. 33, no. 7, pp. 2151–2161, 1994.

[117] G. Yang and D. M. Hansell, "CT image enhancement with wavelet analysis for the detection of small airways disease," *IEEE Trans. Med. Imaging*, vol. 16, no. 6, pp. 953–961, 1997.

[118] Y. Fang and F. Qi, "A method of wavelet image enhancement based on soft threshold," *Comput. Eng. Appl.*, vol. 23, pp. 16–19, 2002.

[119] P. J. Burt and E. H. Adelson, "The laplacian pyramid as a compact image code," *IEEE Trans. Communications*, vol. 31, no. 4, pp. 532–540, April 1983.

[120] R. H. Bamberger and M. J. T. Smith, "A filter bank for the directional decomposition of images: Theory and design," *IEEE Trans. Signal Proc.*, vol. 40, no. 4, pp. 882–893, April 1992.

[121] K. O. Sung, J. H. Y., and M. R. Yong, "Image enhancement with attenuated blocking artifact in transform domain," *IEICE Transactions on Information Systems*, vol. E85-D, no. 1, Jan. 2002.

[122] F. Jean-Luc, S.and Murtagh, J. C. Emmanuel, and L. D. David, "Gray and colour image contrast enhancement by the curvelet transform," *IEEE Transactions on image processing*, vol. 12, no. 6, June 2003.

[123] E. Nezhadarya and M. B. Shamsollahi, "Image contrast enhancement by contourlet transform," in *48th International Symposium on Multimedia Signal Processing and Communication (ELMAR)*, (Zadar, Croatia), pp. 81–84, June 2006.

[124] A. Jiang, P. Ren, and P. Yang, "Medical image enhancement algorithm based on contourlet transform," in *First International Conference on Pervasive Computing, Signal Processing and Applications (PCSPA)*, (Harbin), pp. 624–627, 2010.

[125] W. Ping, L. Junli, L. Dongming, and C. Gang, "A multiscale enhancement method to medical images based on fuzzy logic," in *IEEE Region 10 conference (TENCON)*, (Hong Kong), pp. 1–4, Nov. 2006.

[126] C. Popa, A. Vlaicu, M. Gordan, and B. Orza, "Fuzzy contrast enhancement for images in the compressed domain," *Proceedings of the International Multiconference on computer Science and Information Technology*, pp. 161–170, 2007.

[127] C. Popa, M. Gordan, A. Vlaicu, B. Orza, and O. Gabriel, "Computationally efficient algorithm for fuzzy rule-based enhancement on jpeg compressed colour images," *WSEAS Transactions on signal Processing*, vol. 4, no. 5, pp. 310–319, May 2008.

[128] C. Popa, A. Vlaicu, M. Gordan, and B. Orza, "Fuzzy intensification operator based contrast enhancement in the compressed domain," *Applied soft computing*, vol. 9, no. 3, pp. 1139–1148, 2009.

[129] H. Yuan, Y. Li, and F. He, "An adaptive infrared image enhancement algorithm based on NSCT," in *2011 International Conference on Electronics and OptoElectronics (ICEOE)*, pp. 4–7, July 2011.

[130] N. Hema Rajini and R. Bhavani, "A novel method for brain MRI super-resolution by wavelet-based **??** and adaptive edge zoom," *International Journal on Computer Science and Engineering*, vol. 2, no. 7, pp. 2506–2510, 2010.

[131] M. Yasmin, M. Sharif, S. Masood, M. Raza, and S. Sajjad Mohsin, "Brain image enhancement-a survey," *World Applied Sciences Journal*, pp. 1192–1204, 2012.

[132] K. Hasikin and N. A. M. Isa, "Fuzzy image enhancement for low contrast and non-uniform illumination images," in *IEEE International Conference on Signal and Image Processing Applications (ICSIPA)*, (Melaka), pp. 275–280, Oct. 2003.

[133] W. Liejun and Y. Ting, "A new approach of image enhancement based on improved fuzzy domain algorithm," in *International Conference on Multisensor Fusion and Information Integration for Intelligent Systems (MFI)*, (Beijing), pp. 1–5, Sept. 2014.

[134] B. Girod, *Whats wrong with mean-squared error?* Cambridge, MA: MIT Press, 1993.

[135] Planitz and A. Maeder, "Medical image watermarking: A study on image degradation," in *APRS 2005: Proceedings of Australian Pattern Recognition Society(APRS) Workshop on Digital Image Computing*, (Brisbane, Australia), pp. 8–13, Feb.2005.

[136] S. D. Chen and A. R. Ramli, "Minimum mean brightness error bi-histogram equalization in contrast enhancement," *IEEE Transactions on Consumer Electronics*, vol. 49, pp. 1310–1319, 2003.

[137] J. Sijbers, P. Scheunders, N. Bonnet, D. Van Dyck, and E. Raman, "Quantification and improvement of the signal-to-noise ratio in a magnetic resonance image acquisition procedure," *Magnetic Resonance Imaging*, vol. 14, p. 11571163, 1996.

[138] E. Deniz, G. L. Erik, Y. Rui, C. P. Jose, and R. F. Jeffrey, "Measuring the signal-to-noise ratio in magnetic resonance imaging: a caveat," *Signal processing*, vol. 84, pp. 1035–1040, 2004.

[139] B. Bechara, C. A. McMahan, W. S. Moore, M. Noujeim, H. Geha, and F. B. Teixeira, "Contrast-to-noise ratio difference in small field of view cone beam computed tomography machines," *Journal of Oral Science*, vol. 54, pp. 227–232, 2012.

[140] Schmidt., R. Haskell, B. Eng, and K. O'Riordan, "An experimental time-compression system for satellite television transmission," *Proceedings of the IEEE*, vol. 73, pp. 789–794, 1995.

[141] N. Damera Venkata, T. Kite, W. Geisler, B. Evans, and A. Bovik, "Image quality assessment based on a degradation model," *IEEE Trans. Image Processing*, vol. 4, pp. 636–650, 2000.

[142] Z. Wang and A. C. Bovik, "A universal image quality index," *IEEE Signal Proces. Letters*, vol. 4, pp. 81–84, Sept. 2002.

[143] Z. Wang, A. C. Bovik, H. Sheikh, and E. P. Simoncelli, "Image quality assessment: From error visibility to structural similarity," *IEEE Trans.Image Process*, vol. 13, pp. 600–612, 2004.

[144] H. Sheikh, A. Bovik, and G. de Veciana, "An information fidelity criterion for image quality assessment using natural scene statistics," *IEEE Trans. Image Processing*, vol. 14, pp. 2117–2128, Dec. 2005.

[145] H. Sheikh and A. Bovik, "Image information and visual quality," *IEEE Transactions on Image Processing*, vol. 15, pp. 430– 444, Feb. 2006.

[146] N. Thakur and S. Devi, "A new method for colour image quality assessment," *Internatinal Journal of Computer Applications*, vol. 15, pp. 10–17, Feb. 2011. Published by Foundation of Computer Science, New York, USA.

[147] D. M. Chandler and S. S. Hemami, "VSNR: A wavelet-based visual signal-to-noise ratio for natural images," *IEEE Trans. Image Processing*, vol. 16, pp. 2284–2298, Sep. 2007.

[148] L. Zhang, L. Zhang, and X. Mou, "RFSIM: a feature based image quality assessment metric using riesz transforms," in *ICIP 2010: Proceedings of IEEE International conference on image processing*, (Hong Kong), pp. 321–324, 2010.

[149] L. Zhang, L. Zhang, X. Mou, and D. Zhang, "FSIM: a feature similarity index for image quality assessment," *IEEE Trans. Image Processing*, vol. 20, pp. 2378–2386, Sep. 2011.

[150] S. S. Agaian, K. P. Lentz, and A. M. Grigoryan, "A new measure of image enhancement," in *IASTED 2000: Proceedings of the Int. Conf. Signal Processing and Communication*, pp. 19–22, 2000.

[151] S. S. Agaian, K. Panetta, and A. Grigoryan, "Transform based image enhancement with performance measure," *IEEE Tran. Image Processing*, vol. 10, pp. 367–381, March 2001.

[152] K. Panetta, S. S. Agaian, Z. Yicong, and E. J. Wharton, "Parameterized logarithmic framework for image enhancement," *IEEE transactions on Systems, Man, Cybernetics*, vol. 41, pp. 460–473, 2011.

[153] S. S. Agaian, B. Silver, and K. Panetta, "Transform coefficient histogram-based image enhancement algorithms using contrast entropy," *IEEE Trans. Image Processing*, vol. 16, p. 741758, Mar. 2007.

[154] K. A. Panetta, E. J. Wharton, and S. S. Agaian, "Human visual system based image enhancement and logarithmic contrast measure," *IEEE transactions on Systems, Man, Cybernetics*, vol. 38, p. 174188, Feb. 2008.

[155] R. M. Haralick, "Statistical and structural approaches to texture," *Proceedings of the IEEE*, vol. 67, pp. 786–804, 1979.

[156] Y. Hu, C. Zhao, and H. Wang, "Directional analysis of texture images using gray level co-occurrence matrix," in *PACIIA 2008: Pacific-Asia Workshop on Computational Intelligence and Industrial Application*, pp. 277–281, 2008.

[157] N. Nikhil, J. M. Vishnu, D. Amal, M. Maneesh, and S. Viswam, "Development of a matlab toolbox/toolbar for MRT, UMRT and SMRT," tech. rep., School of Engineering, CUSAT, Kochi, 2014.

[158] C. V. Pranoy, D. J. Rahul, V. M. Sachin, T. P. Athira, and H. Thariq, "Development of a python toolbox / toolbar for MRT, UMRT and SMRT," tech. rep., School of Engineering, CUSAT, Kochi, 2015.

[159] B. Manju, V. L. Jaya, K. Meenakshy, and R. Gopikakumari, "8x8 SMRT based texture descriptors," *Lecture Notes on Software Engineering*, vol. 3, pp. 295–298, Nov. 2015.

[160] M. Gaubatz, "MeTriX MuX visual quality assessment package [online] available." http://www.foulard.ece.cornell.edu/gaubatz/metrix _ mux.

[161] "FSIM MATLAB code [online] available." http://www.comp. polyu.edu.hk/ čslzhang/IQA/FSIM/FSIM.htm.

[162] "RFSIM MATLAB code [online] available." http://www.sse. tongji.edu.cn/linzhang/IQA/RFSIM/RFSIM.htm.

[163] E. C. Larson and D. M. Chandler, "Most apparent distortion: full-reference image quality assessment and the role of strategy," *Journal of Electronic Imaging*, vol. 19, pp. 1–21, March 2010.

[164] "Mini-MIAS database of mammograms [online] available :." http://peipa.essex.ac.uk/info/mias.html.

[165] V. S. Hari, V. P. Jagathy Raj, and R. Gopikakumari, "Unsharp masking using quadratic filter for the enhancement of fingerprints in noisy backgrounds," *Pattern recognition*, vol. 46, no. 12, pp. 3198–3207, 2013.

[166] D. Zhang, B. Zhan, G. Yang, and X. Hu, "An improved edge detection algorithm based on image fuzzy enhancement," in *IEEE Conference on Industrial Electronics and Applications, (ICIEA)*, pp. 2412–2415, May 2009.

Appendix A

Basis Functions

A.1 DCT Basis Functions

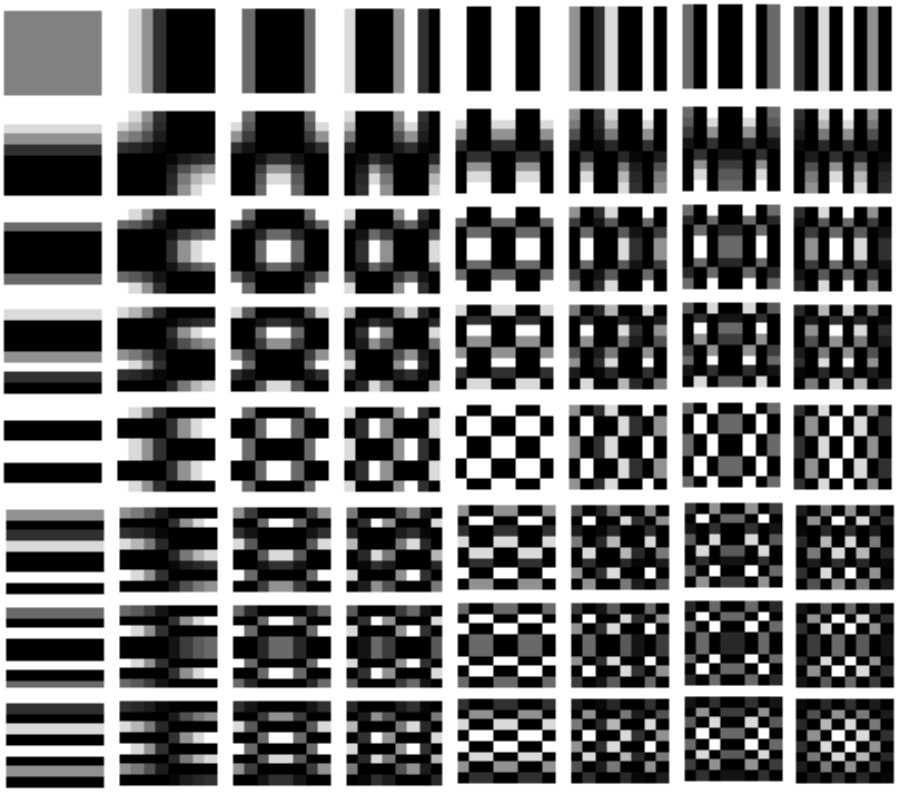

Fig. A.1: Basis functions of DCT for N=8

A.2 WHT Basis Functions

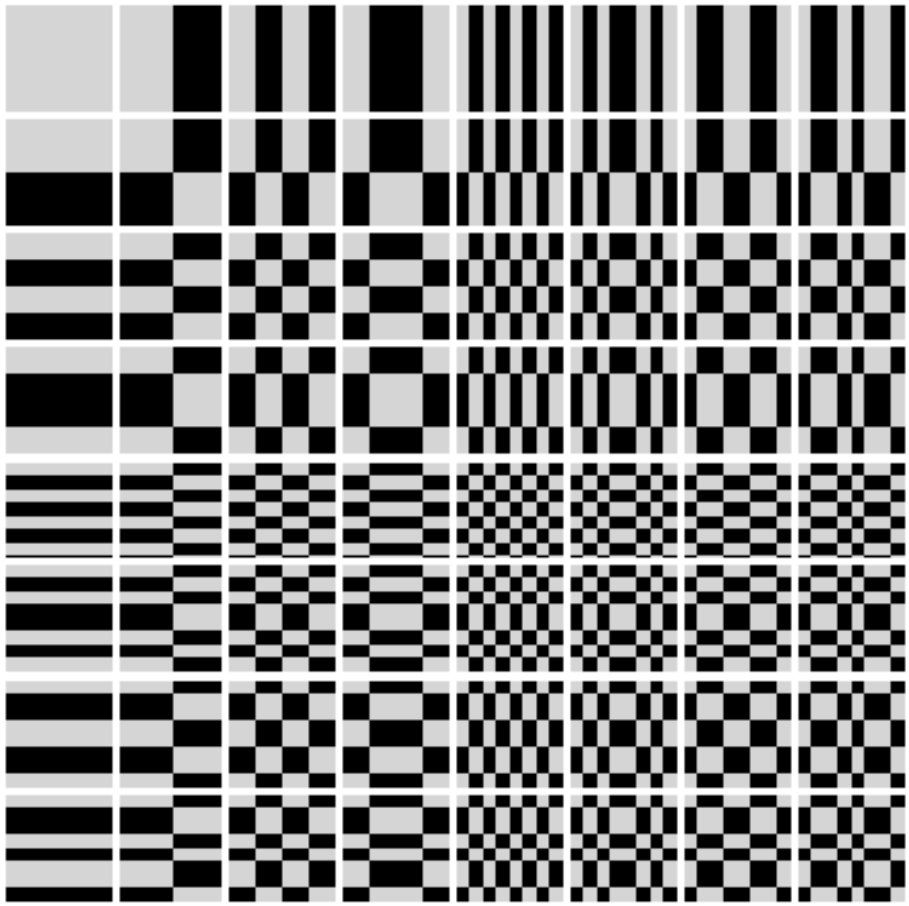

Fig. A.2: Basis functions of Walsh-Hadamard Transform for N=8

Appendix B

Mapping Functions

B.1 Alpha-rooting

In alpha-rooting, DFT coefficients of the image are raised to a power α while the phase part remains unchanged.

$$T(u,v) = |S(u,v)|^{\alpha} e^{jargS(u,v)},\ 0 \leq u,v \leq N-1 \tag{B.1}$$

$S(u,v)$, $T(u,v)$ are the DFT coefficients of the original and modified image and these values are normalized to a maximum value of unity. The function plot for various values of α is shown in Fig. B.1.

B.2 Twicing Function

Twicing function can be expressed as

$$|T(u,v)| = |S(u,v)|(2 - |S(u,v)|) \tag{B.2}$$

Recursively used Twicing functions can be expressed as

$$ie. |T_k(u,v)| = |T_{k-1}(u,v)|(2 - |T_{k-1}(u,v)|) \tag{B.3}$$

where $T_0(u,v)$=$S(u,v)$ and $T_1(u,v) = T(u,v)$.

The mapping function has been modified by Amore et. al. in [107] as

$$|T_k(u,v)| = |T_{k-1}(u,v)|(2 - \beta|T_{k-1}(u,v)|) \tag{B.4}$$

where β value is in the range [0,1]. A plot of the recursive twicing function for different k values is presented in Fig. B.2.

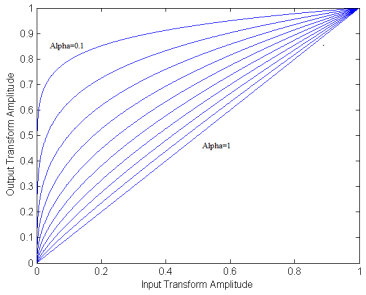

Fig. B.1: Plot of alpha-rooting function for $0.1 < \alpha < 1$.

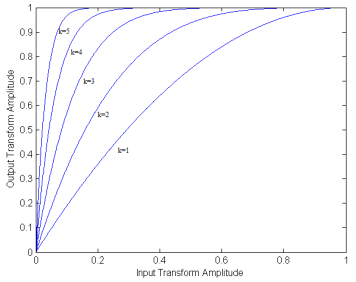

Fig. B.2: Plot of twicing function

B.3 Programmable-S-Function

Functional form of programmable S-function can be expressed as

$$T(u,v) = \begin{cases} n(1 - (1 - \frac{S(u,v)}{m})^{p1}), & \text{if } 0 \le S \le m \\ n + (1-n)(\frac{S(u,v)-m}{1-m})^{p2}, & \text{if } m \le S \le 1 \end{cases} \tag{B.5}$$

where $0 \le m \le n \le 1$ and $p1, p2 > 0$. By varying the values of $p1$, $p2$, m and n, slope and threshold points can be adjusted properly.

Fig. B.3 and Fig. B.4 show the programmable S-function for various values of parameters.

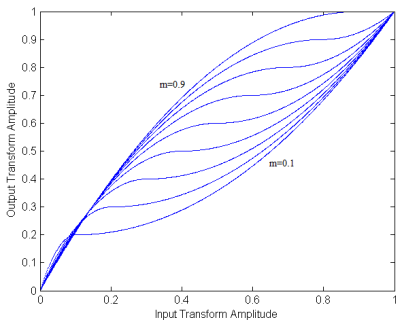

Fig. B.3: Plot of programmable-S-function for $p1 = p2 = 2$

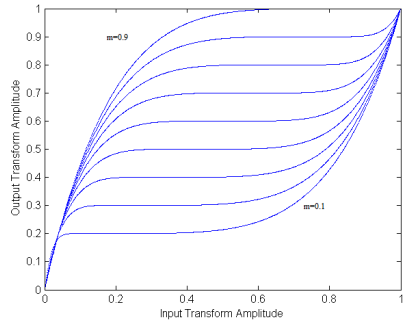

Fig. B.4: Plot of programmable-S-function for $p1 = p2 = 5$

B.4 Function proposed by Lee

A single variable function, proposed by Lee is given by

$$T(u,v) = \frac{1 + S(u,v)^{\frac{1}{\gamma}} - (1 - S(u,v))^{\frac{1}{\gamma}}}{2} \tag{B.6}$$

A plot of this mapping function for various γ is shown in Fig. B.5

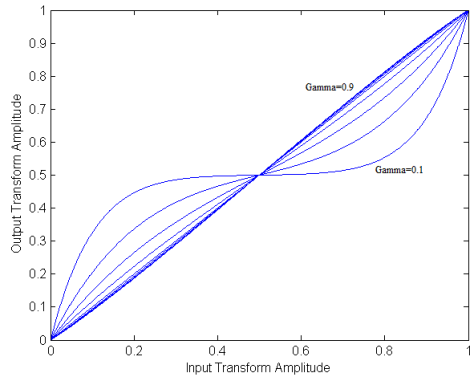

Fig. B.5: Plot of function proposed by Lee for various values of γ

B.5 Intensification Operator

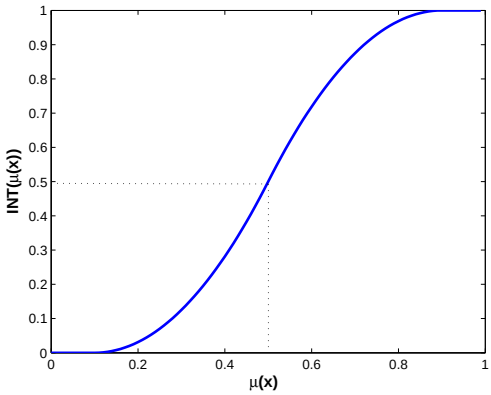

Fig. B.6: Plot of intensification operator in spatial domain

Appendix C

Image Quality Assessment Metrics

C.1 Full-Reference Metrics

Peak Signal-to-Noise Ratio (PSNR) & Mean-Squared Error (MSE) are expressed mathematically as

$$MSE(r,e) = \frac{1}{MN}\sum_{i=0}^{M-1}\sum_{j=0}^{N-1}\left(r(i,j) - e(i,j)\right)^2 \tag{C.1}$$

$$PSNR(r,e) = 10log_{10}\left(\frac{(L-1)^2}{MSE(r,e)}\right)dB \tag{C.2}$$

where r and e denote the reference and enhanced images respectively, MN is the size of the image and L is the dynamic range of pixel values (256 for 8-bit gray-scale images).

Other frequently used metrics are Mean Absolute Error (MAE), Signal-to-Noise Ratio (SNR), Absolute Mean Brightness Error (AMBE), Contrast-to-Noise Ratio (CNR) are defined as

$$MAE(r,e) = \frac{1}{MN}\sum_{i=0}^{M-1}\sum_{j=0}^{N-1}|n(i,j)| \tag{C.3}$$

$$SNR(r,e) = \frac{\sum_{i=0}^{M-1}\sum_{j=0}^{N-1} r(i,j)^2}{\sum_{i=0}^{M-1}\sum_{j=0}^{N-1} n(i,j)^2} \tag{C.4}$$

AMBE is the deviation of the mean intensity of the enhanced image from the mean intensity of the original image.

$$AMBE(r,e) = |\mu_r - \mu_e| \tag{C.5}$$

$$CNR(r,e) = \frac{\mu_r - \mu_n}{\sigma_n} \tag{C.6}$$

where

$$n(i,j) = r(i,j) - e(i,j)$$

$$\mu_r = \frac{1}{MN}\sum_{i=0}^{M-1}\sum_{j=0}^{N-1} r(i,j)$$

$$\mu_n = \frac{1}{MN}\sum_{i=0}^{M-1}\sum_{j=0}^{N-1}(n(i,j))$$

$$\sigma_n^2 = \frac{1}{MN-1}\sum_{i=0}^{M-1}\sum_{j=0}^{N-1}(n(i,j)-\mu_n)^2$$

Universal Quality Index (UQI) is expressed as

$$UQI(r,e) = \frac{4\mu_r\mu_e\sigma_{re}}{(\mu_r^2+\mu_e^2)(\sigma_r^2+\sigma_e^2)} \tag{C.7}$$

where

$$\sigma_{re} = \frac{1}{MN-1}\sum_{i=0}^{M-1}\sum_{j=0}^{N-1}(r(i,j)-\mu_r)(e(i,j)-\mu_e)$$

.

SSIM and Mean SSIM (MSSIM) index are defined as

$$SSIM(r,e) = \frac{(2\mu_r\mu_e + C_1)(2\sigma_{re} + C_2)}{(\mu_r^2 + \mu_e^2 + C_1)(\sigma_r^2 + \sigma_e^2 + C_2)} \tag{C.8}$$

$$MSSIM(r,e) = \frac{1}{K}\sum_{i=1}^{K} SSIM(r_i, e_i) \tag{C.9}$$

where $C_1 = ((L-1)k_1)^2$, $C_2 = ((L-1)k_2)^2$, $k_1, k_2 \ll 1$ and K is the number of local windows in the image.

C.2 Blind-Reference Metrics

EME, EMEE, AME, AMEE are defined as

$$EME(e) = \frac{1}{k_1 k_2}\sum_{m=1}^{k_1}\sum_{l=1}^{k_2} 20ln\left(\frac{I_{max}^{l,m}}{I_{min}^{l,m}}\right) \tag{C.10}$$

$$EMEE(e) = \frac{1}{k_1 k_2}\sum_{m=1}^{k_1}\sum_{l=1}^{k_2} \alpha\left(\frac{I_{max}^{l,m}}{I_{min}^{l,m}}\right)^{\alpha} ln\left(\frac{I_{max}^{l,m}}{I_{min}^{l,m}}\right) \tag{C.11}$$

where the image is divided into $k_1 k_2$ blocks, α is a constant, $I_{max}^{l,m}$ and $I_{min}^{l,m}$ are the maximum and minimum values of the pixels in each block of the enhanced image.

$$AME(e) = -\frac{1}{k_1 k_2}\sum_{m=1}^{k_1}\sum_{l=1}^{k_2} 20ln\,(X) \tag{C.12}$$

$$AMEE(e) = -\frac{1}{k_1 k_2}\sum_{m=1}^{k_1}\sum_{l=1}^{k_2} \alpha\,(X)^{\alpha}\,ln\,(X) \tag{C.13}$$

where $X = \frac{I_{max}^{l,m} - I_{min}^{l,m}}{I_{max}^{l,m} + I_{min}^{l,m}}$. All these metrics divide an image into $k_1 k_2$ blocks and calculate the average value of the measured results of all blocks in the entire image.

$$SDME(e) = -\frac{1}{k_1 k_2} \sum_{m=1}^{k_1} \sum_{l=1}^{k_2} 20ln \left| \frac{I_{max}^{l,m} - 2I_{cen}^{l,m} + I_{min}^{l,m}}{I_{max}^{l,m} + 2I_{cen}^{l,m} + I_{min}^{l,m}} \right| \quad \text{(C.14)}$$

where $I_{cen}^{l,m}$ refers to the centre pixel value of each block.

C.3 Statistical Feature Metrics

$$Entropy = -\sum_i \sum_j P(i,j) log P(i,j) \quad \text{(C.15)}$$

$$Contrast = \sum_i \sum_j (i-j)^2 P(i,j) \quad \text{(C.16)}$$

$$Homogeneity = \sum_i \sum_j \frac{P(i,j)}{1+|i-j|} \quad \text{(C.17)}$$

$$Energy = \sum_i \sum_j P(i,j)^2 \quad \text{(C.18)}$$

$$Correlation = \sum_i \sum_j \frac{(i-\mu_i)(j-\mu_j)}{\sigma_i \sigma_j} P(i,j) \quad \text{(C.19)}$$

where i and j are two different gray levels of the image and P is the number of the co-appearance of gray levels i and j.

Appendix D

Mex Compilation of SMRT

Algorithms for SMRT and ISMRT can be coded in MATLAB for signal processing applications. They are coded in MATLAB using well known C language and integrated to MATLAB via MEX file compilation. MATLAB toolbox has been developed for SMRT and its inverse.

D.1 Mex Compilation

C is one of the most popular languages in coding. It is powerful, flexible, portable and elegantly structured language. Another important reason for selecting C is that the platform of MATLAB software is written in C. It also provides means to integrate functions written in C to MATLAB library. Hence the functions written can be optimized to the maximum extent possible by using C.

Register variables are used to improve the speed in C. They are a special case of variables. Unlike normal variables, stored in the main memory of the computer, these are stored in the registers of CPU.

The registers can be stored and accessed quickly. Normally the compiler decides which all variables are stored in the register, but in C language the programmer can suggest to store some variables in the registers.

Other improvisation techniques were not required for the C programs since the computation algorithm of transforms does not contain any complex arithmetic operations or equations other than simple additions and comparisons.

The programs written in C cannot be used directly in MATLAB. Proper interfacing is required to integrate it back to MATLAB by using MEX files. MEX files are MATLAB Executable files. They are dynamically-linked subroutines that the MATLAB interpreter loads and executes. MEX files have a definite structure, different from ordinary C program, and must be compiled to form the actual executable files. MEX-file can be called using the name of the file, without the file extension. It contains only one function or subroutine with the name same as the MEX-file name.

A difficulty associated with the MEX file compilation is the debugging of MEX files. MATLAB does not have any provision to debug the MEX files, making it difficult for error correction via MATLAB. Any error occurring while creating a MEX file needs to be corrected by trial and error method. In addition, there is no C compiler present in the versions of MATLAB released after 2009. So creating MEX files will require external compiler for versions after 2009.

D.2 MATLAB Toolbox

One of the prime advantages of using MEX files is that they can be invoked in a manner similar to the inbuilt MATLAB functions, provided they are already included in MATLAB working directory.

Here comes the role of MATLAB toolbox. Toolbox is basically a collection of user-written functions designed for a specific purpose. Creation of toolbox is a simple task if all the program files are ready. All the program files for implementation of the transform are initially put together in a single folder. A file named startup.m has to be added in the default working directory of MATLAB. It has the path of the folder in which the files are saved. The tool box is integrated automatically when MATLAB is launched from startup.m. The computation time for SMRT and its inverse are reduced considerably with the help of C Programming and MEX file integration. The better performance of MEX files over MATLAB is accomplished by the usage of pointers, dynamically assigned during program run and cleared after program execution.